Supporting Information For:

A Nanocrystalline Hf(IV) MOF for Precise Fluorometric Recognition of Carcinogenic Nicotine and Herbicide Benfluralin: Characterization, Real-Life Application and Mechanistic Investigation

Srijan Mukherjee, [a, ‡] *Sandip Roy,* [a, ‡] *Pitam Chakrabarti,* [b] *Vishal Trivedi,*[b,] *and Shyam Biswas*[a,]*

[a] Department of Chemistry, Indian Institute of Technology Guwahati, 781039 Assam, India

[b] Department of Biosciences and Bioengineering, Indian Institute of Technology Guwahati, 781039 Assam, India

[‡] Equal contribution

* Corresponding author. Tel: 91-3612583309, Fax: 91-3612582349.

E-mail address: sbiswas@iitg.ac.in.

1.1. Materials and Characterization Methods:

All the reagents and solvents were procured from commercial sources and used without purification, except the 2-benzamido terephthalic acid (H_2BDC-NH-CH_2-Py) linker. The ligand synthesis procedure is discussed below (Scheme S1) and its purity was verified by the ATR-IR, ^{1}H NMR, ^{13}C NMR and mass spectrometric analysis. The notations used for characterization of the bands are broad (br), strong (s), very strong (vs), medium (m), weak (w) and shoulder (sh). PXRD data were collected by using Rigaku Smartlab X-ray diffractometer with Cu-*K*α radiation (λ = 1.54056 Å), 50 kV of operating voltage and 100 mA of operating current. The Attenuated Total Reflectance Infrared (ATR-IR) spectra were recorded using PerkinElmer UATR Two at ambient condition in the region 400-4000 cm^{-1}. Thermogravimetric analysis (TGA) was carried out with a TG 209 F1 Libra Netzsch, thermogravimetric analyzer in the temperature range of 30 - 700 ℃ in an N_2 atmosphere at the rate of 4 ℃ min^{-1}. N_2 sorption isotherms were recorded by using Quantachrome Autosorb iQ-MP volumetric gas adsorption equipment at − 196 ℃. Before the sorption analysis, the degassing of the compound was carried out at 100 ℃ under a high vacuum for 24 h. Fluorescence sensing studies were performed with a HORIBA JOBIN YVON Fluoromax-4 spectrofluorometer. FE-SEM images were captured with a Zeiss (Sigma) scanning electron microscope. A Bruker Avance III 600 NMR spectrometer was used for recording ^{1}H NMR spectra at 400 MHz. Mass spectra were recorded with an Agilent 6520 QTOF high-resolution mass spectrometer (HR-MS). Fluorescence lifetimes were measured using Picosecond Time-resolved and Steady State Luminescence Spectrometer on an Edinburg Instruments Lifespec II & FSP 920 instrument. Pawley refinement was carried out using Materials Studio software package.

1.2. Synthesis of H_2BDC-NH-CH_2-Py or ((Pyridin-2-ylmethyl)amino)Terephthalic Acid Linker:

Firstly, 2-aminoterephthalic acid (1500 mg, 8.28 mmol) and anhydrous methanol (60 mL) were poured into a 100 mL round bottom flask and dissolved by sonication. Thereafter, 2-pyridinecaboxaldehyde (800 μL, 8.28 mmol) was added dropwise to the aforementioned mixture under reflux condition at 70 ℃ in N_2 atmosphere for 12 h. After that a white colour precipitate appeared. The obtained product was kept at 0 ℃ under stirring conditions and $NaBH_3CN$ (1040 mg, 16.56 mmol) was added into the reaction mixture. The reaction mixture was kept in cold conditions for 2 h under N_2 atmosphere. Finally, the reaction mixture was kept in stirring conditions for 12 h under N_2 atmosphere at room temperature. The product was filtered and washed with water to obtain a very light-yellow precipitate and product was kept in oven for drying at 60 ℃ for 6 h. Yield: 1.25 g (4.59 mmol, 56%). Purity of the obtained powder product was verified by ^{1}H NMR (Figure S1), ^{13}C NMR (Figure S2), IR (Figure S3), and HR-MS (Figure S4) techniques.

^{1}H NMR (400 MHz, DMSO-d_6): δ = 13.07 (s, 1H,), 8.56 (s, 1H,), 7.89-7.91 (d, 1H), 7.75-7.77-7.79 (t, 1H), 7.72-7.74 (m, 2H), 7.59-7.66 (m, 4H) ppm. ^{13}C NMR (100 MHz, DMSO-d_6): δ = 169.27, 167.10, 157.82, 149.09, 136.92, 135.72, 132.03, 122.36, 121.39, 114.90, 113.79, 112.41, 47.62. HR-MS (m/z): Calculated mass [M - H^+] (m/z): 273.26, obtained mass [M - H^+] (m/z): 273.09.

1.3. Fluorescence Detection of Nicotine:

The probe **1′** (3 mg) was taken in a 5 mL glass vial containing 3 mL deionized water. Then, the suspension was sonicated for 15 min and kept it for overnight to make the suspension stable. Aliquot (100 μL) of the resulting suspension was taken as a probe and mixed well with 3000 μL of water in a quartz fluorescence cuvette. During titration experiments, sequential addition of 10 mM aqueous solution of few analytes was performed in 3 mL of **1′** suspension in water. In all the fluorescence titrations, excitation wavelength was 366 nm. The selectivity study was executed with 10 mM aqueous solution of all the analytes prepared by proper dilution, where I_0 refers to the initial fluorescence emission intensity of the probe and I refers to the emission fluorescence intensity after the addition of the analyte.

1.4. Fluorescence Detection of Benfluralin:

The probe **1′** (3 mg) was taken in a 5 mL glass vial containing 3 mL methanol. Then, the suspension was sonicated for 15 min and kept it for overnight to make the suspension stable. Aliquot (100 μL) of the resulting suspension was taken as a probe and mixed well with 3000 μL of methanol respectively in a quartz fluorescence cuvette. During titration experiments, sequential addition of 10 mM methanol solution of few analytes was performed in 3 mL of **1′** suspension in methanol. In all the fluorescence titrations, excitation wavelength was 366 nm. The selectivity study was executed with 10 mM methanol solution of all the analytes prepared by proper dilution. Quenching efficiency was calculated by the formula: $\left(1-\frac{I}{I_0}\right)\times 100\%$, where I_0 refers to the initial fluorescence emission intensity of the probe and I refers to the emission fluorescence intensity after the addition of the analyte.

1.5. Fluorescence Detection of Nicotine in Human Blood Serum Samples:

Firstly, 10 mL of blood sample was collected from the right arm vein of a healthy person (blood group (A+) and the blood plasma was separated by centrifuging the sample at 10,000 rpm for 15 min. The light-yellow blood serum was collected in a Falcon tube and stored at -20 ℃ in a refrigerator. For fluorescence detection experiments, aliquots of different concentrations of nicotine (NIC) were spiked into the blood serum sample, which contained HEPES buffer suspension of the MOF.

1.6. Fluorescence Detection of Nicotine in Artificial Sweat samples:

Artificial sweat was prepared according to the reference test method EN 1811:2011 on the same day as the fluorescence sensing experiment carried out. It was prepared by dissolving urea [100 mg (0.1 wt%)], NaCl [500 mg (0.5 wt%)] and lactic acid [100 mg (0.1 wt%)] in 100 mL of deionized water. The pH of the comprehensive artificial sweat was adjusted from pH 3.9 to the final pH of 6.5 by adding 0.1 M NaOH and 0.1 M HCl, while continuously monitoring the solution pH. In fluorescence detection experiments, aliquots of different nicotine (NIC) concentrations prepared in sweat specimens were spiked in the suspension of the **1′**.

1.7. Fluorescence Detection of Nicotine in Different Environmental Aqueous Media:

Probe **1′** (3 mg) was taken in a 5 mL glass vial containing 3 mL deionized water. Then, the suspension was sonicated for 15 min and kept it overnight to make it stable.

Different water samples (lake water, river water, tap water and distilled water) were collected from their respective sources and filtered well to remove all the solid particles present in the water. Various nicotine solutions were prepared in different water samples with proper dilution. Fluorescence titration experiments were performed by spiking prepared NIC solution into the probe suspension in water.

1.8. Fluorometric Detection of Nicotine in Human Urine Sample:

A 10 mL urine sample was collected from a healthy individual and treated with 500 mL of HNO_3 to eliminate any interfering living organisms. The sample was then centrifuged at 8000 rpm for 10 min, and the supernatant was used for the experiments. To conduct fluorescence experiments, various amounts of nicotine were added to the urine samples containing a HEPES buffer suspension of the probe.

1.9. Extraction and Fluorometric Detection of Nicotine from Tobacco Leaves:

Nicotine was extracted from tobacco leaves based on the alkaloid property of nicotine, which involves different ranges of solubility in water and organic solvents. Firstly, tobacco leaf was dried for 4 h at 60 °C. After that, 20 g of the dried tobacco leaves was boiled with 300 mL of water at 80 ± 5 ℃ for 30 min. Then, 4 g of sodium carbonate was added, and the mixture was heated for 20 min. After filtration, the resultant filtrate was adjusted to pH 12 using 0.1 M NaOH and extracted with chloroform (50 mL × 2 times) utilizing the liquid-liquid extraction technique. The chloroform of the filtrate was separated using a rotary evaporator at 50 ℃ under vacuum to get brown colour crude extract. For fluorescence experiments, the crude extract was diluted ten times with deionized water and fluorescence titration experiments were performed by spiking prepared nicotine (NIC) extract into the probe suspension in water.

1.10. Preparation of 1′@Chitosan@Paper Composites:

Cellulose acetate filter papers were washed by stirring in ethanol over 12 h, after changing ethanol every 3 h. The filter papers were dried well at 60 ℃ for overnight. Chitosan (80 mg) was taken in a clean vial and mixed well with 500 µL of acetic acid and 7.5 mL of distilled water over 12 h to obtain a clear aqueous chitosan solution (1%, w/w). In a second vial, 30 mg of **1′** MOF was placed and dispersed well in 2 mL of water. Then, 1 mL of 1% chitosan solution (w/w) was added and left under stirring conditions to make a homogeneous solution. Finally, the solution was drop cast on the washed cellulose acetate filter paper (4 cm × 4 cm) and dried in an oven at 60 ℃ for 24 h to make it completely dry. The filter paper was washed three times with 20 mL of distilled water to remove the entire unwanted residue and left for drying for 24 h at 60 ℃.

1.11. Cell Culture and Cell Imaging Experiments:

Breast cancer MDAMB-231 cells were cultured in DMEM:F12 cells supplemented with 10% FBS and 1% antibiotic cocktails. MDAMB-231 cells (10,000 cells) were plated in 96 well cell culture plates in complete medium and allowed them to adhere to the dish. The cells were washed with PBS and incubated with probe (10µg/mL) overnight. Next day, the cells were washed with PBS and treated with nicotine (25µg/mL) for 4 h in HEPES buffer at 37 °C. Post-treatment, the cells were washed with HEPES buffer and the cells were observed under the inverted fluorescence microscope.

1.12 Quantum Yield Measurement:

Here, we have utilised the Parker-Rees method to calculate the quantum yield of the prepared MOF, using a 0.5 M H_2SO_4 solution of quinine sulphate as a standard reference.[1] The formula for this calculation is provided as follows:

$$\Phi_s = (A_r F_S n_s^2 / A_s F_r n_r^2)\, \Phi_r \quad \text{.....(Equation-1)}$$

In this equation, Φ_r represents the quantum yield of the quinine sulphate reference solution, while Φ_s represents the quantum yield of the sample. The values of A_r and A_s correspond to the absorbance of the reference and sample, respectively, whereas F_r and F_s refer to the integrated area of fluorescence intensity for the reference and sample, respectively. The refractive indices of the reference and sample are represented by n_r and n_s, respectively. Table S1 contains the relevant photophysical parameters and quantum yield values.

Table S1. Quantum yield of quinine sulphate, **1′** and **1′** treated with nicotine.

Sl. No.	Sample Name	Excitation Wavelength λ_{ex} (nm)	Absorbance (A)	Area of Integrated Fluorescence Intensity (F)	Quantum Yield (Φ)
1	Quinine Sulphate	344	0.059	7.12 9	0.546
2	**1'**	366	0.080	1.12E8	0.006
3	**1'** after treatment with nicotine	366	0.057	3.11E9	0.194

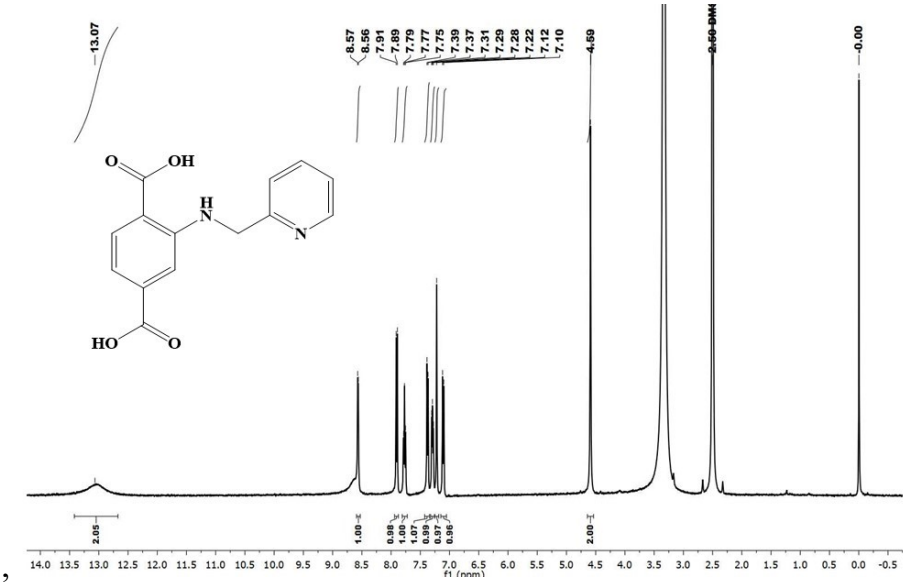

Figure S1. ^{1}H NMR spectrum of ((pyridin-2-ylmethyl)amino)terephthalic acid ligand in DMSO-d_6.

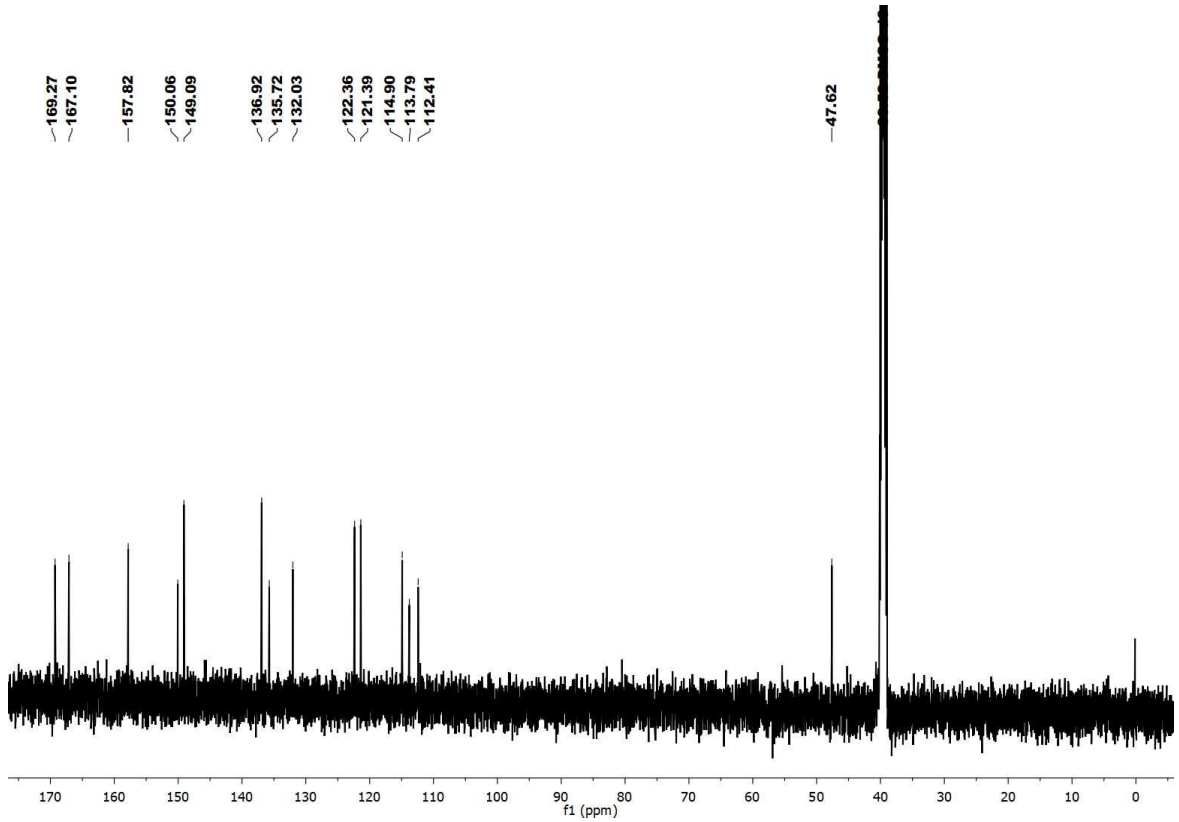

Figure S2. ^{13}C NMR spectrum (125 MHz, DMSO-d_6) of ((pyridin-2-ylmethyl)amino)terephthalic acid linker.

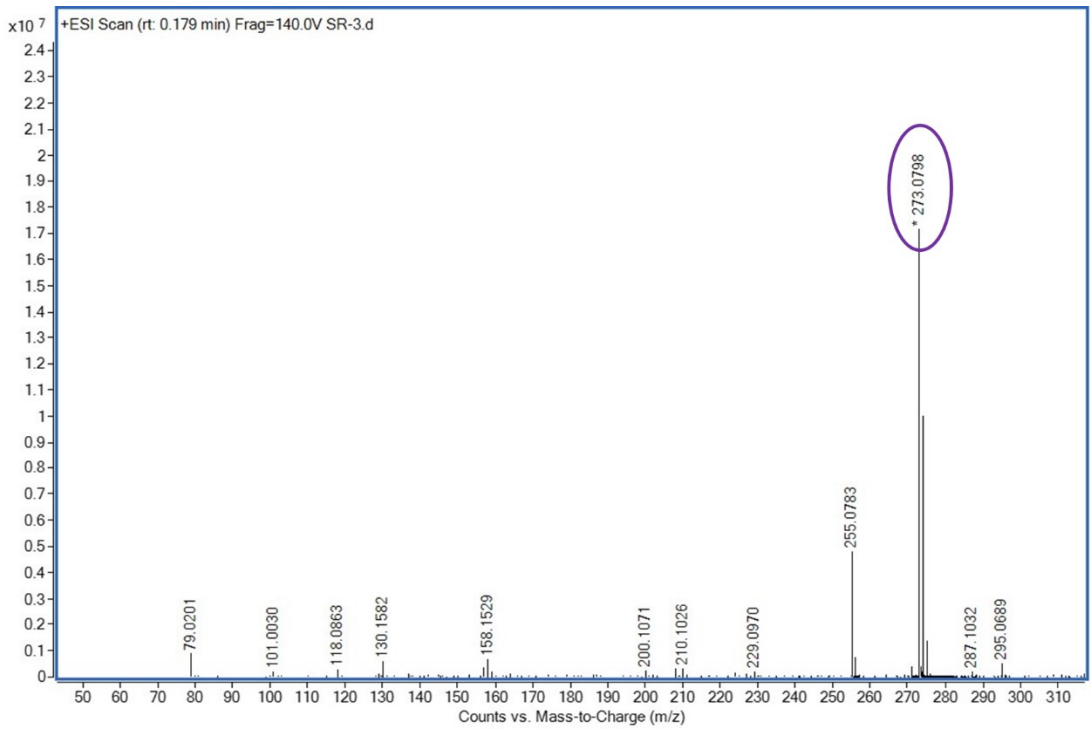

Figure S3. Mass spectrum of ((pyridin-2-ylmethyl)amino)terephthalic acid linker measured in MeOH. The spectrum shows m/z peak at 273.0789, which corresponds to ($M-H^+$) ion (M = mass of ((pyridin-2-ylmethyl)amino)terephthalic acid linker).

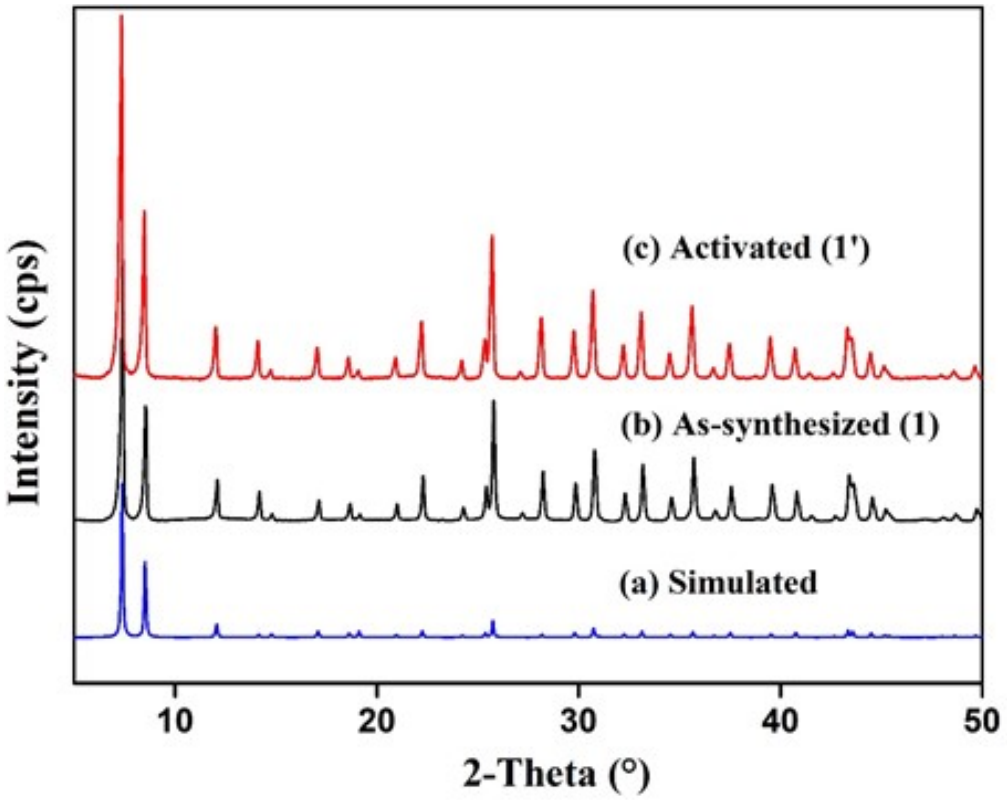

Figure S4. PXRD patterns of simulated (black), as-synthesized **1** (red) and activated **1′** (blue).

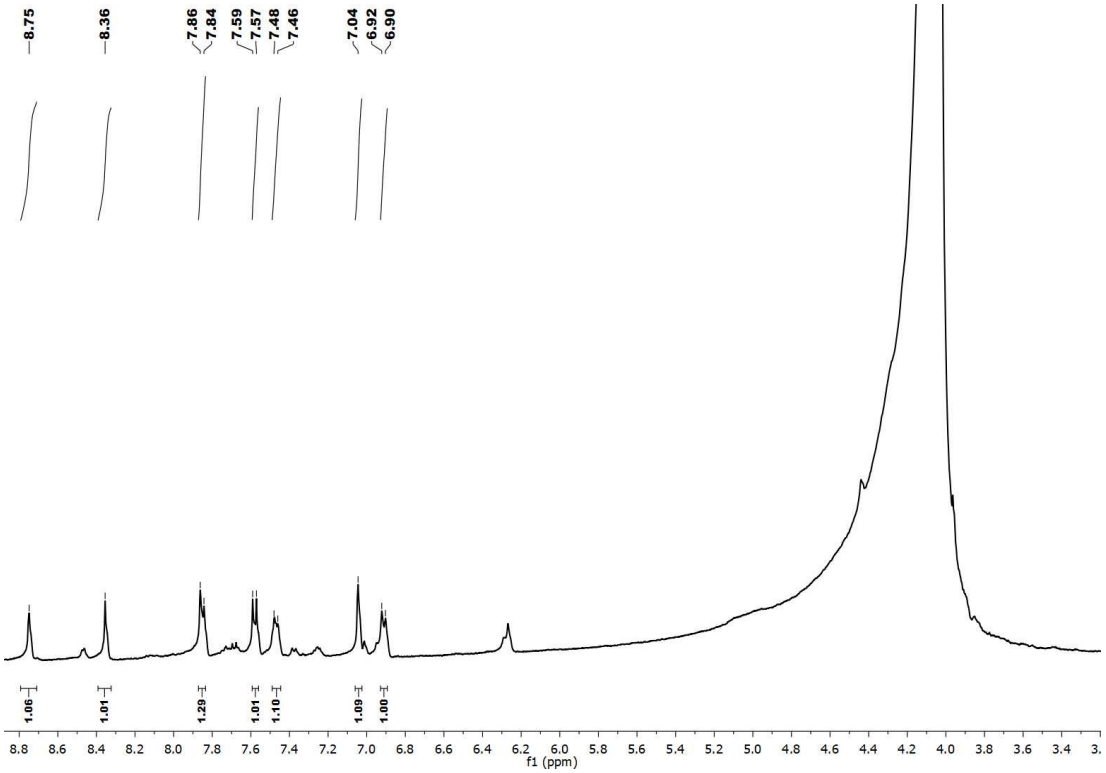

Figure S5. ^{1}H NMR spectrum of ((pyridin-2-ylmethyl)amino)terepthalic acid linker (after digestion of **1′**) in K_3PO_4 in D_2O and DMSO-d_6.

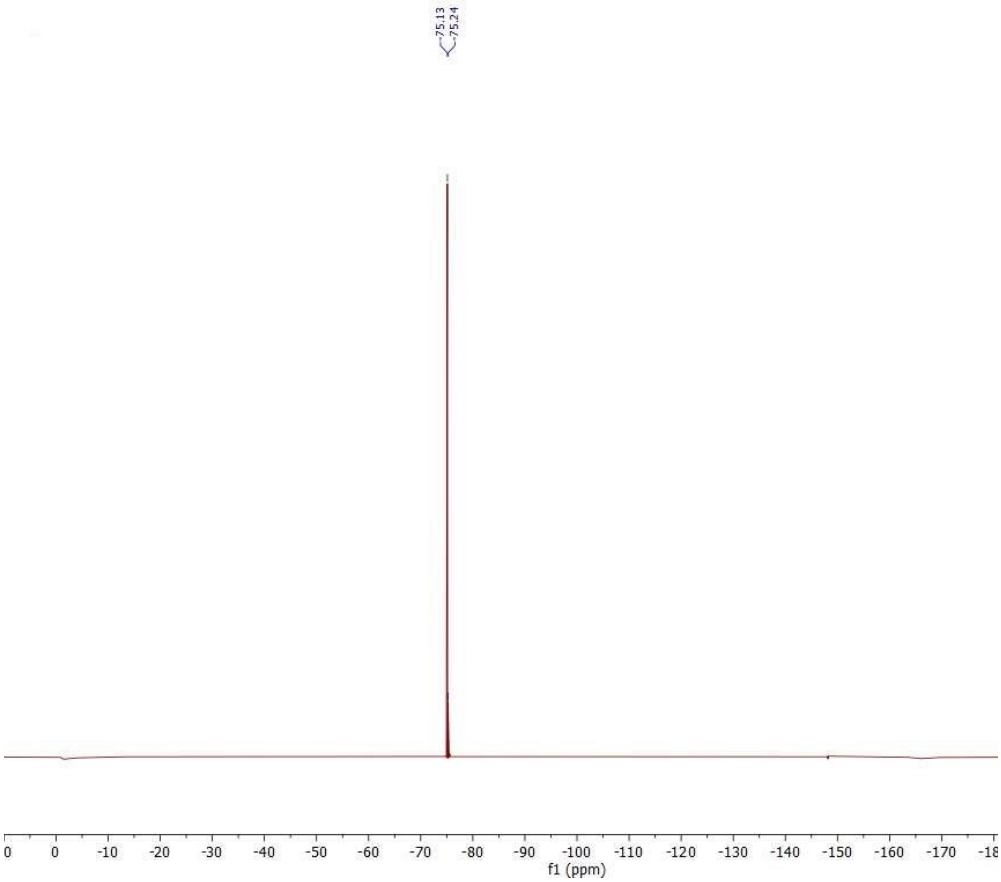

Figure S6. ^{19}F NMR spectrum of ((pyridin-2-ylmethyl)amino)terepthalic acid linker (after digestion of **1′**) in K_3PO_4 in D_2O and DMSO-d_6.

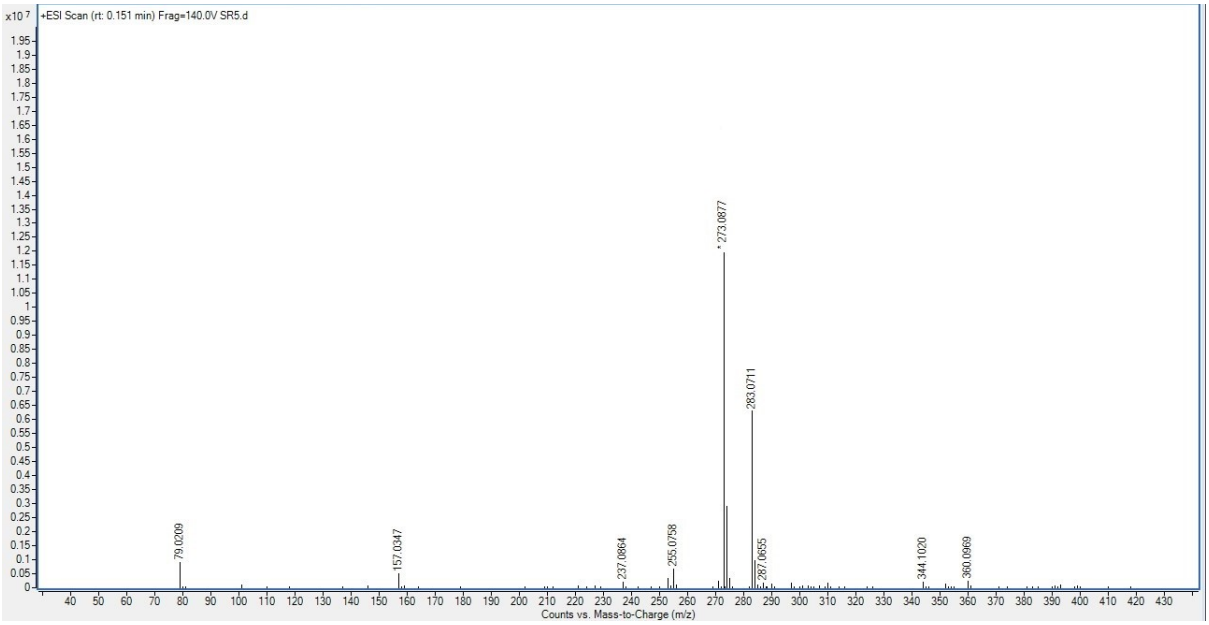

Figure S7. Mass spectrum of **1′** after digestion with 20 μL of HF. The spectrum shows m/z peak at 273.0789, which corresponds to ($M\text{-}H^+$) ion (M = mass of $H_2BDC\text{-}NH\text{-}CH_2\text{-}Py$ linker).

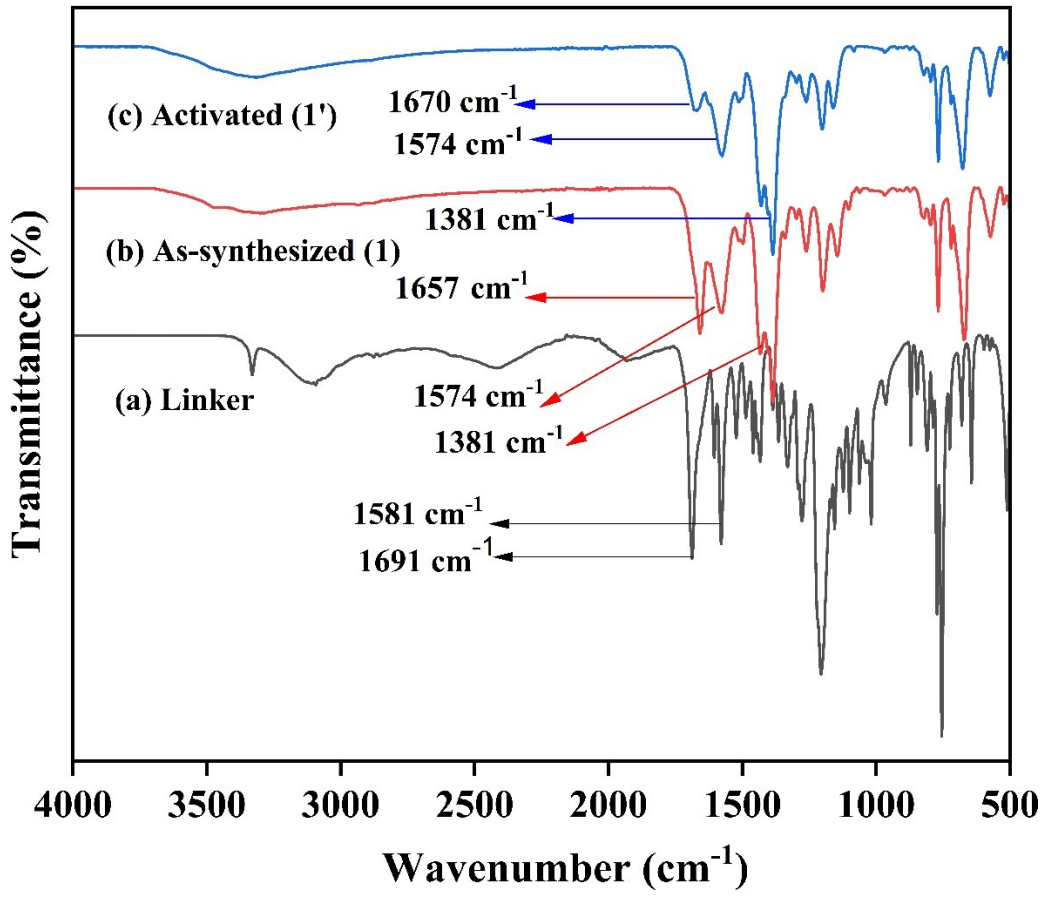

Figure S8. IR spectra of (a) ((pyridin-2-ylmethyl)amino)terephthalic acid linker (black), (b) as-synthesized **1** (red), (c) activated **1′** (blue).

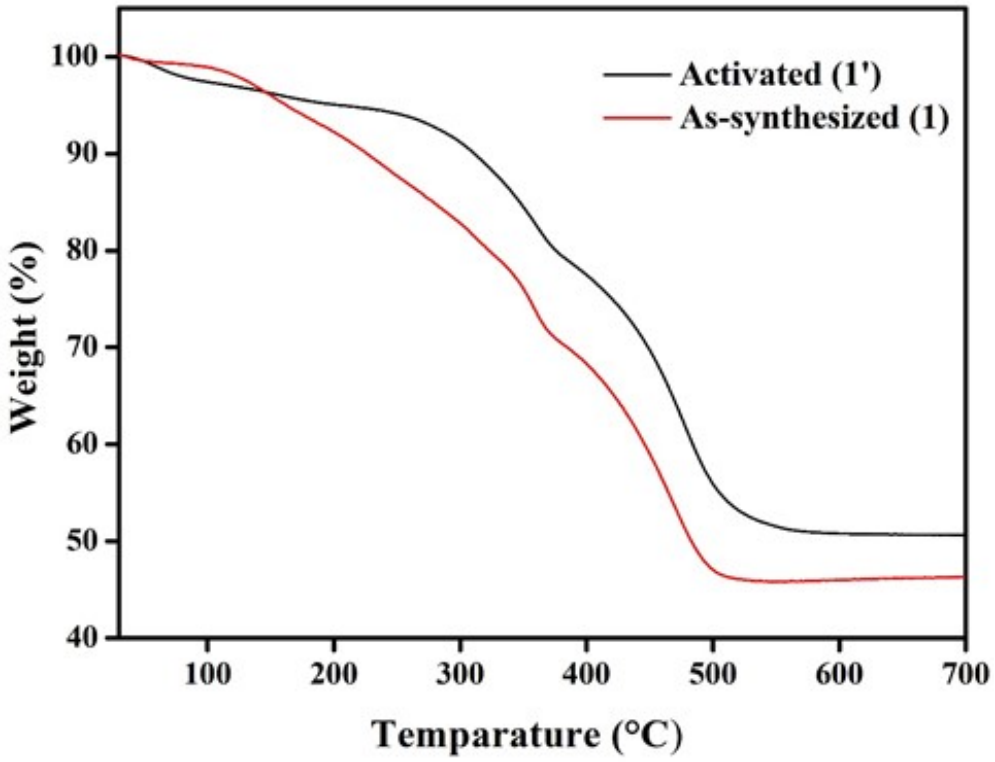

Figure S9. TGA curves of as-synthesized **1** (red) and activated **1′** (black) recorded under O_2 atmosphere in the temperature range of 30-700 °C with a heating rate of 4 °C min^{-1}.

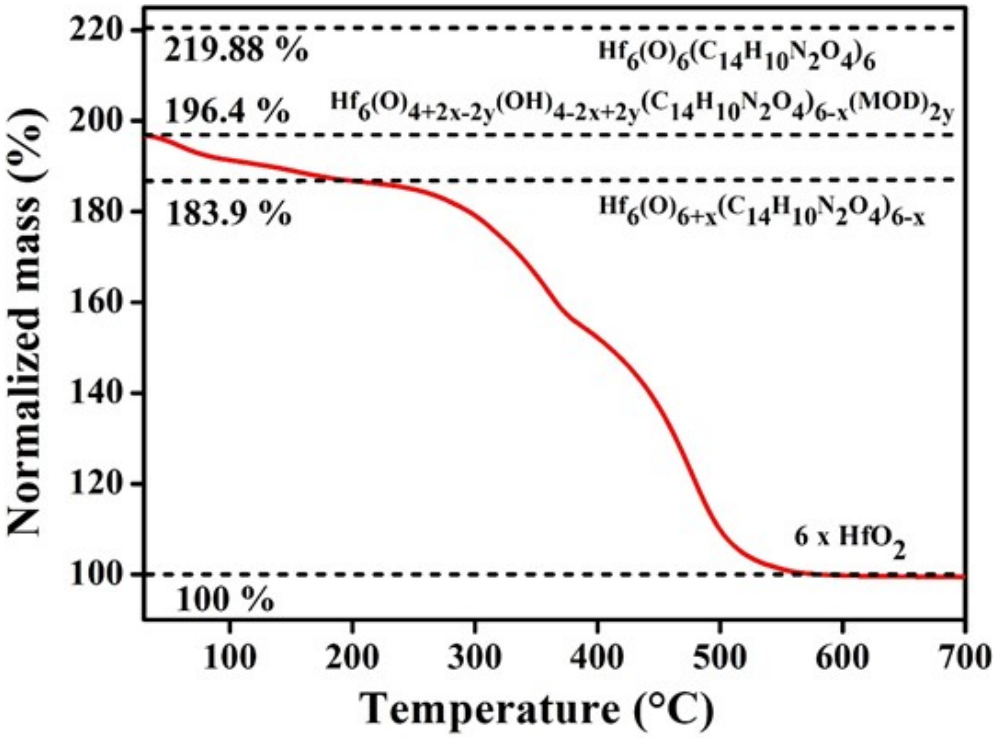

Figure S10. Calculation of missing ligand defects from the TG curve of activated **1′**. The vertical dashed line pinpoints $T_{Plat.}$, the temperature at which the plateau ($W_{Exp.\ Plat.}$) is reached. The horizontal dashed lines pinpoint the relevant TGA plateaus.

Calculation of Linker Defects for 1′ from TGA Data:

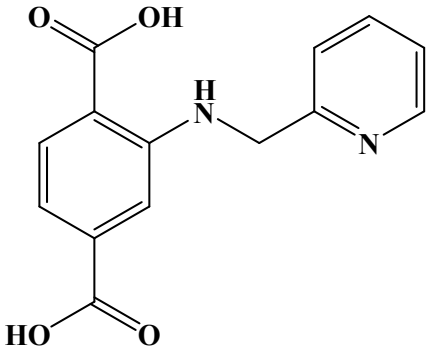

Formula of MOF = $(Hf_6(O)_4(OH)_4(C_{14}H_{10}O_4N_2)_6)$

Molecular Weight = 2832.054 g/mol

- The dehydroxylated and modulator free formula of MOF is $[Hf_6(O)_6(C_{14}H_{10}O_4N_2)_6]$ (ideal),
- Molecular Weight = 2796.033 g/mol
- The dehydroxylated and modulator free formula of MOF is $[Hf_6(O)_{6+x}(C_{14}H_{10}O_4N_2)_{6-x}]$ (experimental), Molecular Weight = 2796.033 g/mol (x = number of linker defect).
- From TGA data, after the final weight loss step, the remaining mass is due to 6 moles of HfO_2 i.e. 6 × 123.2 = 1271.618 g/mol.
- The ideal Weight of $[Hf_6(O)_6(C_{14}H_{10}O_4N_2]$ is 2.198 times of 6 moles of HfO_2.
- The remaining flat mass obtained at the last mass on TGA curve was normalized to 100%.
- The ideal normalized mass percentage for $[Hf_6(O)_6(C_{14}H_{10}O_4N_2]$ is 219.87 %.
- The experimental normalized mass percentage of $[Hf_6(O)_{6+x}(C_{14}H_{10}O_4N_2)_{6-x}]$ from TGA is 183.9%.
- $x = 6 – (W_{wt.\ Plat} - W_{end}/Wt._{PL\cdot Theo})$.

where

- $W_{wt.\ Plat}$ is the (normalized) Weight of the sample at the second TGA plateau.
- W_{end} is 100 %
- $Wt._{PL.Theo} = (W_{wt.\ ideal\ Plat.} – W_{end})/NL_{ideal}$
- NL_{ideal} = number of linkers per unit formula ideally (6)
- $Wt._{PL.Theo} = ((183.92-100)/6) = 19.97\%$
- $x = 6 - ((183.92 – 100)/19.97) = 6 – 4.20 = 1.80$
- The number of linker defects per unit formula is 1.8

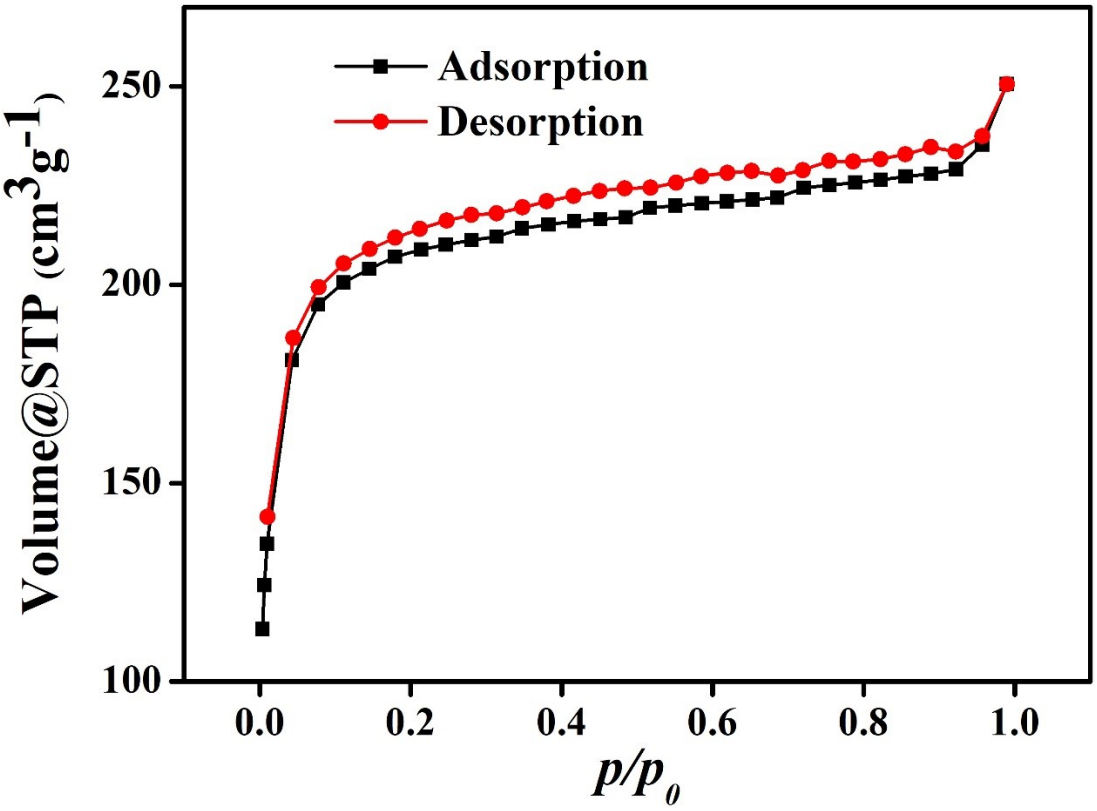

Figure S11. N_2 sorption isotherms of activated **1′** recorded at -196 ℃.

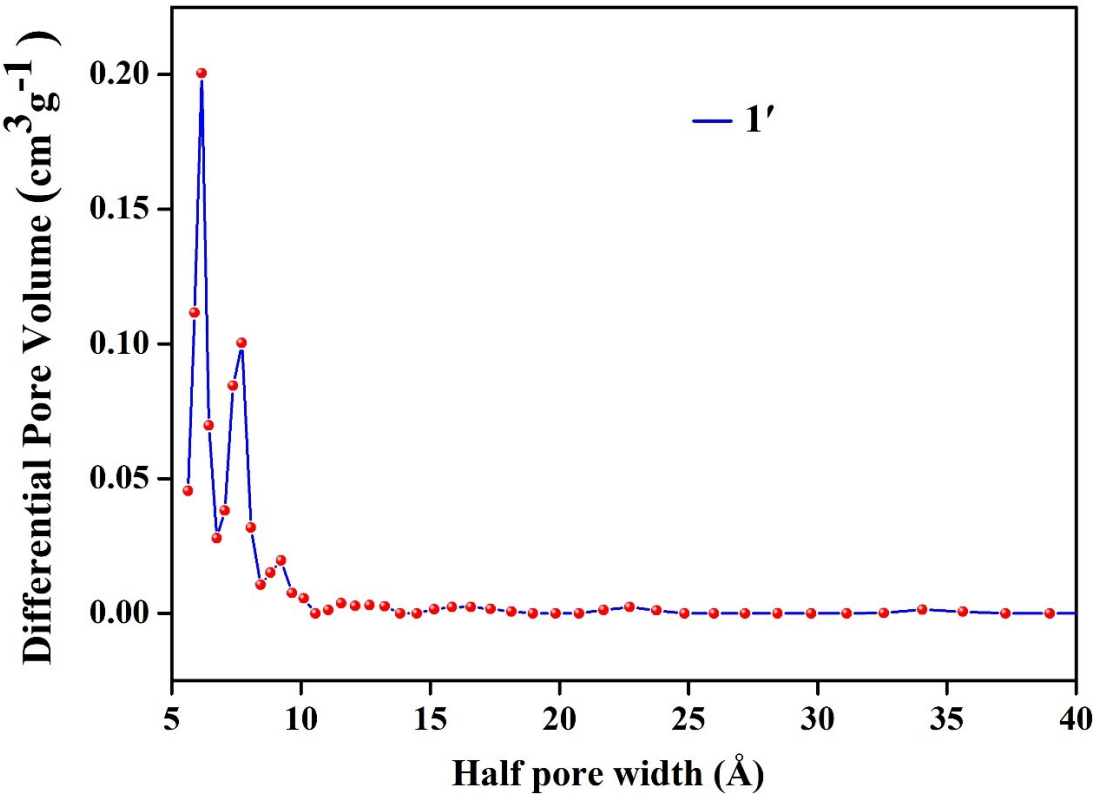

Figure S12. Pore size distribution curve of activated **1**.

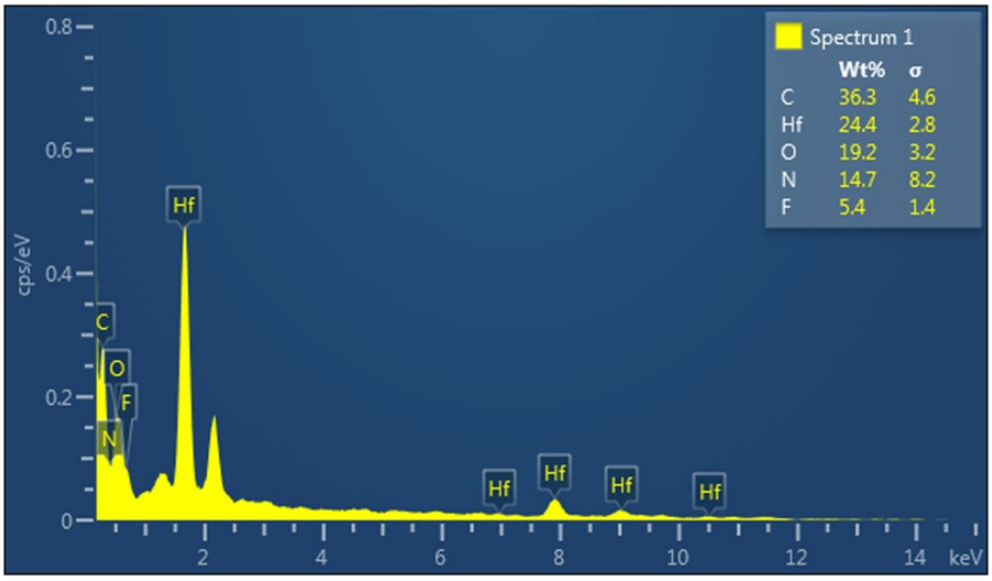

Figure S13. EDX spectrum of **1′**.

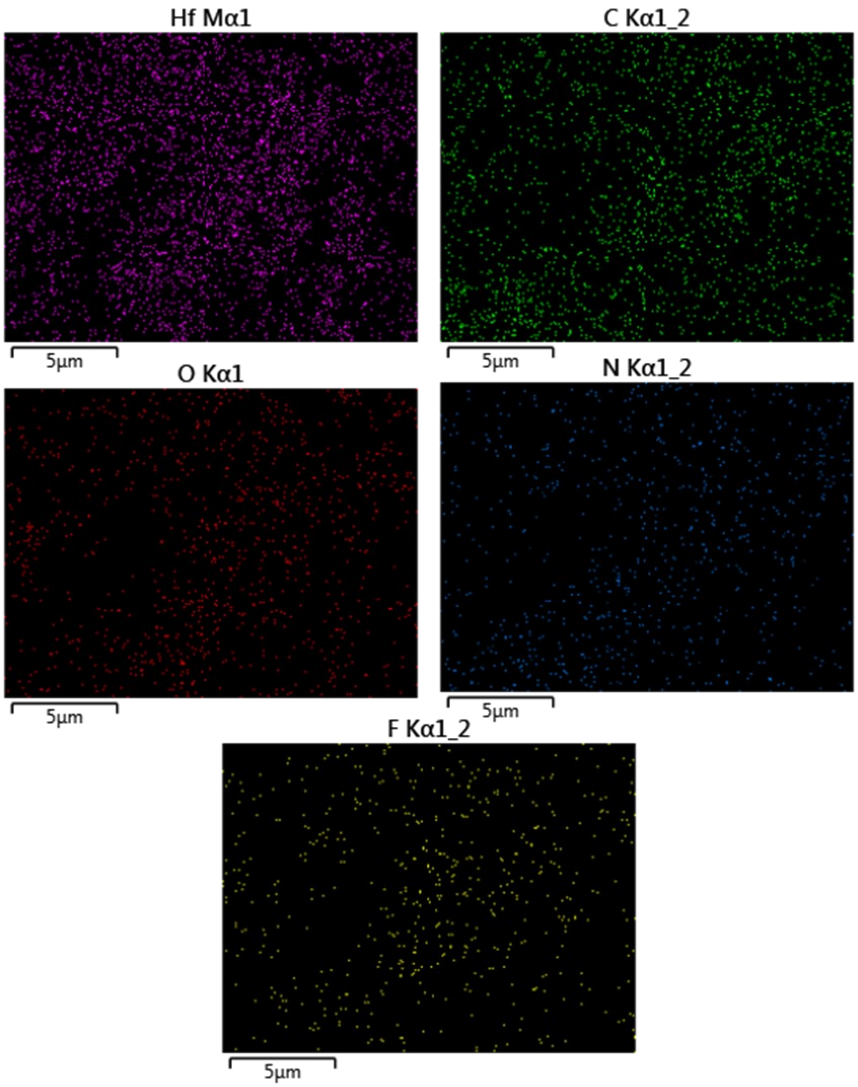

Figure S14. EDX elemental mapping of **1′**.

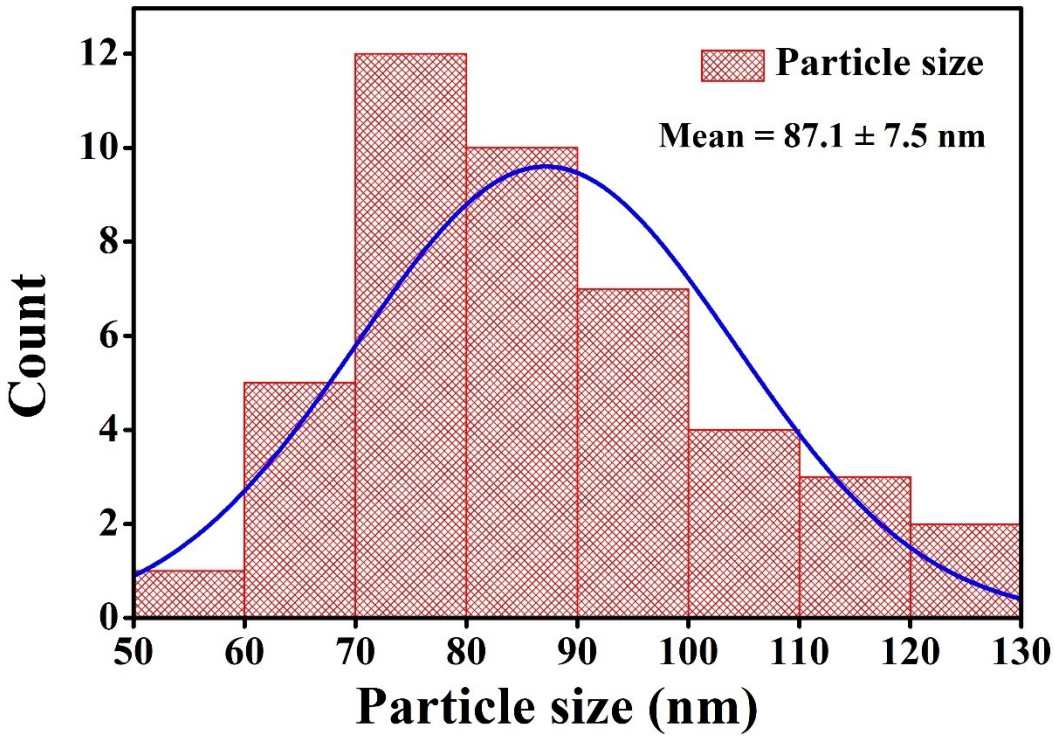

Figure S15. Particle size distribution curve of **1′** obtained from the FETEM images.

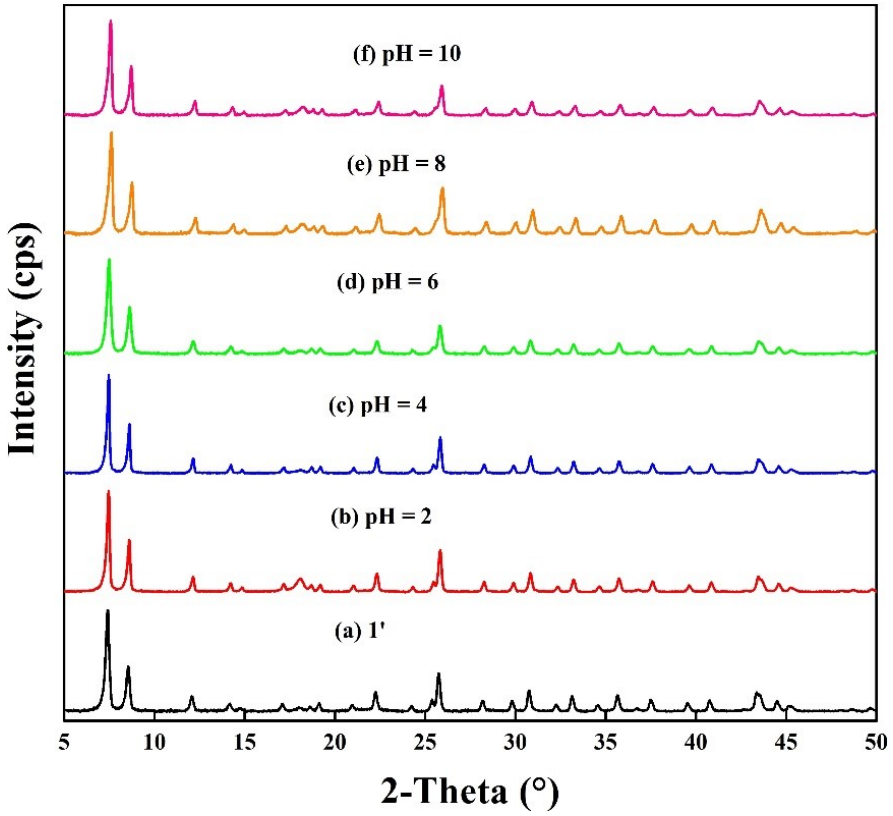

Figure S16. (i) PXRD patterns of (a) activated **1′** (black), after stirring in (b) pH 2 (red), (c) pH 4 (blue), (d) pH 6 (green), (e) pH 8 (orange), and (f) pH 10 (pink) solutions.

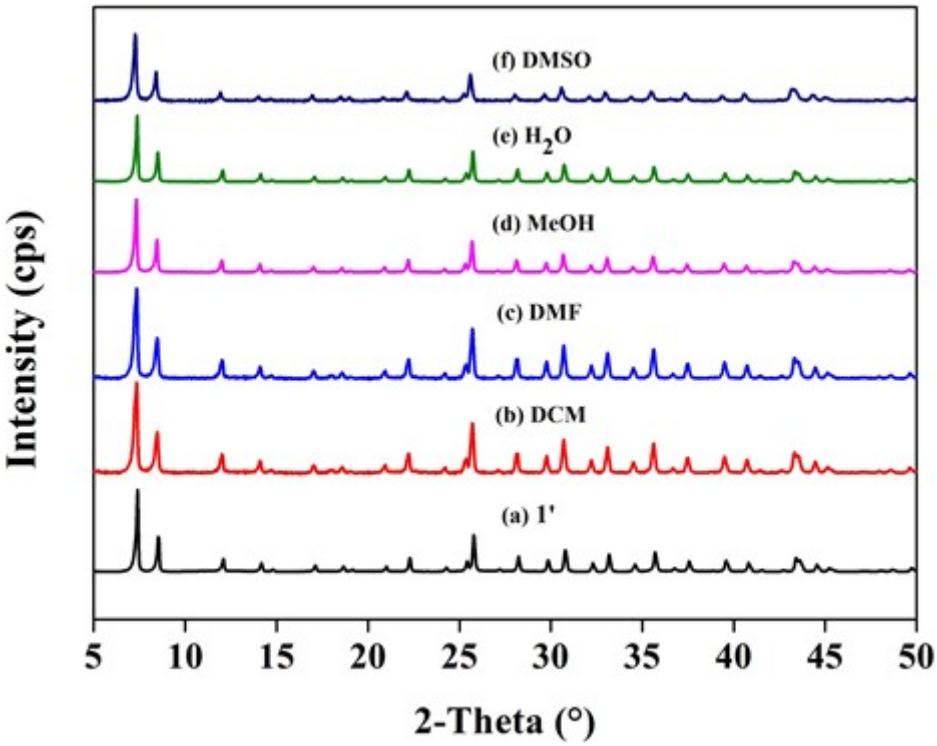

Figure S17. PXRD patterns of (a) activated **1′** (black), after stirring in (b) DCM (red), (c) DMSO (indigo), (d) MeOH (purple), (e) H_2O (green), (f) DMSO (navy blue) solutions.

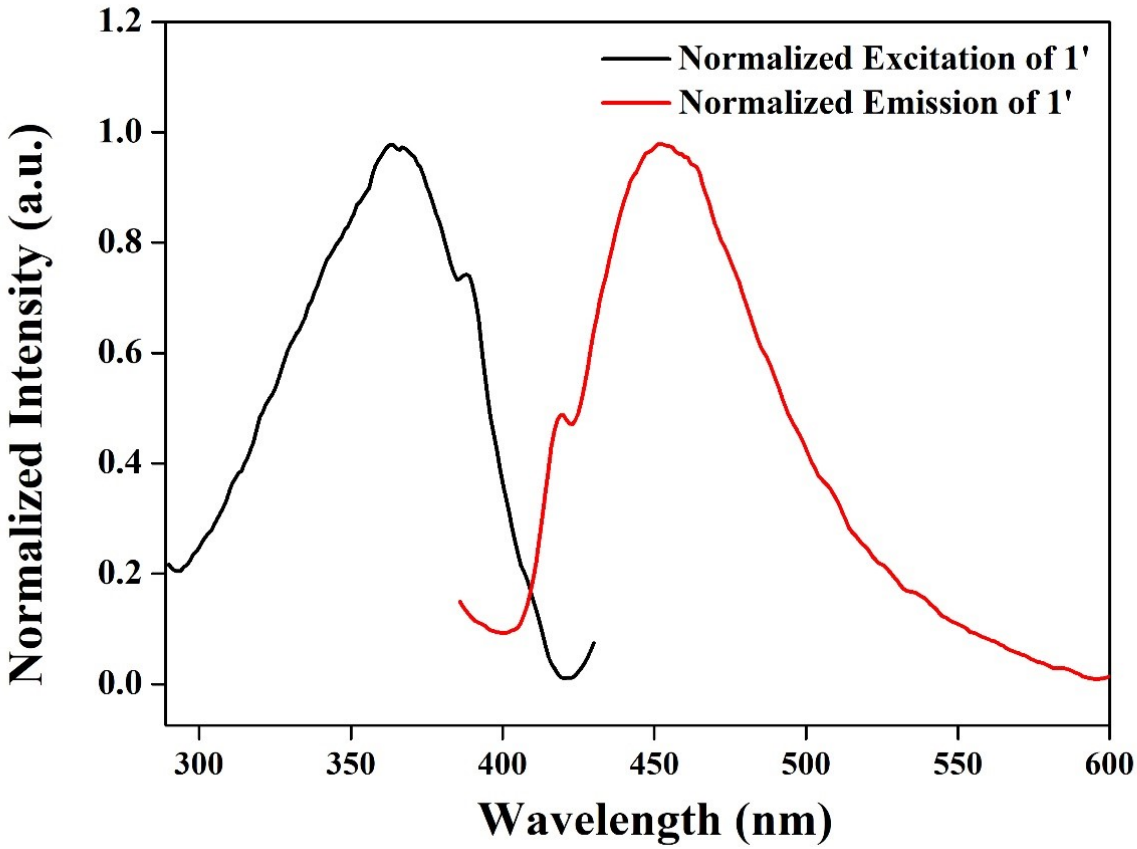

Figure S18. Excitation (black) and emission (red) spectra of **1′** in aqueous medium.

Figure S19. Excitation (black) and emission (red) spectra of **1′** in methanol medium.

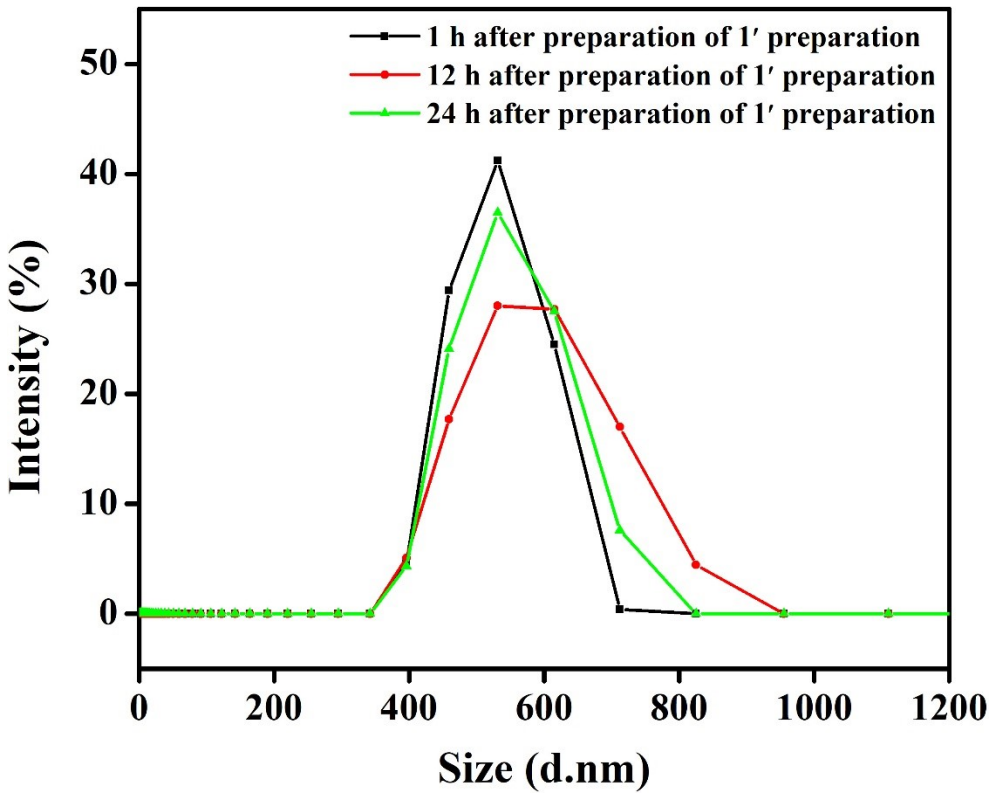

Figure S20. Particle size distribution of the aqueous dispersion of **1′** measured by DLS method in different time intervals.

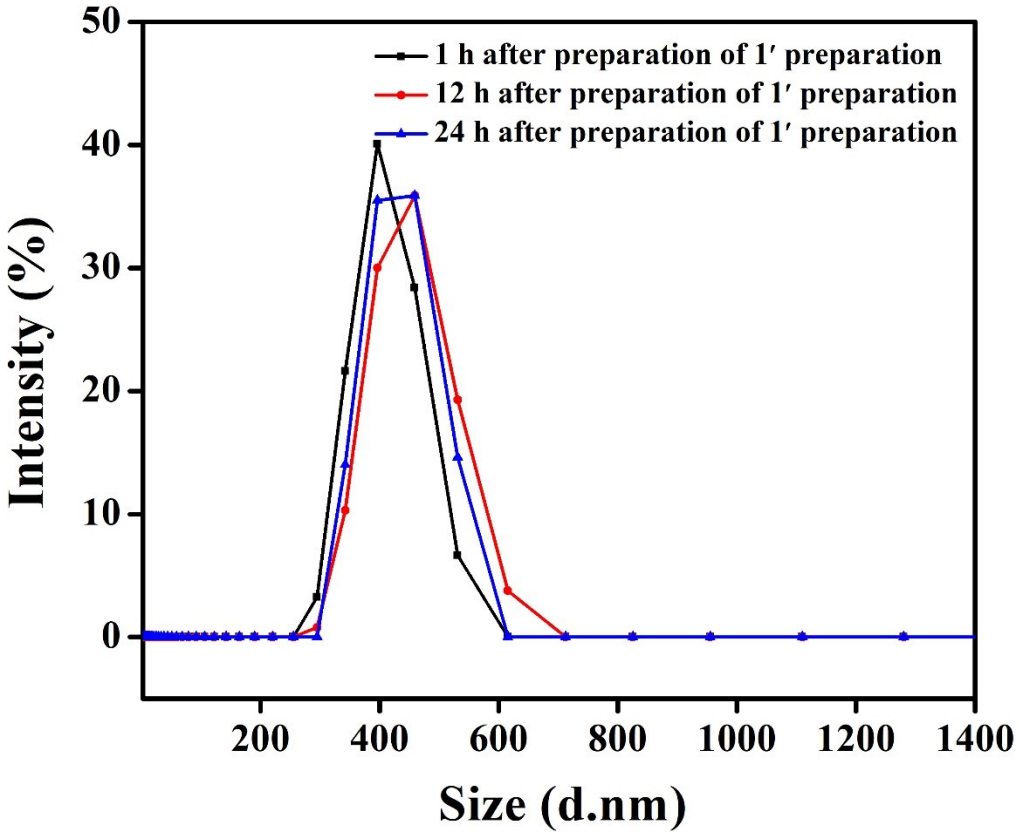

Figure S21. Particle size distribution of the dispersion of **1′** in MeOH, measured by DLS method in different time intervals.

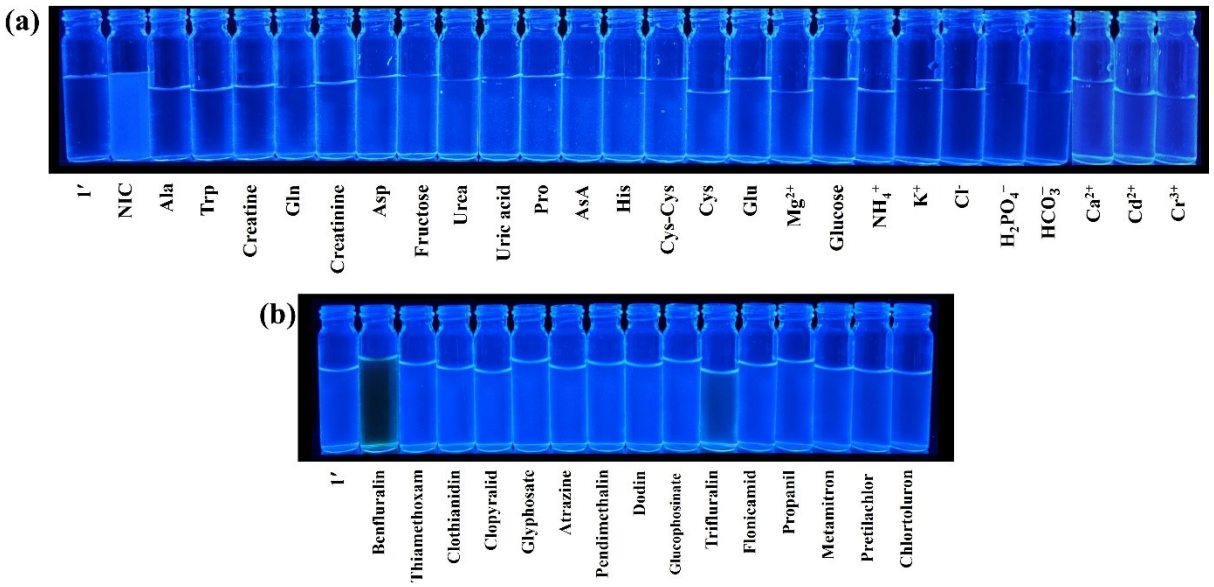

Figure S22. (a) Aqueous phase visible fluorescence response of **1′** in coexistence of 100 µL of 10 mM nicotine (NIC) and other competitive analytes. (b) Visible fluorescence response of **1′** in coexistence of 300 µL of 10 mM benfluralin and other competitive analytes in MeOH medium.

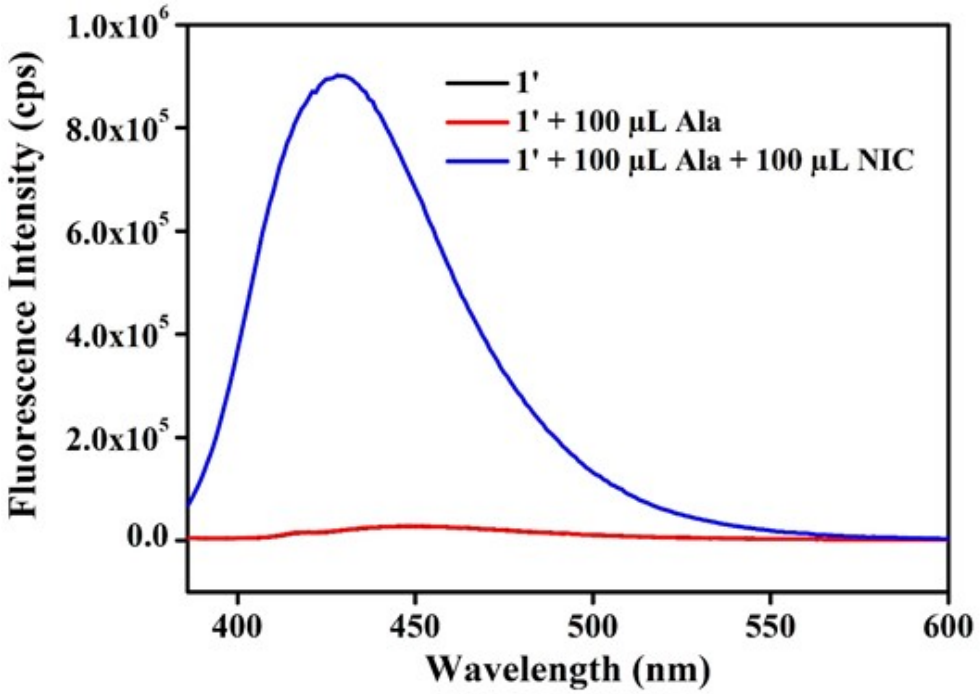

Figure S23. Change in fluorescence emission intensity of activated **1′** in aqueous medium upon addition of 100 µL of 10 mM NIC in presence of 100 µL of 10 mM alanine (Ala) solution (λ_{ex} = 366 nm and λ_{em} = 431 nm).

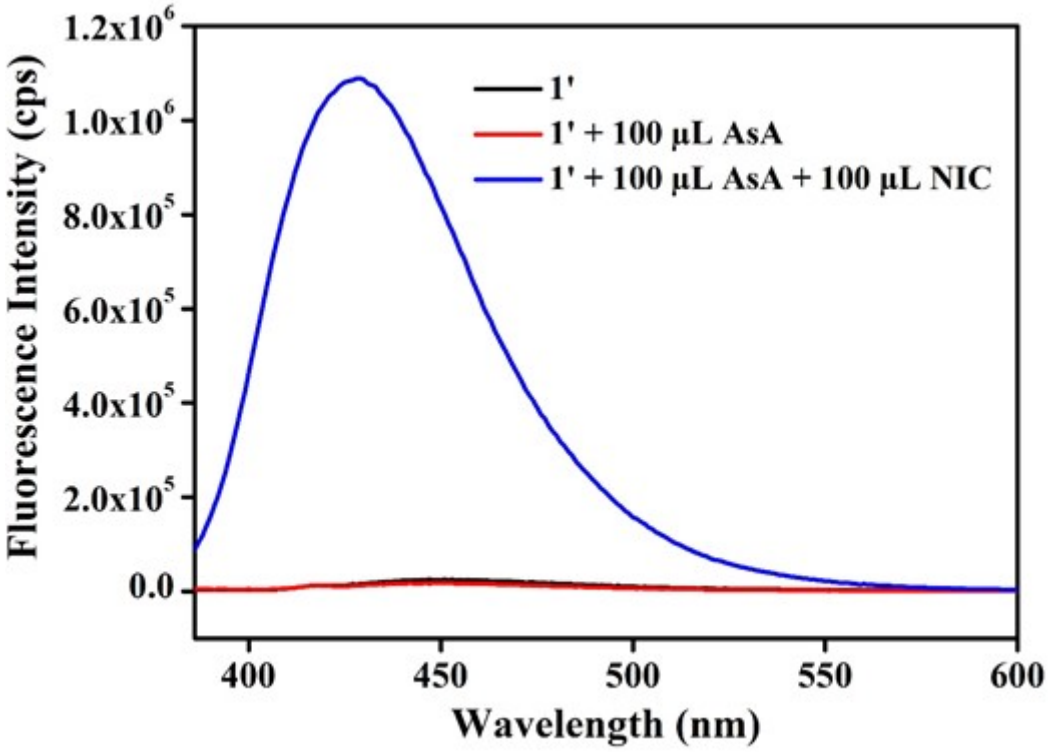

Figure S24. Change in fluorescence emission intensity of activated **1′** in aqueous medium upon addition of 100 µL of 10 mM NIC in presence of 100 µL of 10 mM ascobic acid (AsA) (λ_{ex} = 366 nm and λ_{em} = 431 nm).

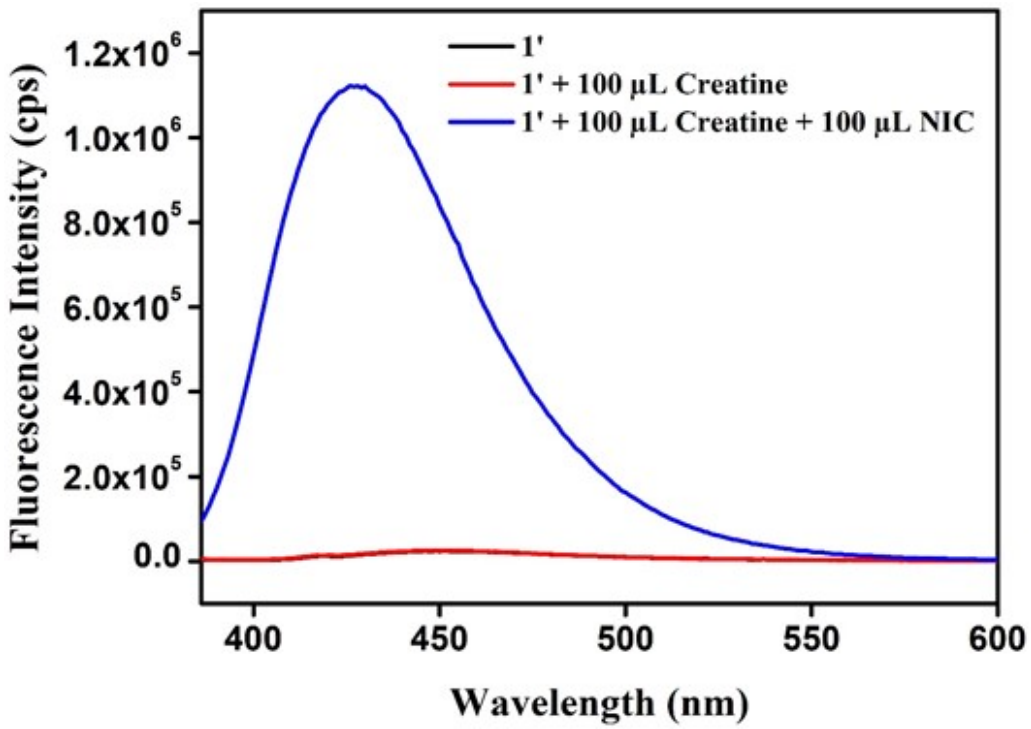

Figure S25. Change in fluorescence emission intensity of activated **1′** in aqueous medium upon addition of 100 µL of 10 mM NIC in presence of 100 µL of 10 mM creatine (λ_{ex} = 366 nm and λ_{em} = 431 nm).

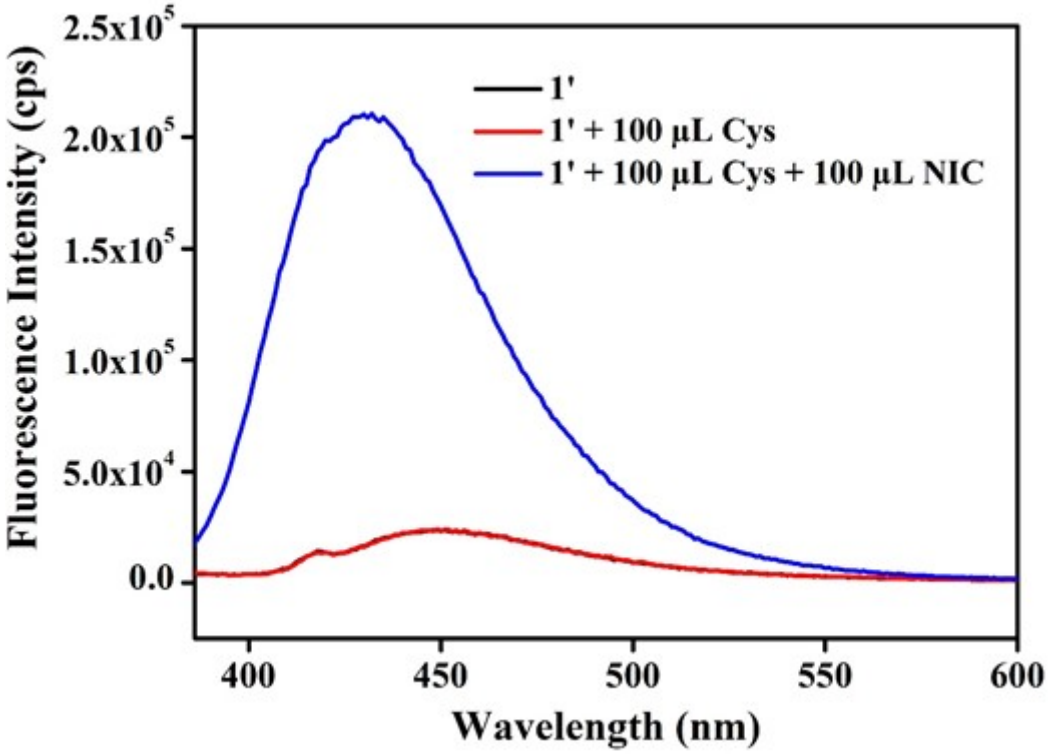

Figure S26. Change in fluorescence emission intensity of activated **1′** in aqueous medium upon addition of 100 µL of 10 mM NIC in presence of 100 µL of 10 mM cysteine (Cys) (λ_{ex} = 366 nm and λ_{em} = 431 nm).

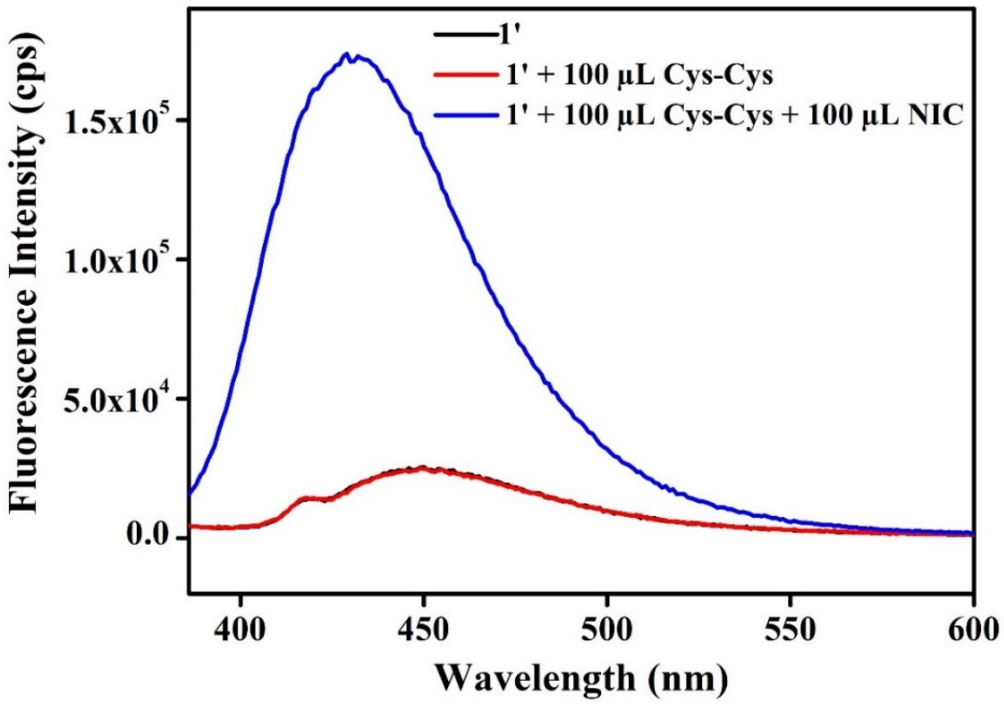

Figure S27. Change in fluorescence emission intensity of activated **1′** in aqueous medium upon addition of 100 µL of 10 mM NIC in presence of 100 µL of 10 mM cystine (Cys-Cys) (λ_{ex} = 366 nm and λ_{em} = 431 nm).

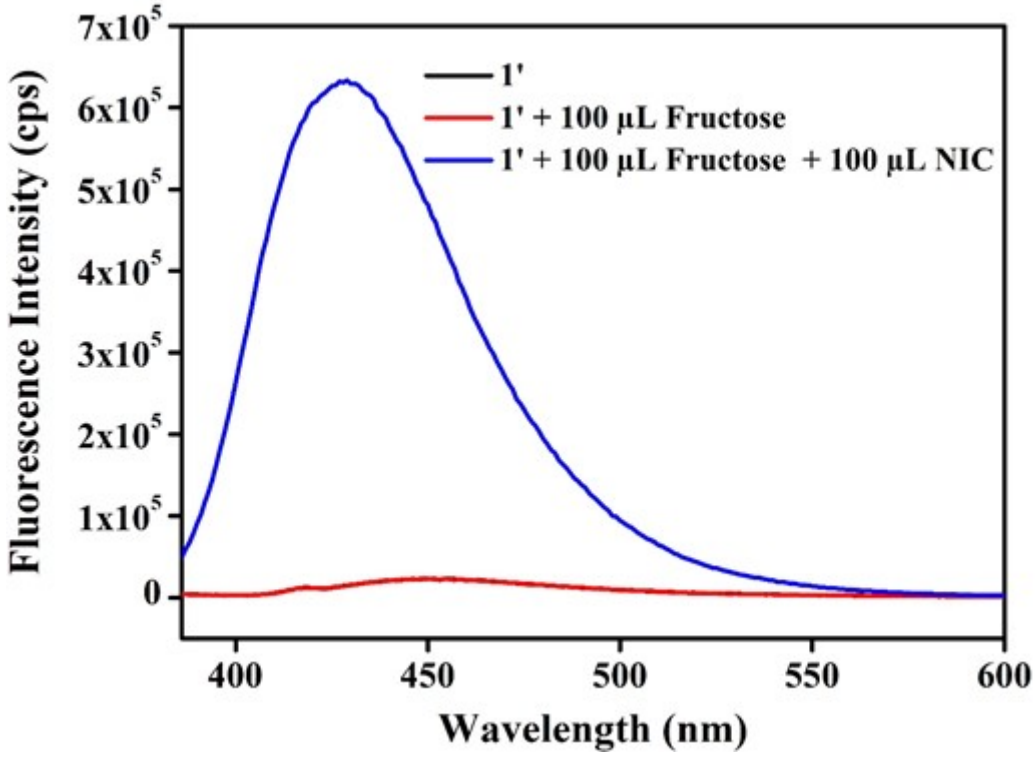

Figure S28. Change in fluorescence emission intensity of activated **1′** in aqueous medium upon addition of 100 µL of 10 mM NIC in presence of 100 µL of 10 mM fructose (λ_{ex} = 340 nm and λ_{em} = 425 nm).

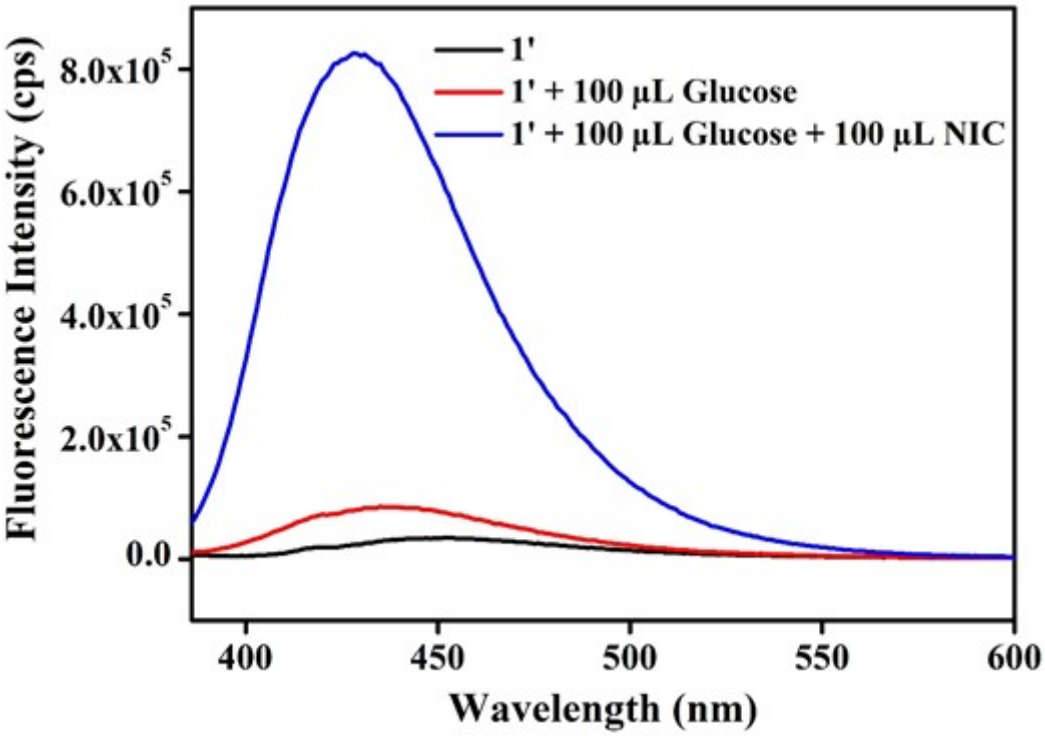

Figure S29. Change in fluorescence emission intensity of activated **1′** in aqueous medium upon addition of 100 µL of 10 mM NIC in presence of 100 µL of 10 mM glucose (λ_{ex} = 366 nm and λ_{em} = 431 nm).

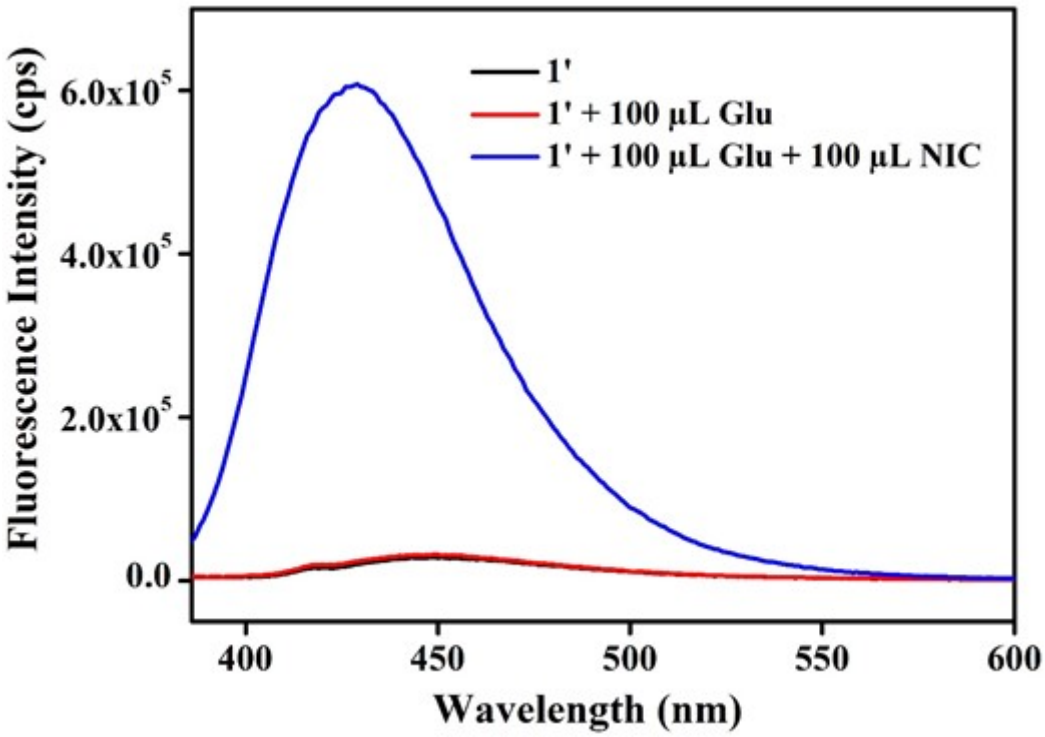

Figure S30. Change in fluorescence emission intensity of activated **1′** in aqueous medium upon addition of 100 µL of 10 mM NIC in presence of 100 µL of 10 mM glutamic acid (Glu) (λ_{ex} = 366 nm and λ_{em} = 431 nm).

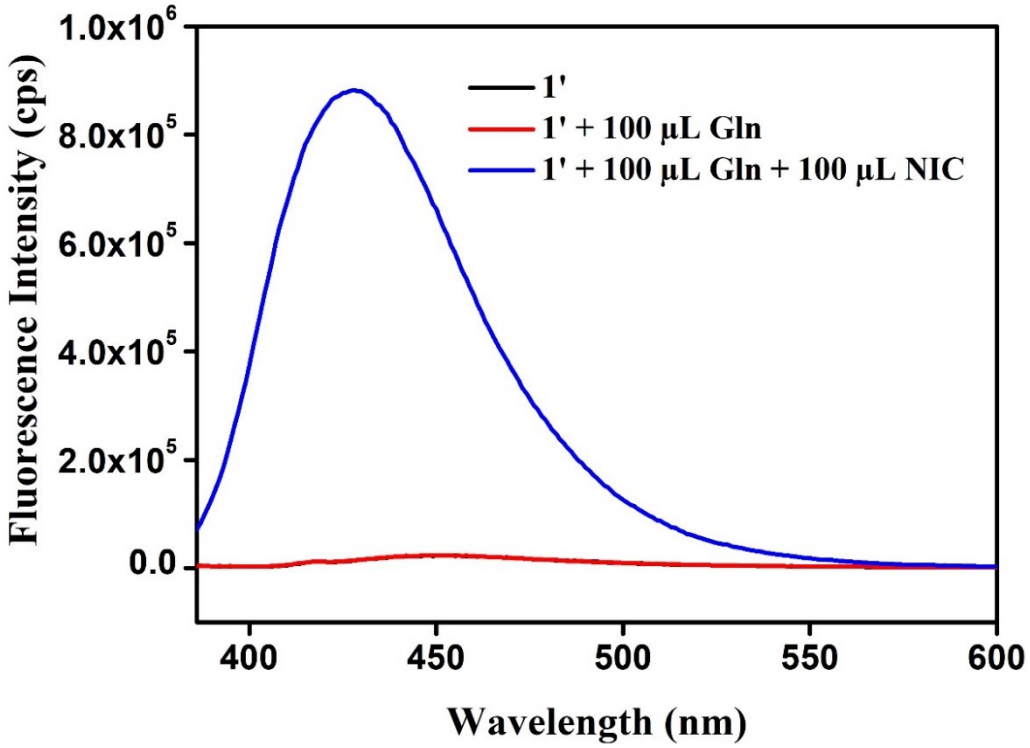

Figure S31. Change in fluorescence emission intensity of activated **1′** in aqueous medium upon addition of 100 µL of 10 mM NIC in presence of 100 µL of 10 mM glutamine (Gln) (λ_{ex} = 366 nm and λ_{em} = 431 nm).

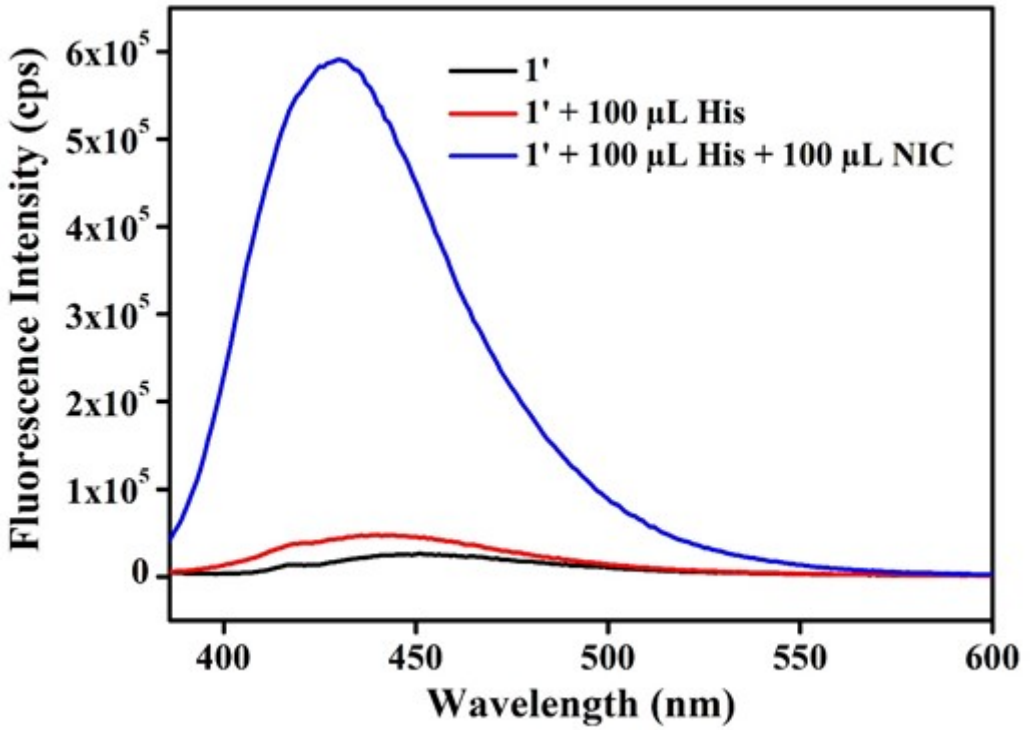

Figure S32. Change in fluorescence emission intensity of activated **1′** in aqueous medium upon addition of 100 µL of 10 mM NIC in presence of 100 µL of 10 mM histidine (His) (λ_{ex} = 366 nm and λ_{em} = 431 nm).

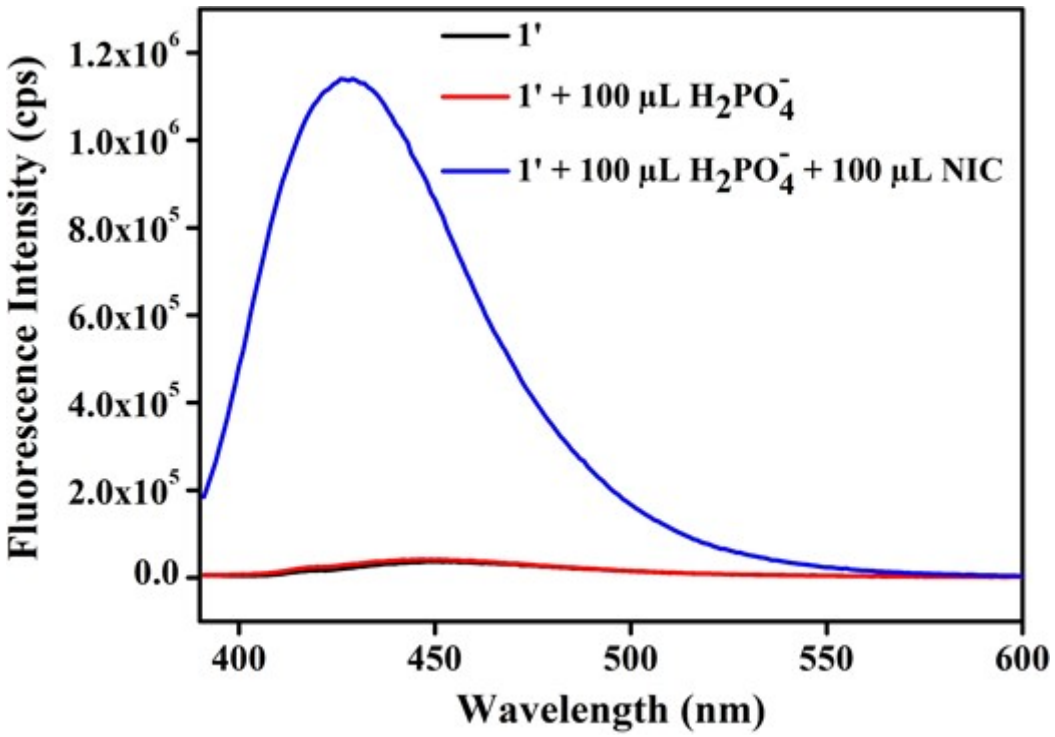

Figure S33. Change in fluorescence emission intensity of activated **1′** in aqueous medium upon addition of 100 µL of 10 mM NIC in presence of 100 µL of 10 mM $H_2PO_4^-$ (λ_{ex} = 366 nm and λ_{em} = 431 nm).

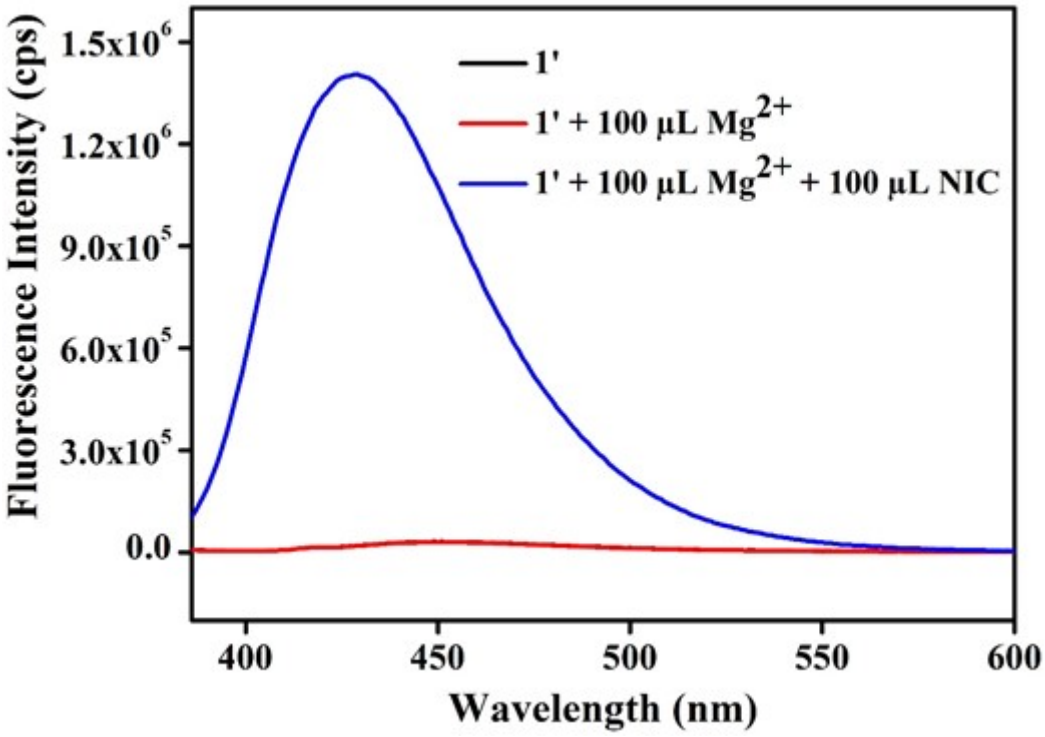

Figure S34. Change in fluorescence emission intensity of activated **1′** in aqueous medium upon addition of 100 µL of 10 mM NIC in presence of 100 µL of 10 mM Mg^{2+} (λ_{ex} = 366 nm and λ_{em} = 431 nm).

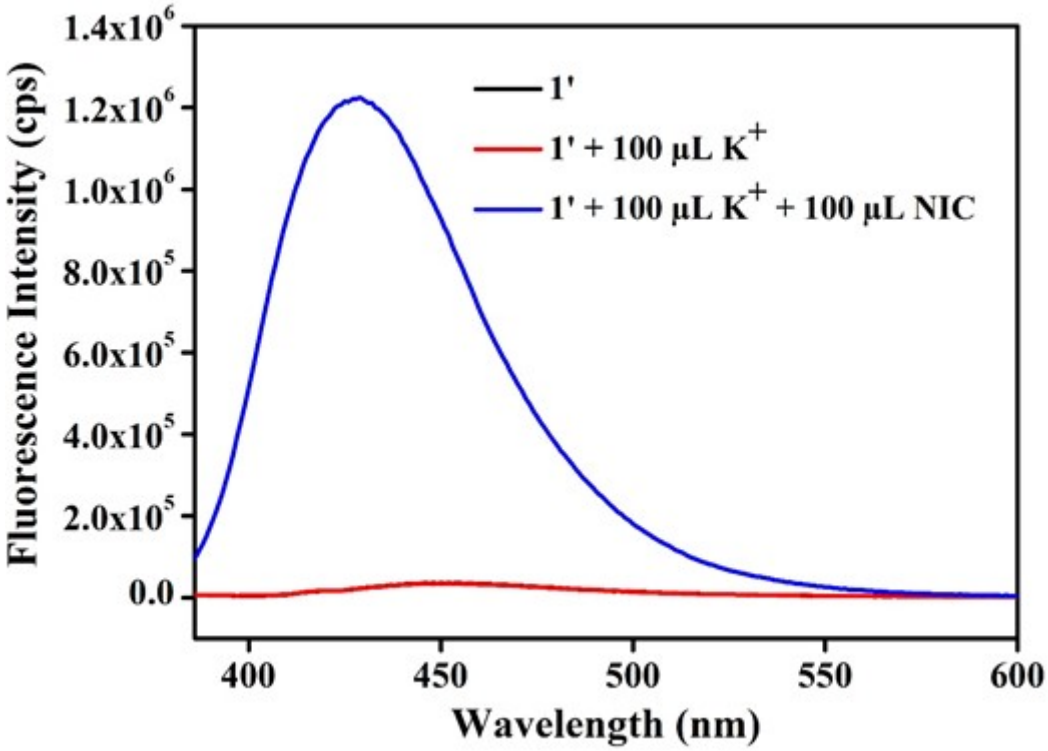

Figure S35. Change in fluorescence emission intensity of activated **1′** in aqueous medium upon addition of 100 µL of 10 mM NIC in presence of 100 µL of 10 mM K^+ (λ_{ex} = 366 nm and λ_{em} = 431 nm).

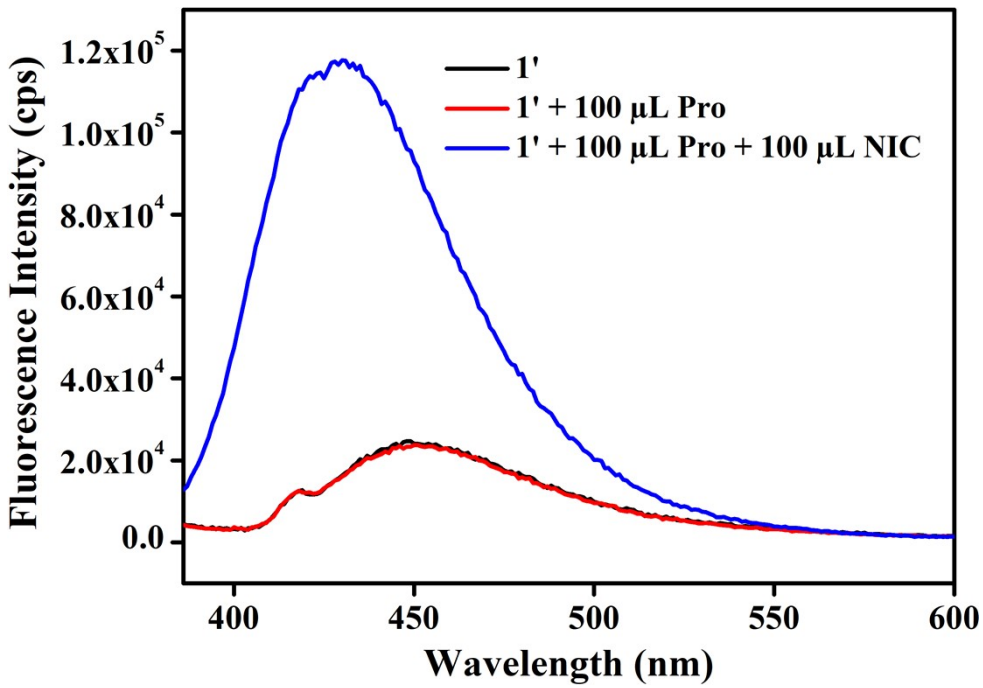

Figure S36. Change in fluorescence emission intensity of activated **1′** in aqueous medium upon addition of 100 µL of 10 mM NIC in presence of 100 µL of 10 mM proline (Pro) (λ_{ex} = 366 nm and λ_{em} = 431 nm).

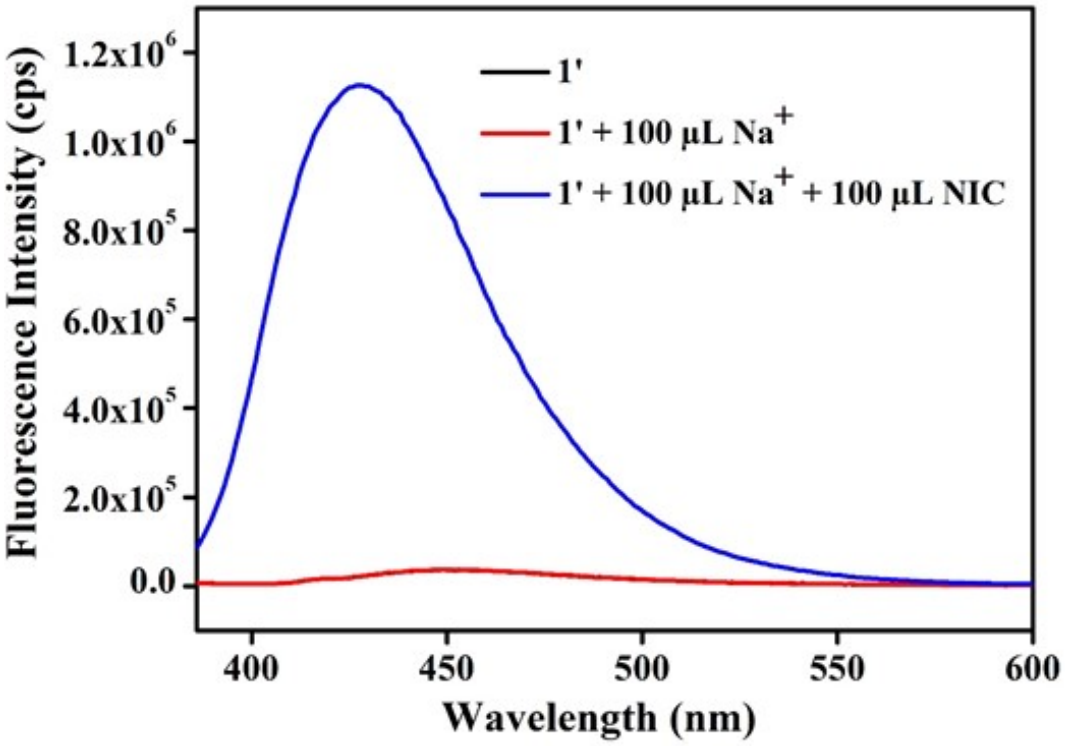

Figure S37. Change in fluorescence emission intensity of activated **1′** in aqueous medium upon addition of 100 µL of 10 mM NIC in presence of 100 µL of 10 mM Na^+ (λ_{ex} = 366 nm and λ_{em} = 431 nm).

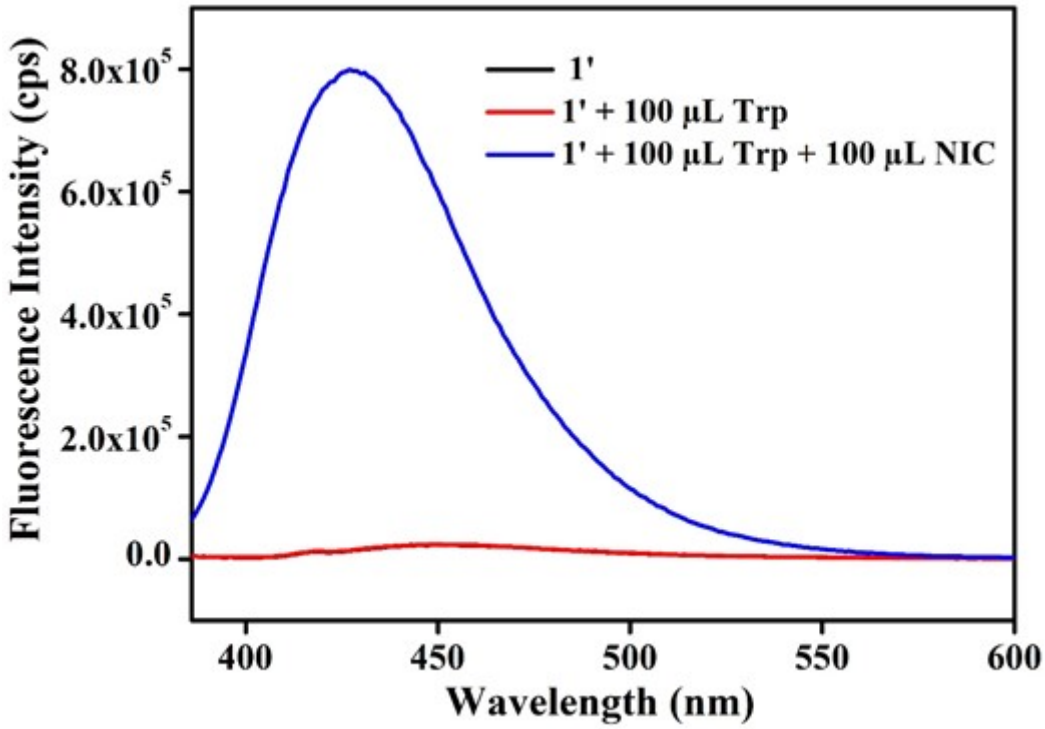

Figure S38. Change in fluorescence emission intensity of activated **1′** in aqueous medium upon addition of 100 µL of 10 mM NIC in presence of 100 µL of 10 mM tryptophan (Trp) (λ_{ex} = 366 nm and λ_{em} = 431 nm).

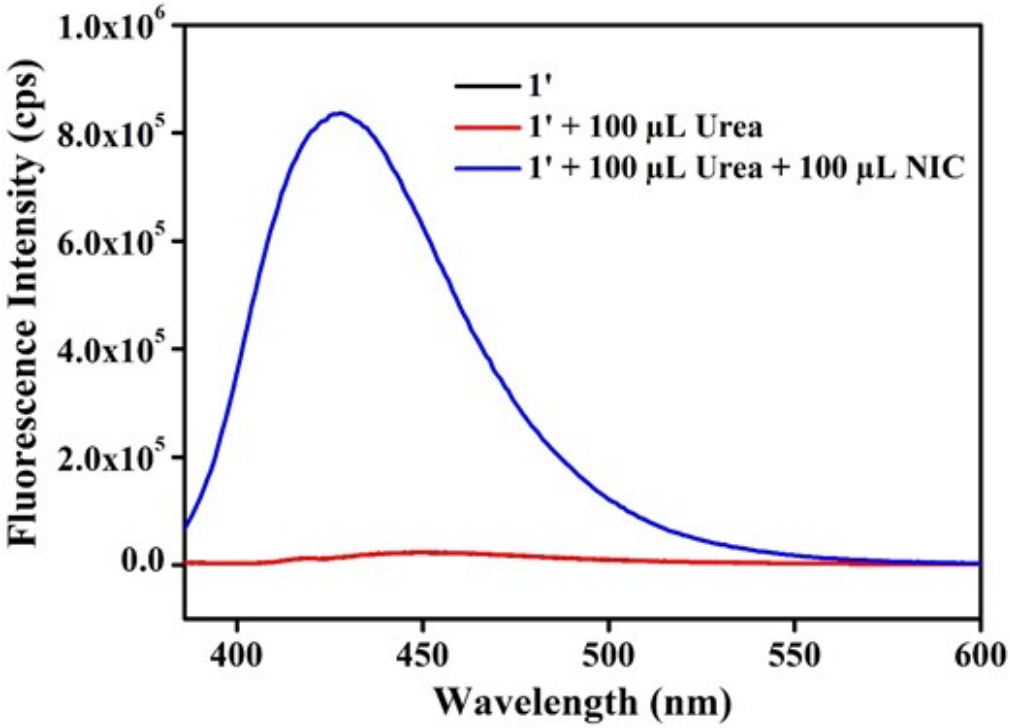

Figure S39. Change in fluorescence emission intensity of activated **1′** in aqueous medium upon addition of 100 µL of 10 mM NIC in presence of 100 µL of 10 mM urea (λ_{ex} = 366 nm and λ_{em} = 431 nm).

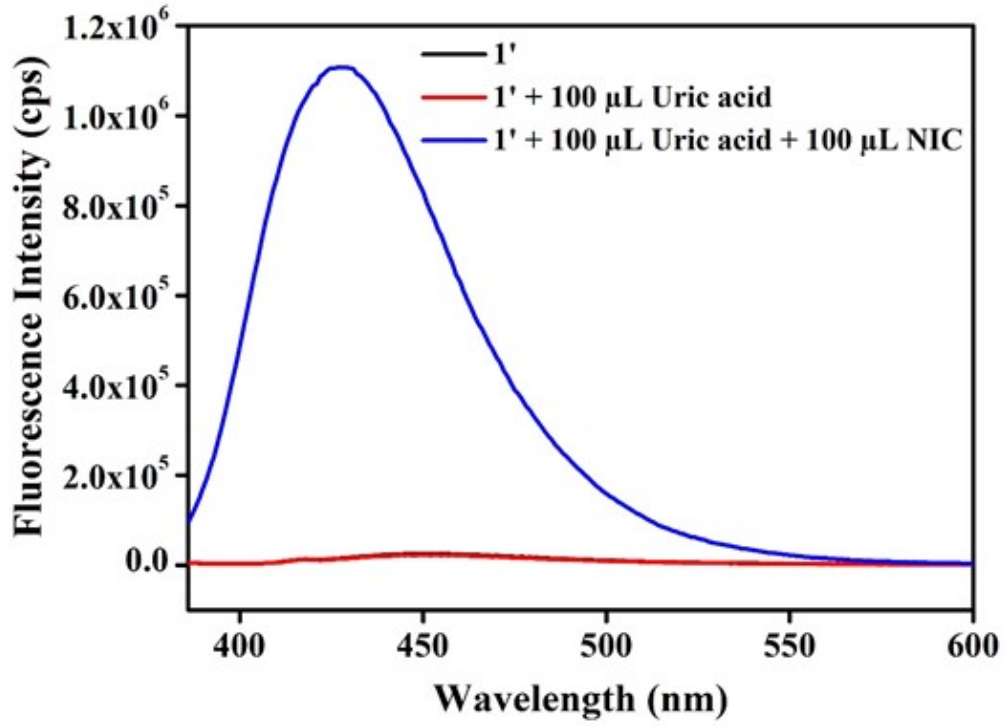

Figure S40. Change in fluorescence emission intensity of activated **1′** in aqueous medium upon addition of 100 µL of 10 mM NIC in presence of 100 µL of 10 mM uric acid (λ_{ex} = 366 nm and λ_{em} = 431 nm).

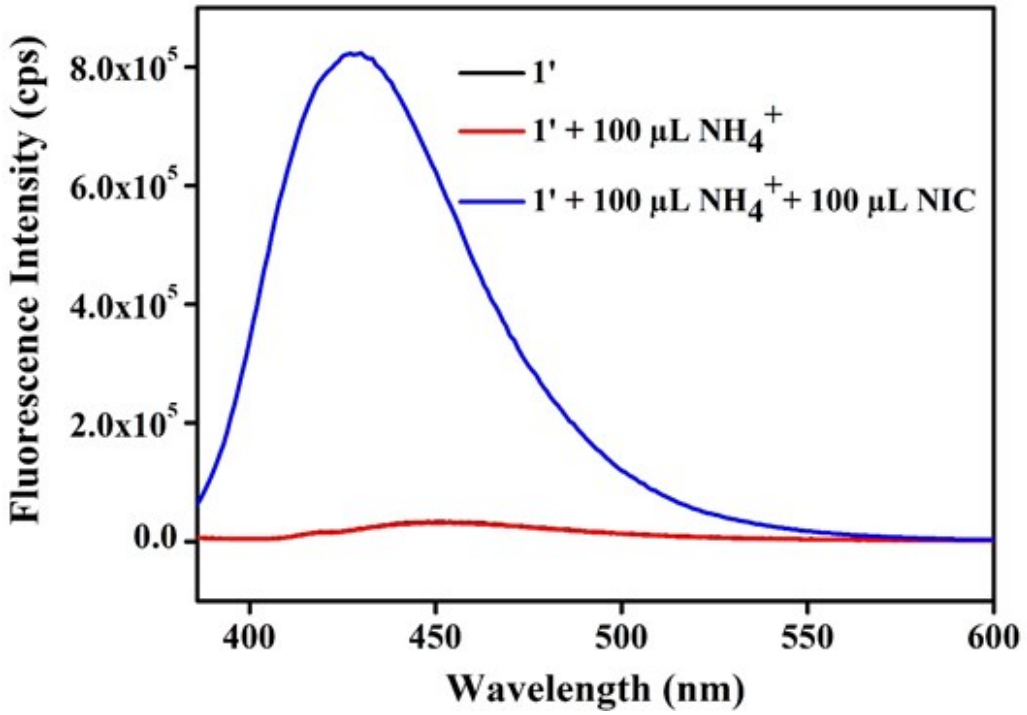

Figure S41. Change in fluorescence emission intensity of activated **1′** in aqueous medium upon addition of 100 µL of 10 mM NIC in presence of 100 µL of 10 mM NH_4^+ (λ_{ex} = 366 nm and λ_{em} = 431 nm).

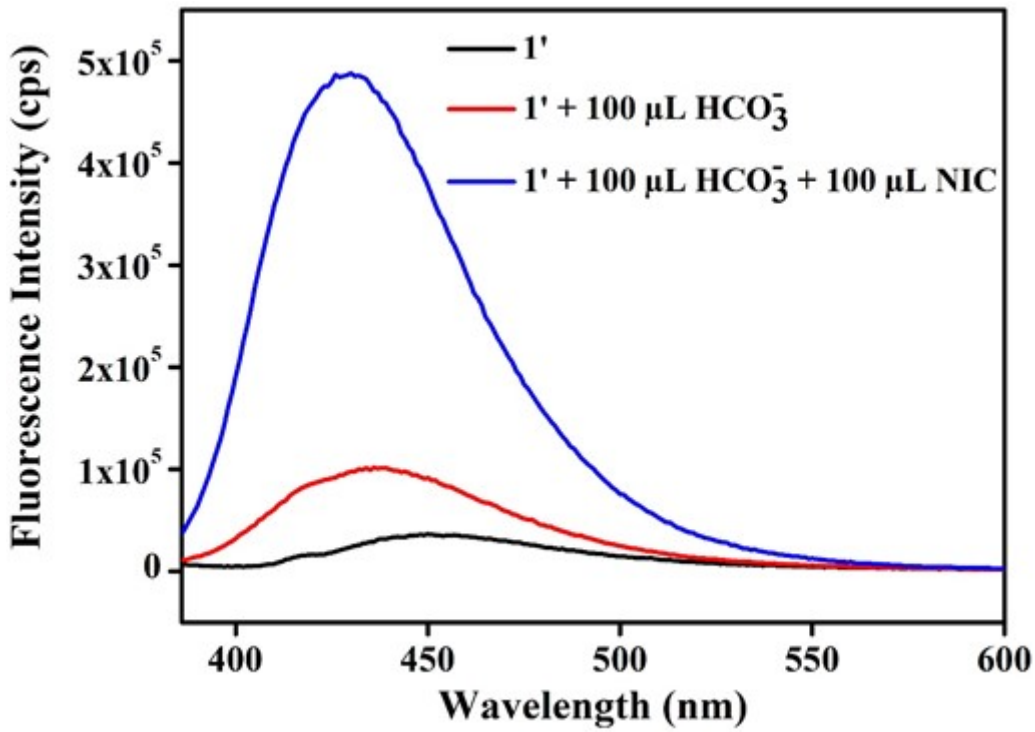

Figure S42. Change in fluorescence emission intensity of activated **1′** in aqueous medium upon addition of 100 µL of 10 mM NIC in presence of 100 µL of 10 mM HCO_3^- (λ_{ex} = 366 nm and λ_{em} = 431 nm).

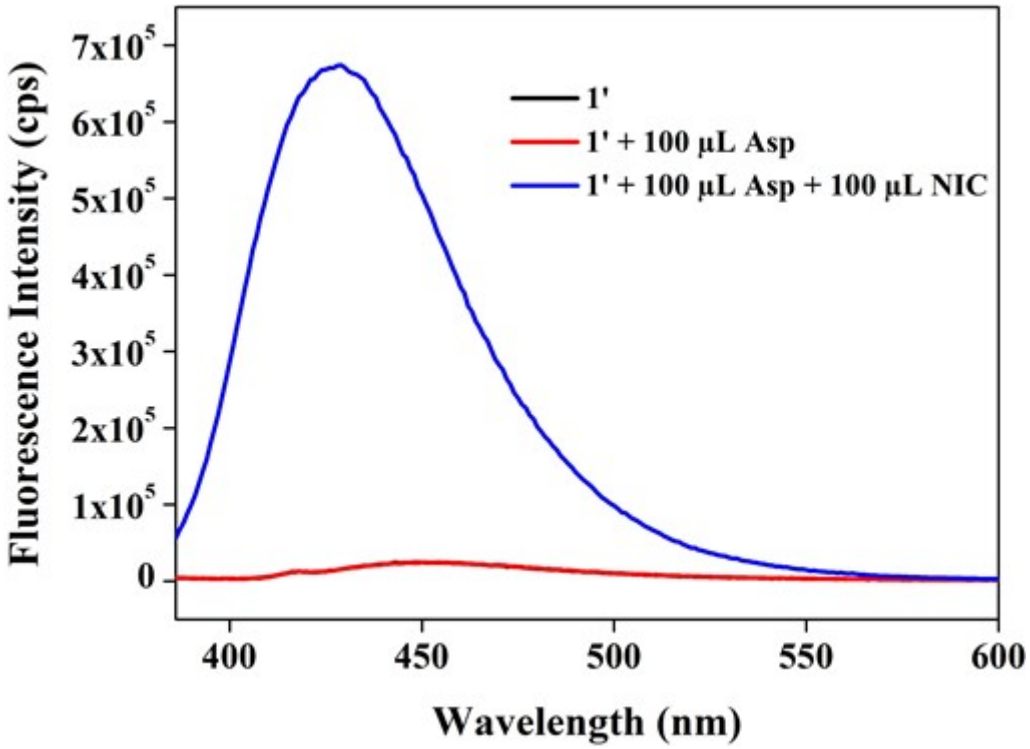

Figure S43. Change in fluorescence emission intensity of activated **1′** in aqueous medium upon addition of 100 µL of 10 mM NIC in presence of 100 µL of 10 mM aspartic acid (asp) (λ_{ex} = 366 nm and λ_{em} = 431 nm).

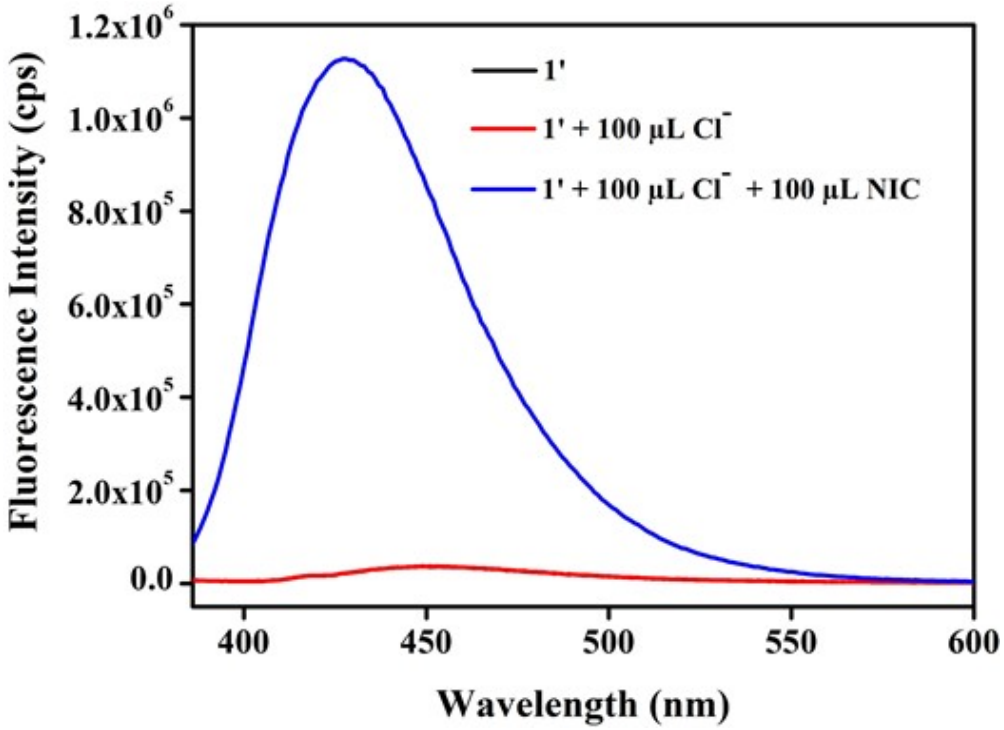

Figure S44. Change in fluorescence emission intensity of activated **1′** in aqueous medium upon addition of 100 µL of 10 mM NIC in presence of 100 µL of 10 mM Cl^- (λ_{ex} = 366 nm and λ_{em} = 431 nm).

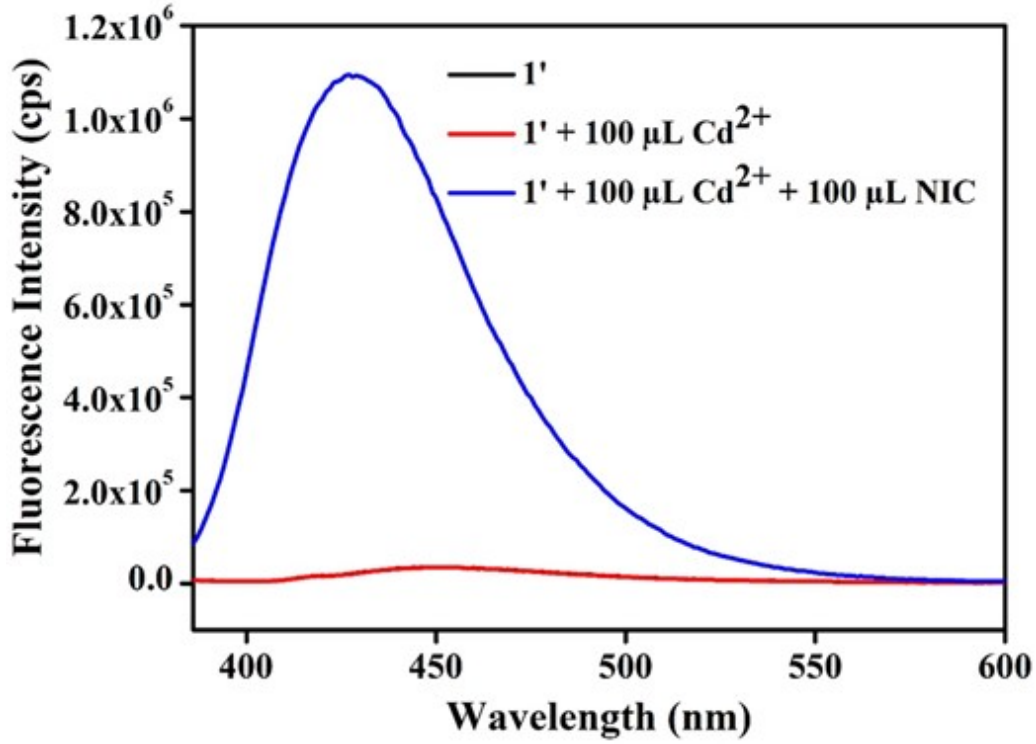

Figure S45. Change in fluorescence emission intensity of activated **1′** in aqueous medium upon addition of 100 µL of 10 mM NIC in presence of 100 µL of 10 mM Cd^{2+} (λ_{ex} = 366 nm and λ_{em} = 431 nm).

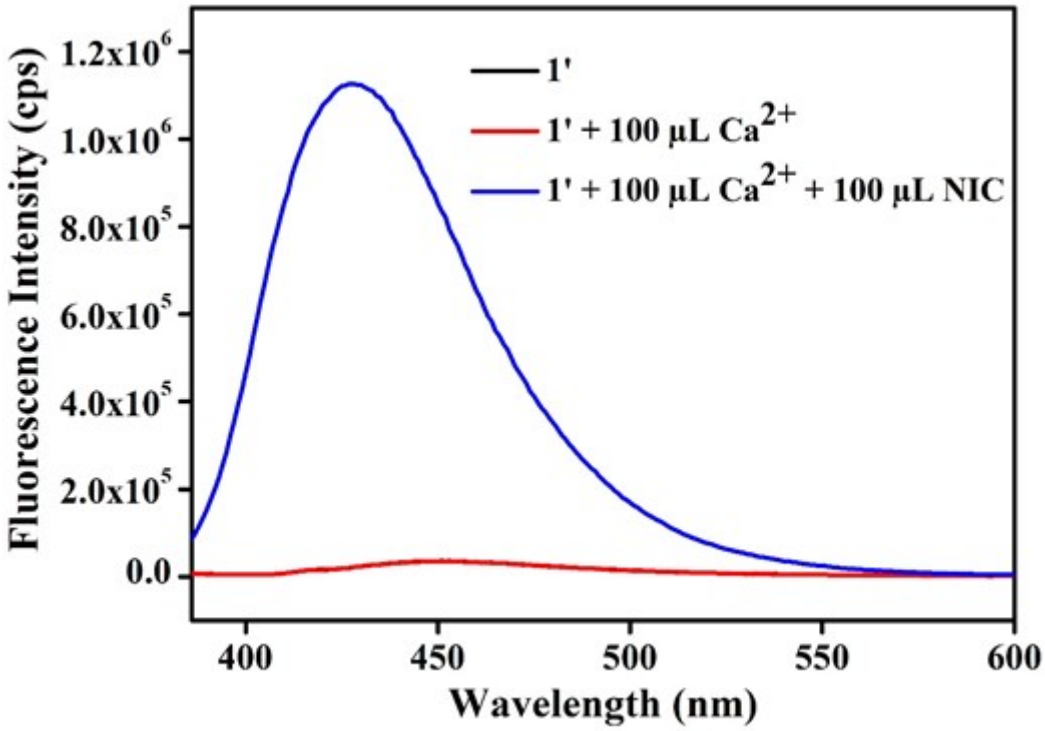

Figure S46. Change in fluorescence emission intensity of activated **1′** in aqueous medium upon addition of 100 µL of 10 mM NIC in presence of 100 µL of 10 mM Ca^{2+} (λ_{ex} = 366 nm and λ_{em} = 431 nm).

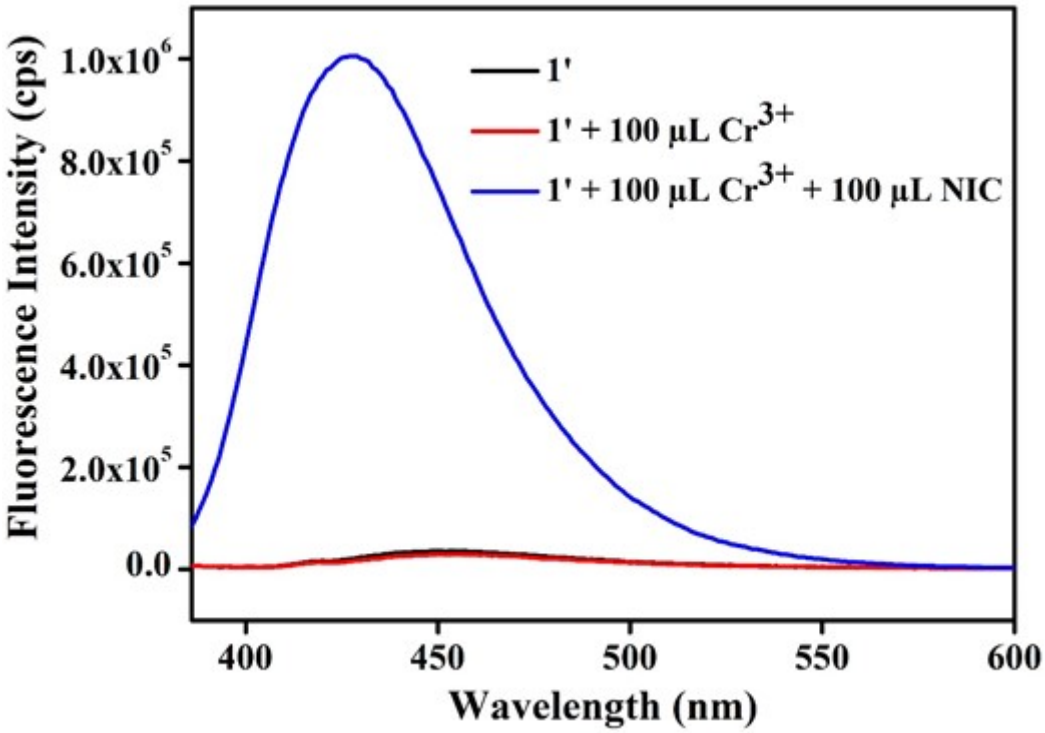

Figure S47. Change in fluorescence emission intensity of activated **1′** in aqueous medium upon addition of 100 µL of 10 mM NIC in presence of 100 µL of 10 mM Cr^{3+} (λ_{ex} = 366 nm and λ_{em} = 431 nm).

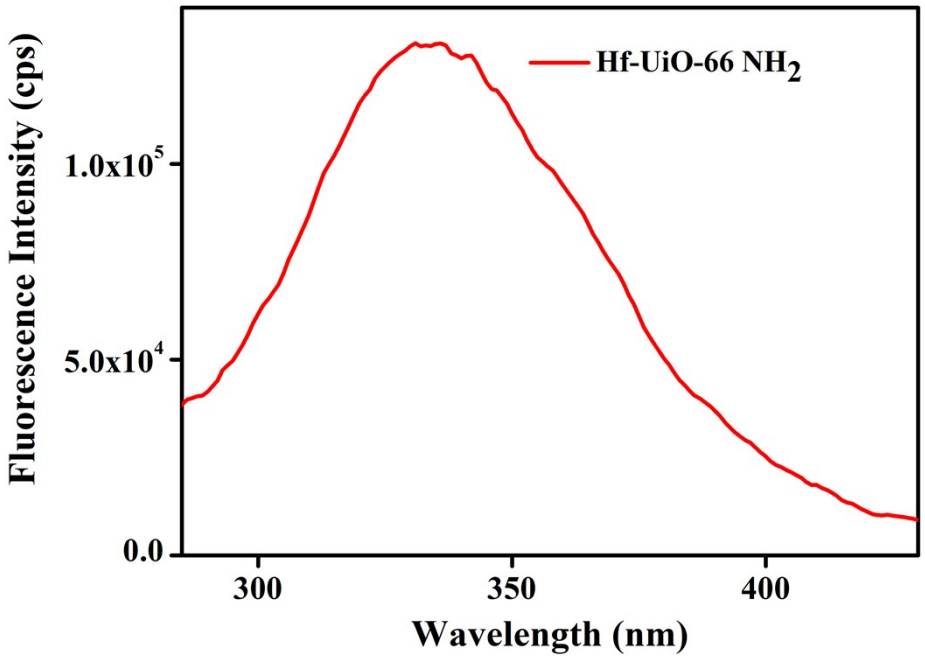

Figure S48. Excitation spectra of Hf-UiO-66-NH_2 MOF in water.

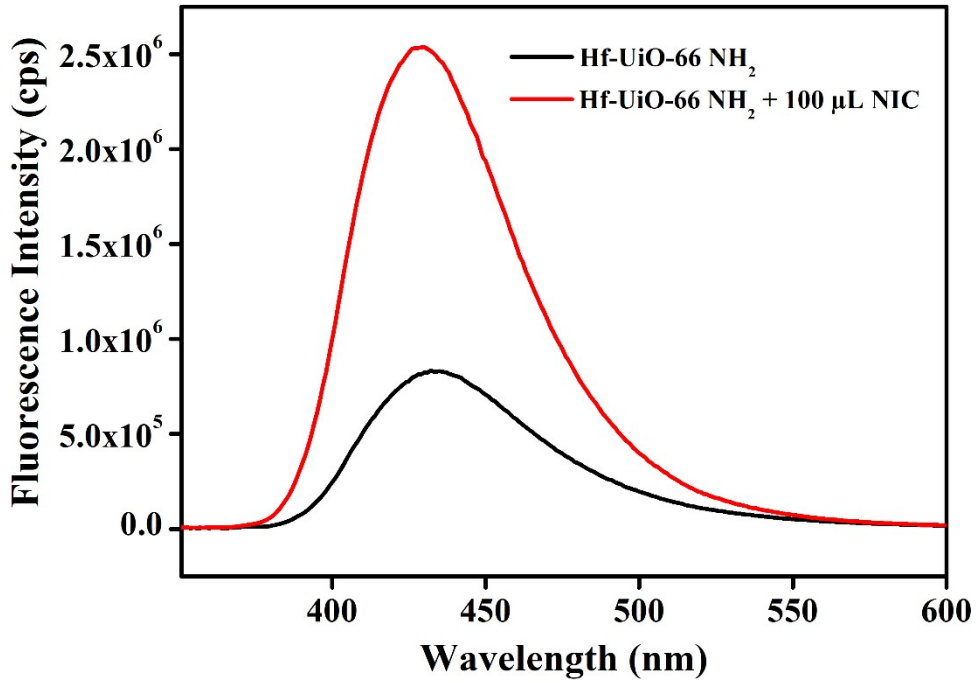

Figure S49. Change in fluorescence emission intensity of activated Hf-UiO-66-NH_2 in aqueous medium upon addition of 100 µL of 10 mM (λ_{ex} = 331 nm and λ_{em} = 432 nm).

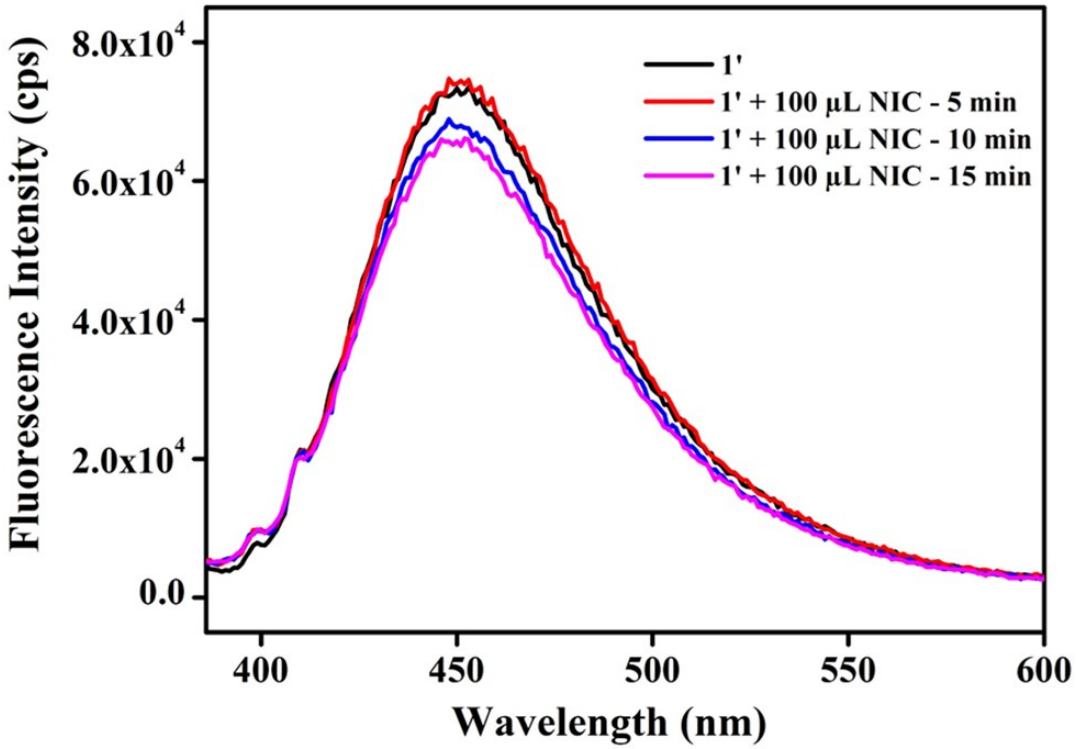

Figure S50. Change in fluorescence emission intensity of activated **1′** in acetonitrile medium upon addition of 100 µL of 10 mM NIC (λ_{ex} = 366 nm and λ_{em} = 431 nm).

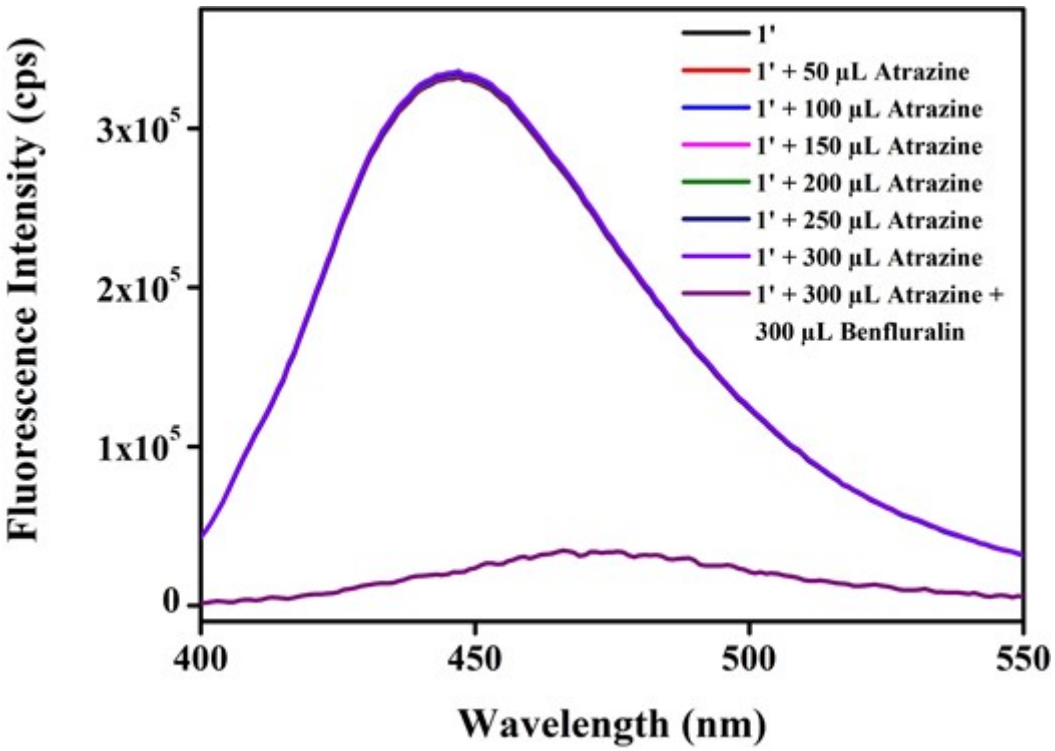

Figure S51. Change in fluorescence emission intensity of activated **1′** in methanol medium upon addition of 300 µL of 10 mM benfluralin in presence of 300 µL of 10 mM atrazine (λ_{ex} = 366 nm and λ_{em} = 450 nm).

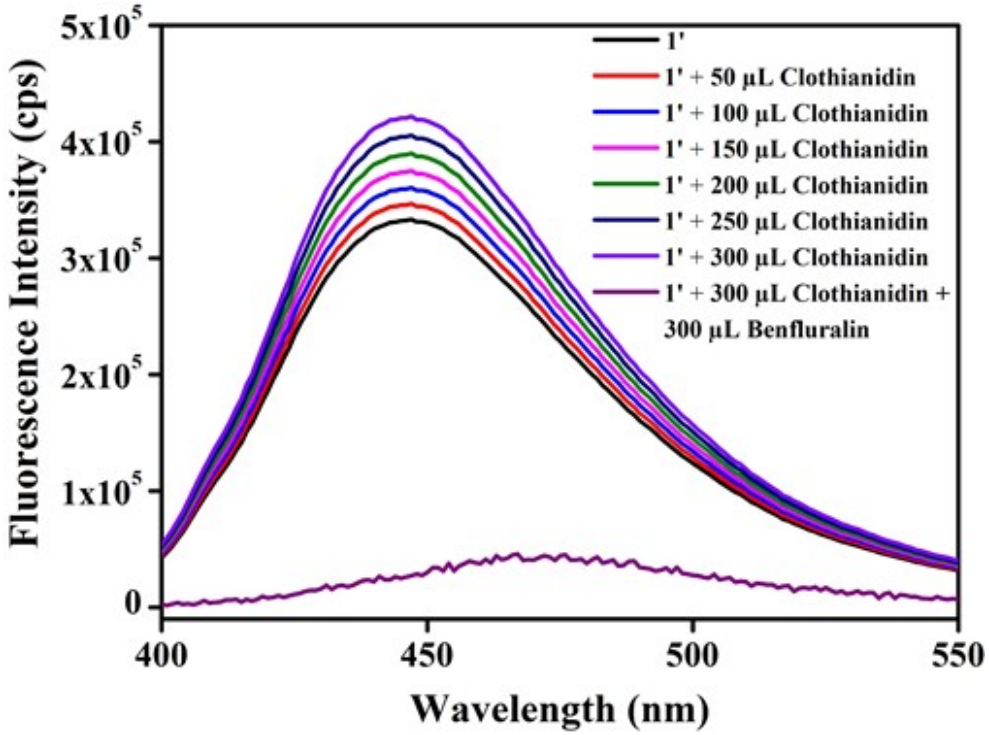

Figure S52. Change in fluorescence emission intensity of activated **1′** in methanol medium upon addition of 300 µL of 10 mM benfluralin in presence of 300 µL of 10 mM clothianidin (λ_{ex} = 366 nm and λ_{em} = 450 nm).

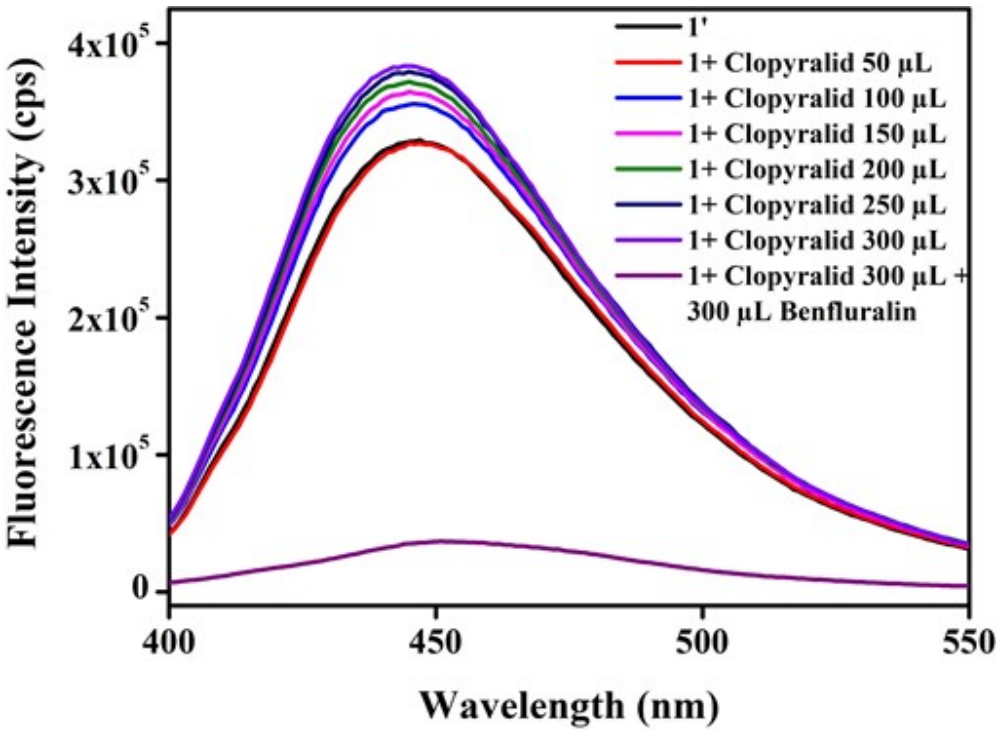

Fig S53. Change in fluorescence emission intensity of activated **1′** in methanol medium upon addition of 300 µL of 10 mM benfluralin in presence of 300 µL of 10 mM clopyralid (λ_{ex} = 366 nm and λ_{em} = 450 nm).

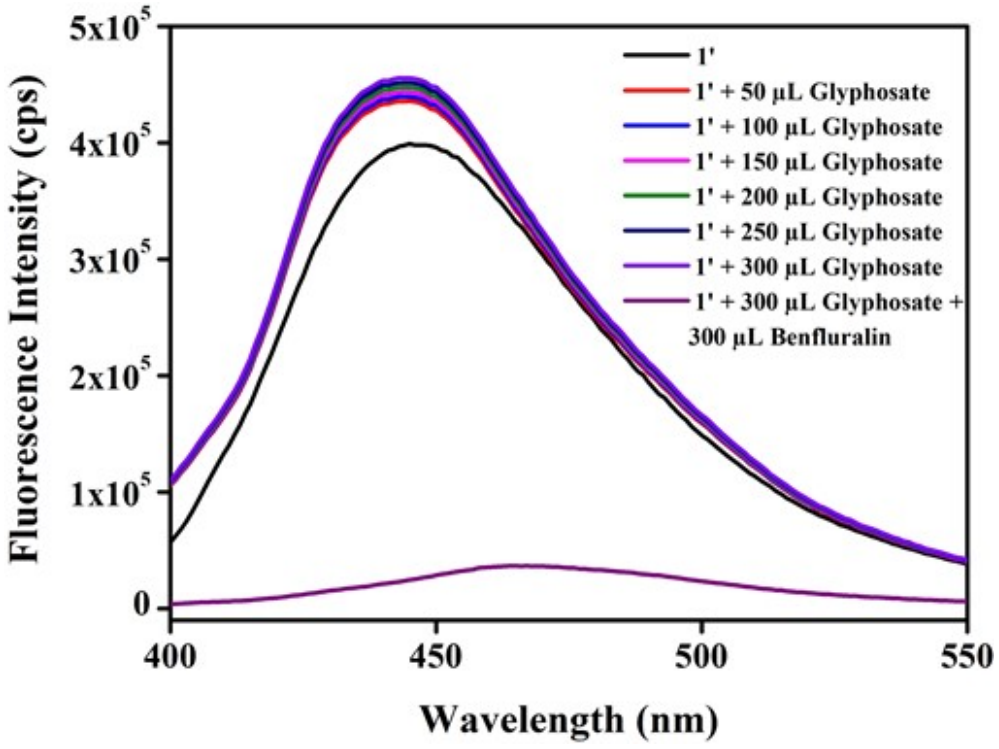

Figure S54. Change in fluorescence emission intensity of activated **1′** in methanol medium upon addition of 300 µL of 10 mM benfluralin in presence of 300 µL of 10 mM glyphosate (λ_{ex} = 366 nm and λ_{em} = 450 nm).

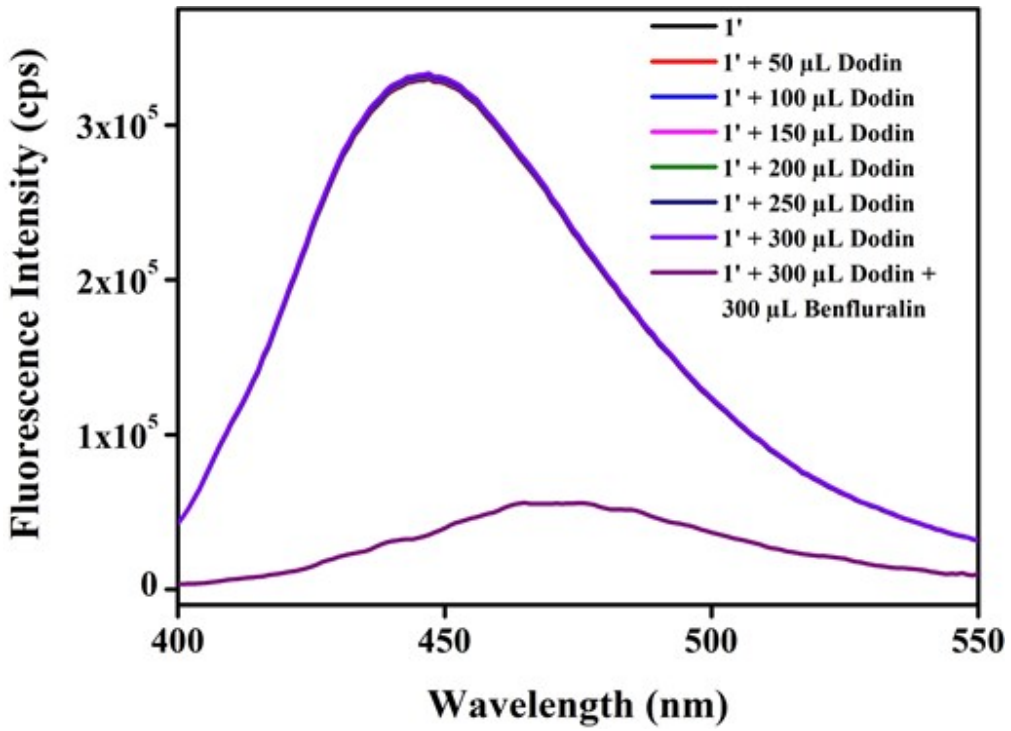

Figure S55. Change in fluorescence emission intensity of activated **1′** in methanol medium upon addition of 300 µL of 10 mM benfluralin in presence of 300 µL of 10 mM dodin (λ_{ex} = 366 nm and λ_{em} = 450 nm).

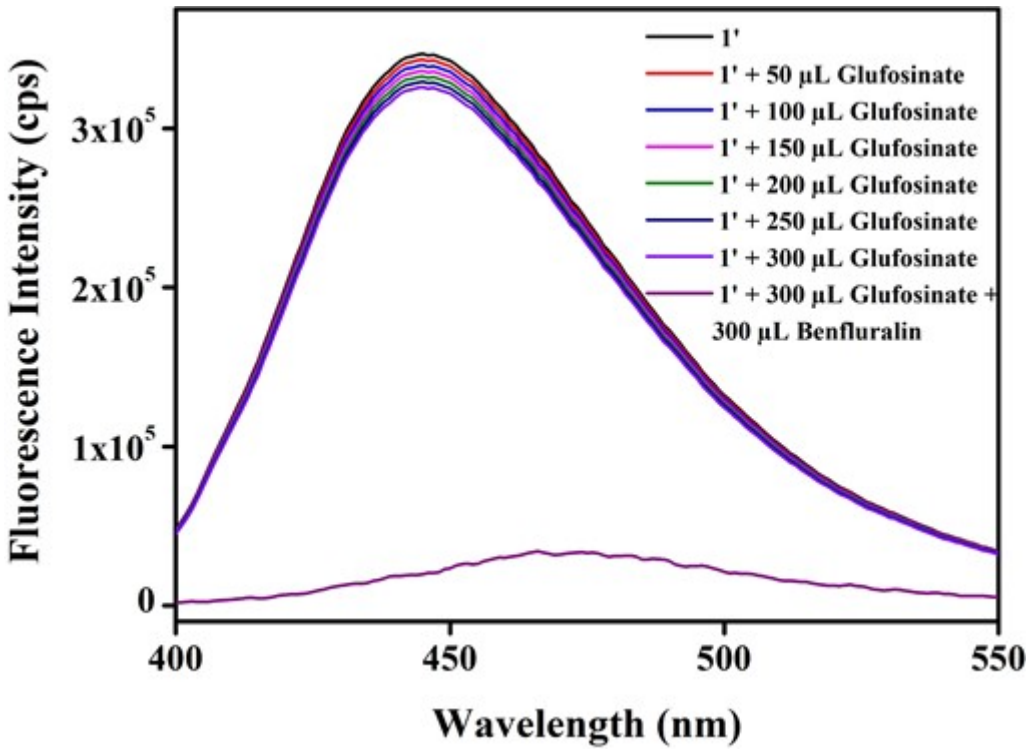

Figure S56. Change in fluorescence emission intensity of activated **1′** in methanol medium upon addition of 300 µL of 10 mM benfluralin in presence of 300 µL of 10 mM glufosinate (λ_{ex} = 366 nm and λ_{em} = 450 nm).

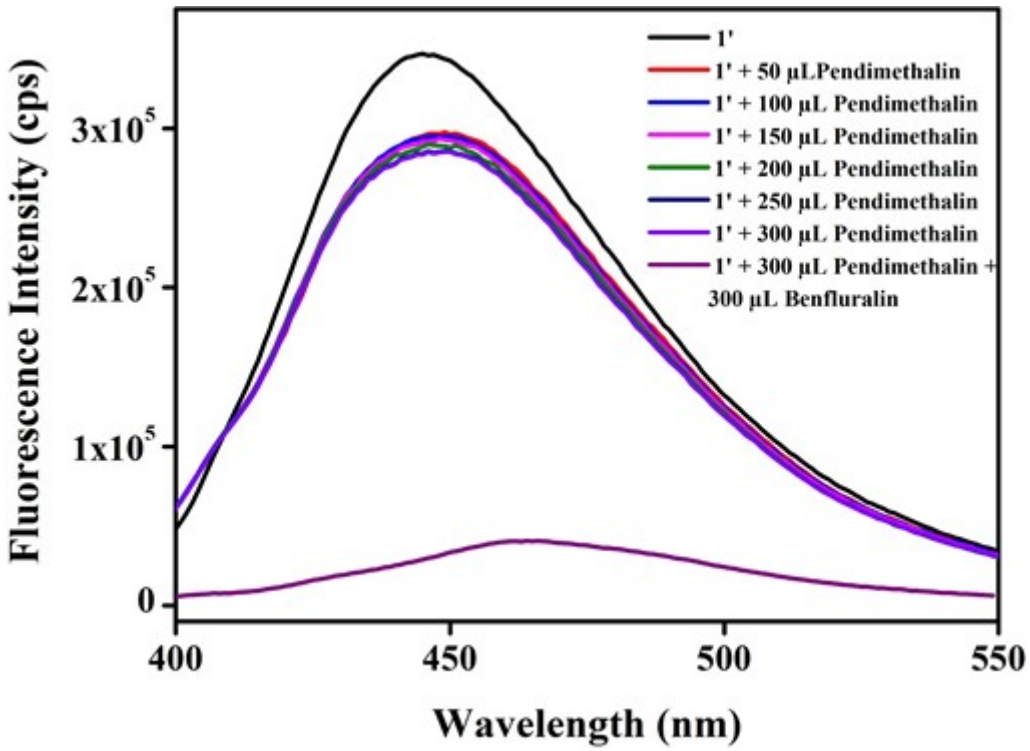

Figure S57. Change in fluorescence emission intensity of activated **1′** in methanol medium upon addition of 300 µL of 10 mM benfluralin in presence of 300 µL of 10 mM pendimethalin (λ_{ex} = 366 nm and λ_{em} = 450 nm).

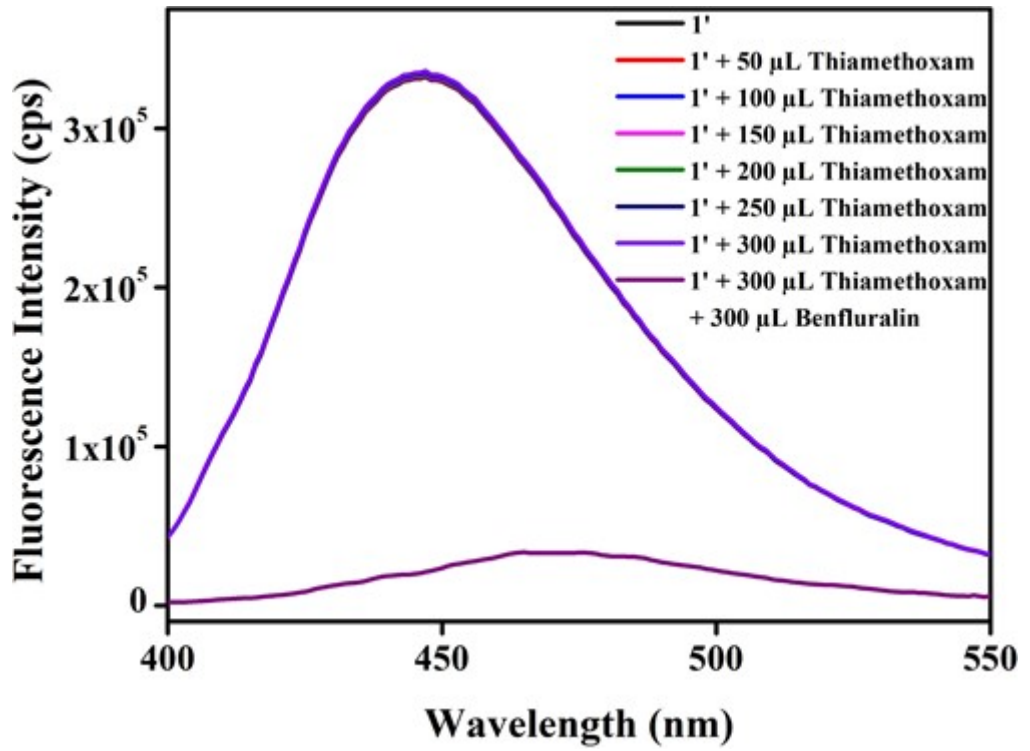

Figure S58. Change in fluorescence emission intensity of activated **1′** in methanol medium upon addition of 300 µL of 10 mM benfluralin in presence of 300 µL of 10 mM thiamethoxam (λ_{ex} = 366 nm and λ_{em} = 450 nm).

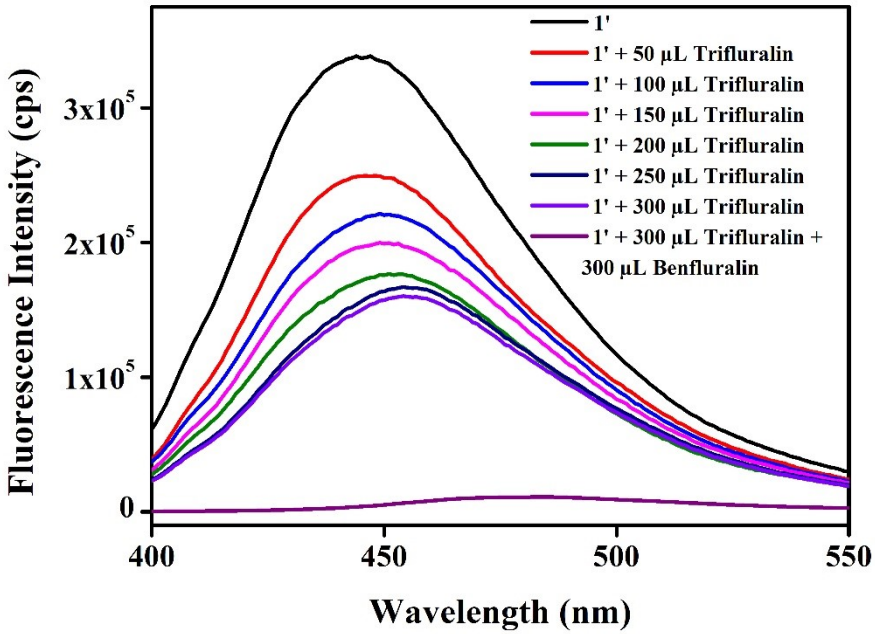

Figure S59. Change in fluorescence emission intensity of activated **1′** in methanol medium upon addition of 300 µL of 10 mM benfluralin in presence of 300 µL of 10 mM trifluralin (λ_{ex} = 366 nm and λ_{em} = 450 nm).

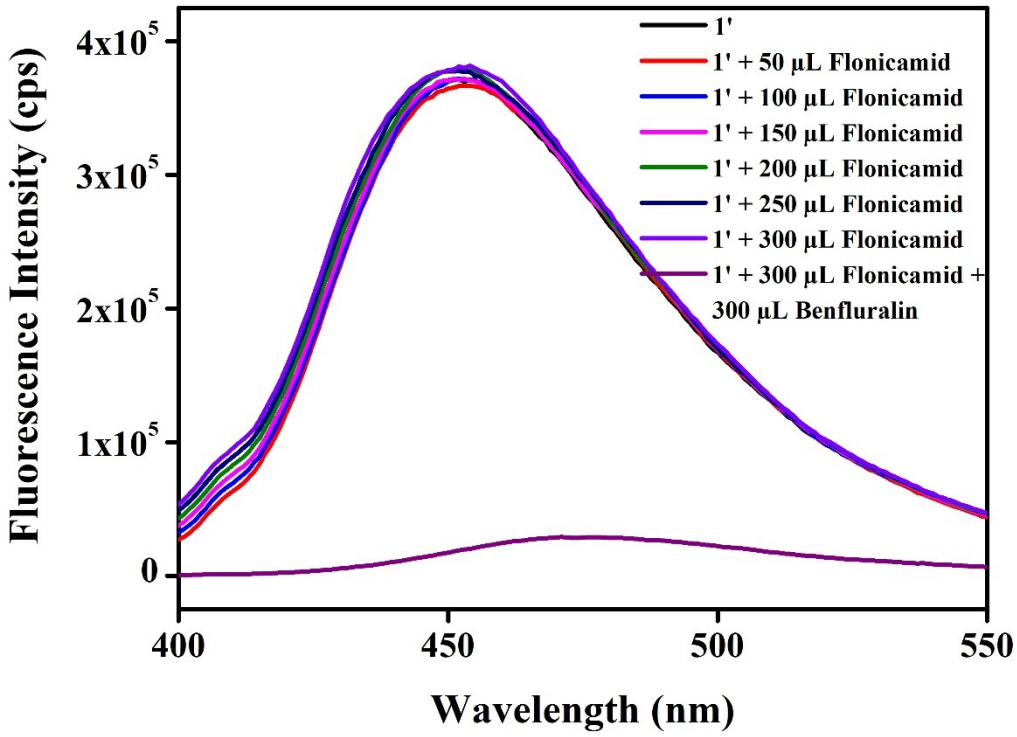

Figure S60. Change in fluorescence emission intensity of activated **1′** in methanol medium upon addition of 300 µL of 10 mM benfluralin in presence of 300 µL of 10 mM flonicamid (λ_{ex} = 366 nm and λ_{em} = 450 nm).

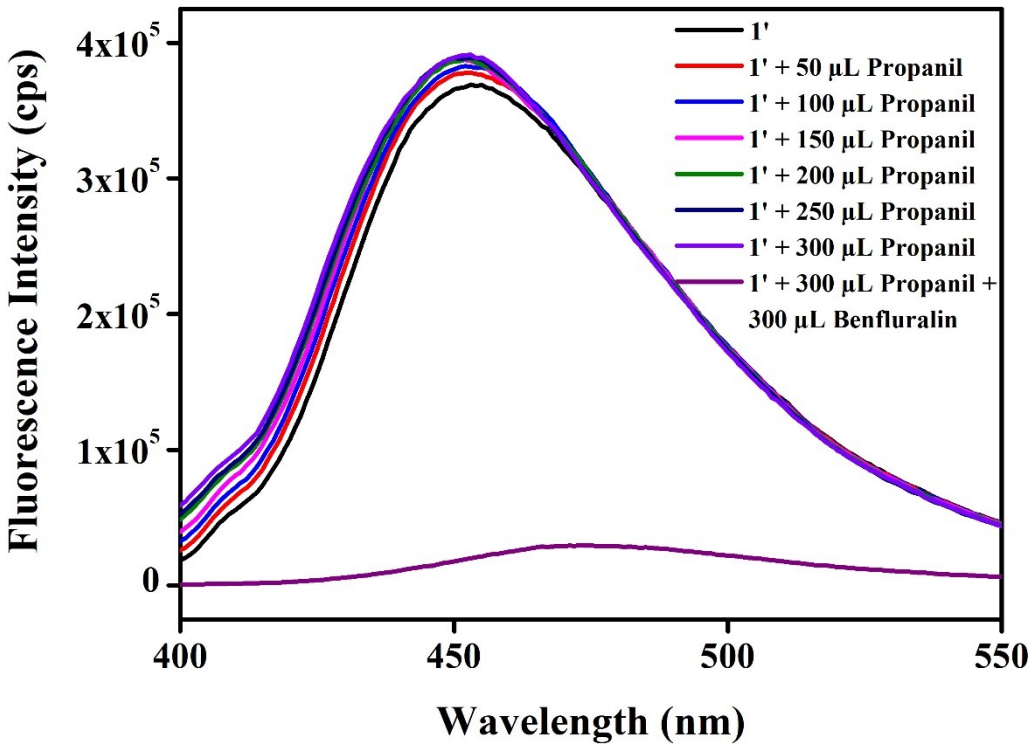

Figure S61. Change in fluorescence emission intensity of activated **1′** in methanol medium upon addition of 300 µL of 10 mM benfluralin in presence of 300 µL of 10 mM propanil (λ_{ex} = 366 nm and λ_{em} = 450 nm).

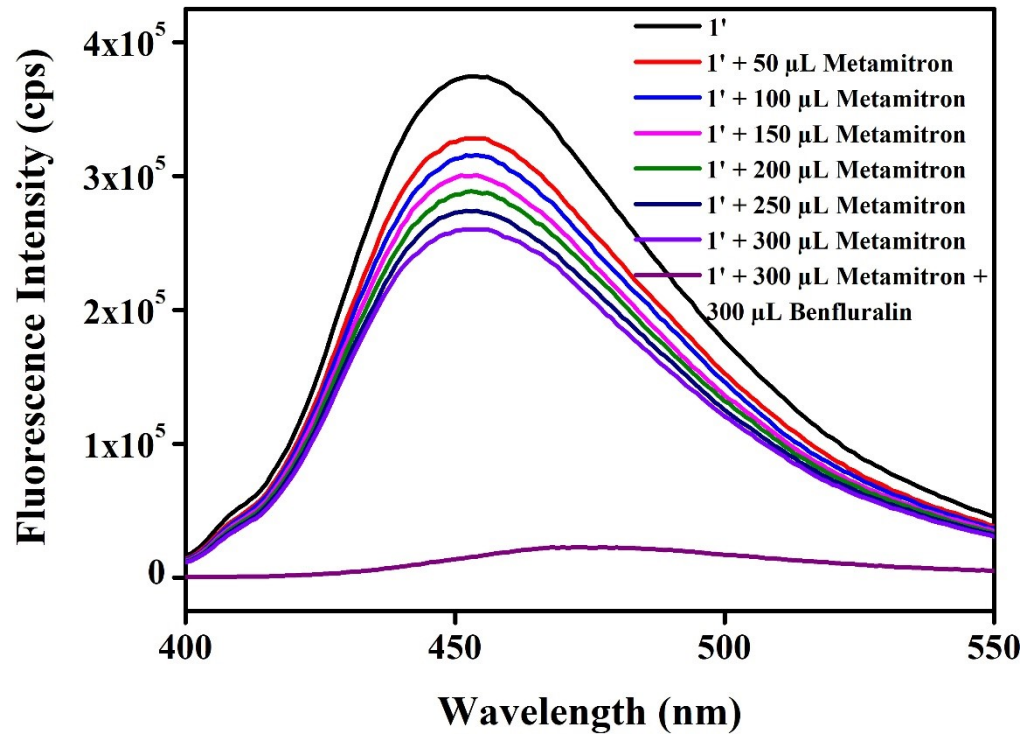

Figure S62. Change in fluorescence emission intensity of activated **1′** in methanol medium upon addition of 300 µL of 10 mM benfluralin in presence of 300 µL of 10 mM metamitron (λ_{ex} = 366 nm and λ_{em} = 450 nm).

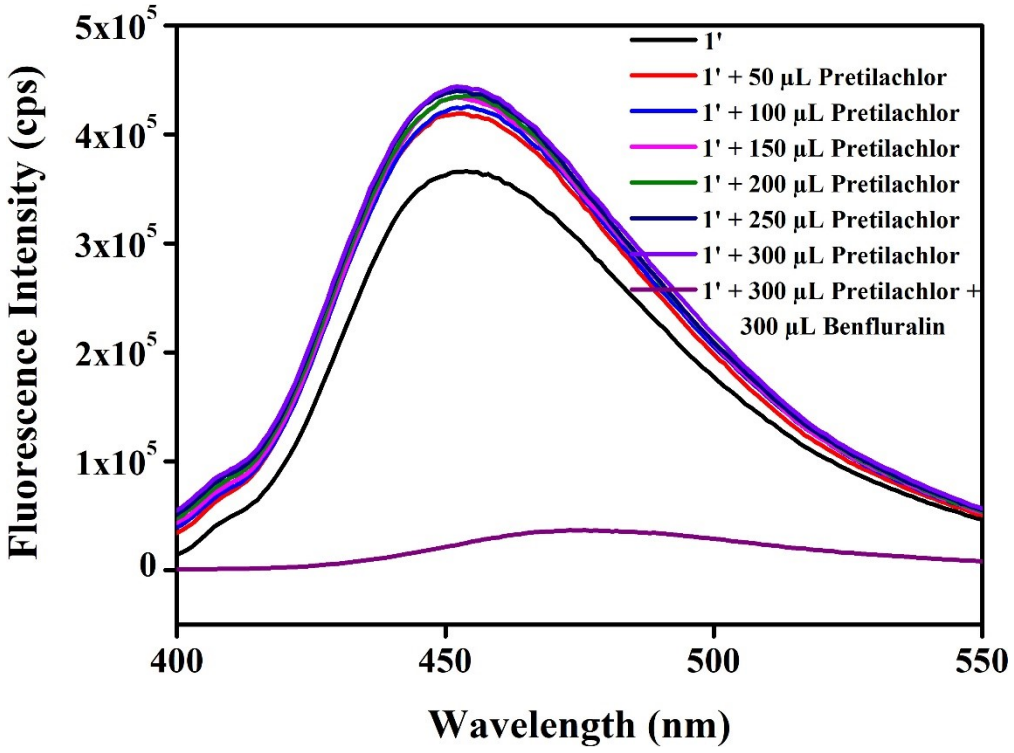

Figure S63. Change in fluorescence emission intensity of activated **1′** in methanol medium upon addition of 300 µL of 10 mM benfluralin in presence of 300 µL of 10 mM pretilachlor (λ_{ex} = 366 nm and λ_{em} = 450 nm).

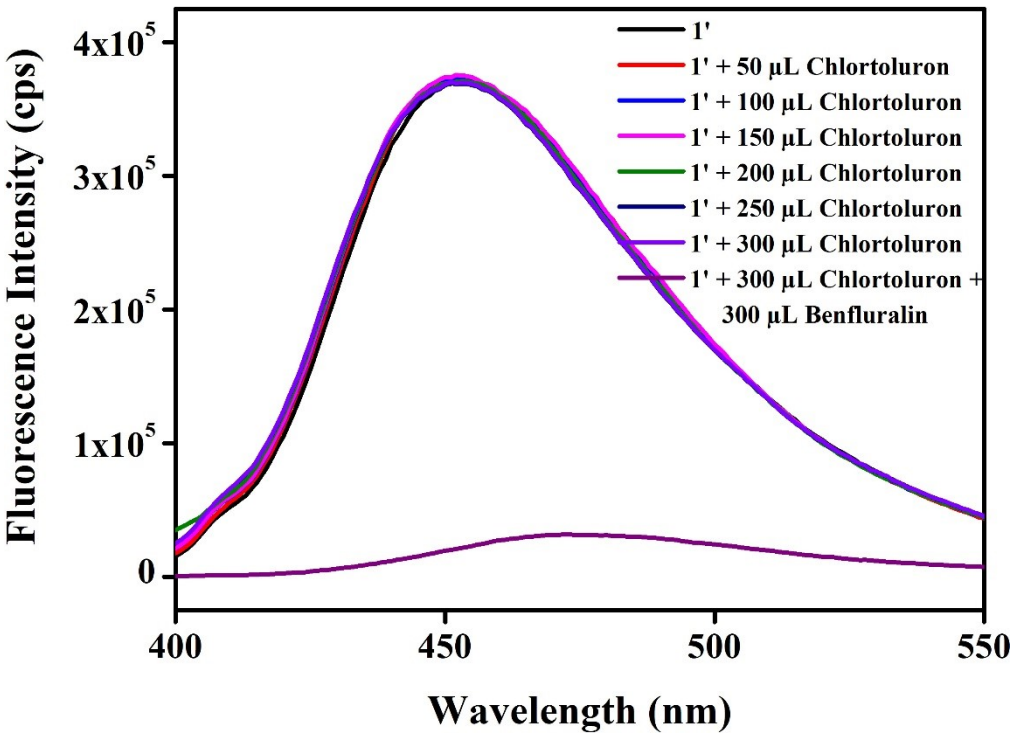

Figure S64. Change in fluorescence emission intensity of activated **1′** in methanol medium upon addition of 300 µL of 10 mM benfluralin in presence of 300 µL of 10 mM chlortoluron (λ_{ex} = 366 nm and λ_{em} = 450 nm).

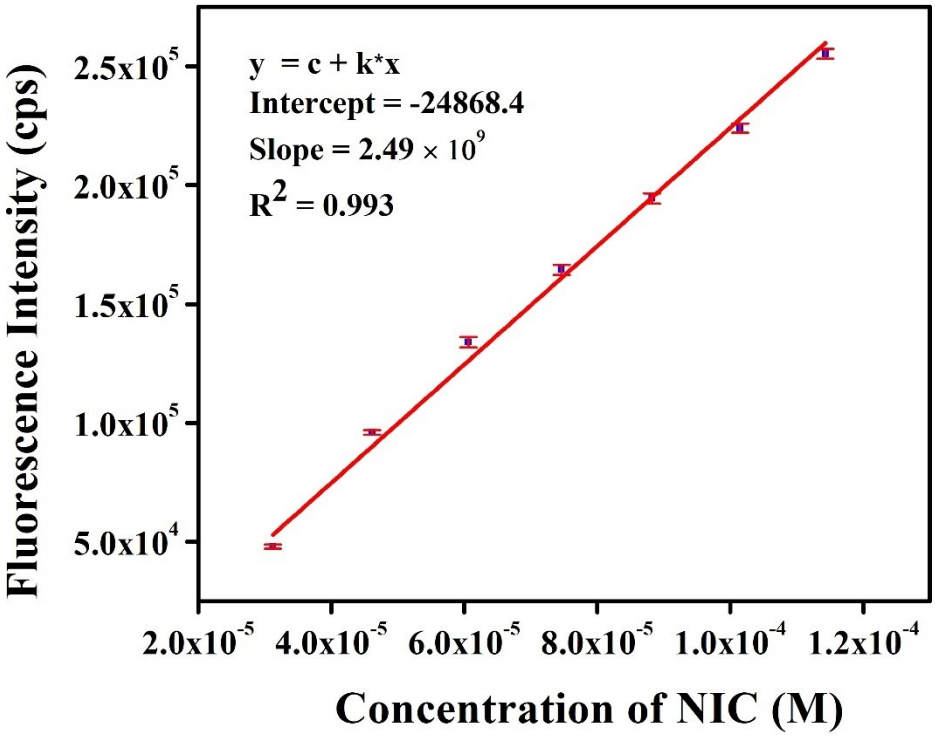

Figure S65. Change in fluorescence emission intensity of activated **1′** in water medium as a function of NIC concentration.

Table S2. Calculation of standard deviation of fluorescence intensity and limit of detection towards NIC.

Blank Readings	**Fluorescence Intensity (cps)**
Reading 1	32982.56
Reading 2	33063.39
Reading 3	33087.93
Reading 4	33290.68
Reading 5	33178.78
Reading 6	33368.93
Standard Deviation (σ)	133.49
Slope form Graph (K)	2.49E+09
LOD	160.8 nM

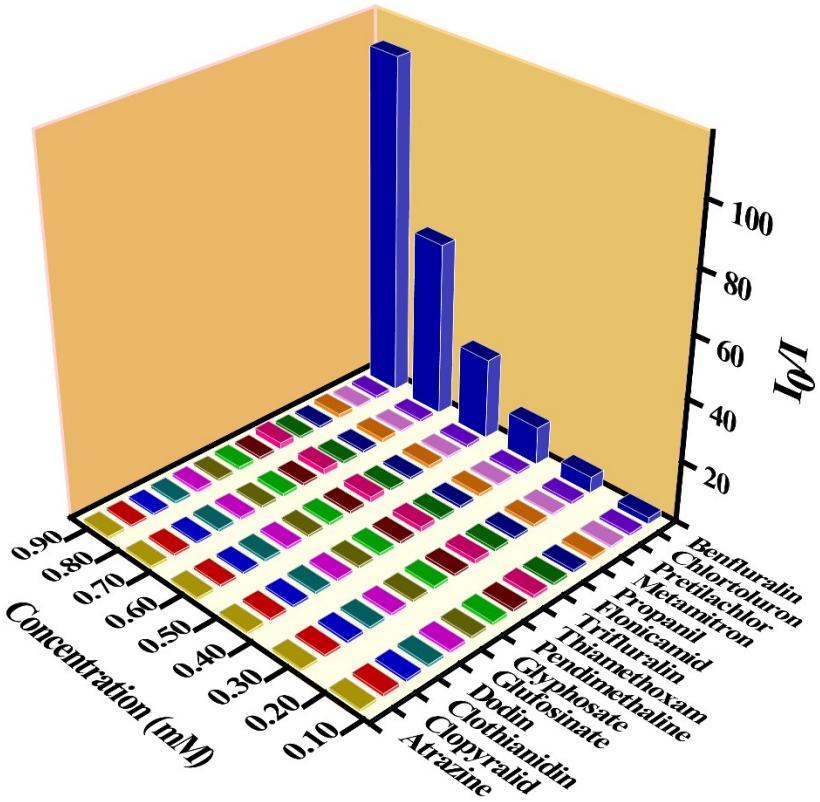

Figure S66. S-V plot for the decrease in fluorescence emission intensities of 1′ with gradual addition of various analytes in case of benfluralin sensing.

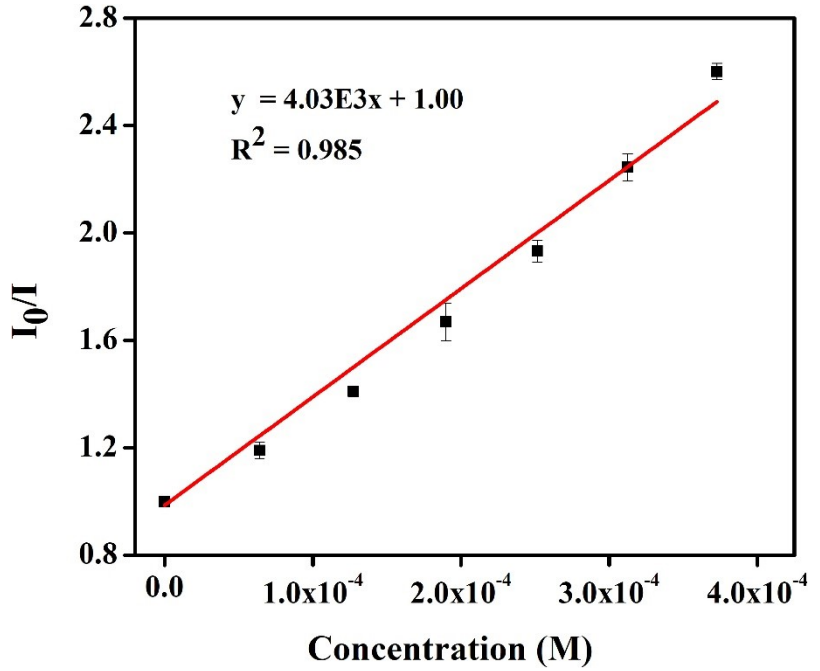

Figure S67. Stern-Volmer plot for fluorescence quenching of activated **1′** in methanol against increasing concentration of benfluralin.

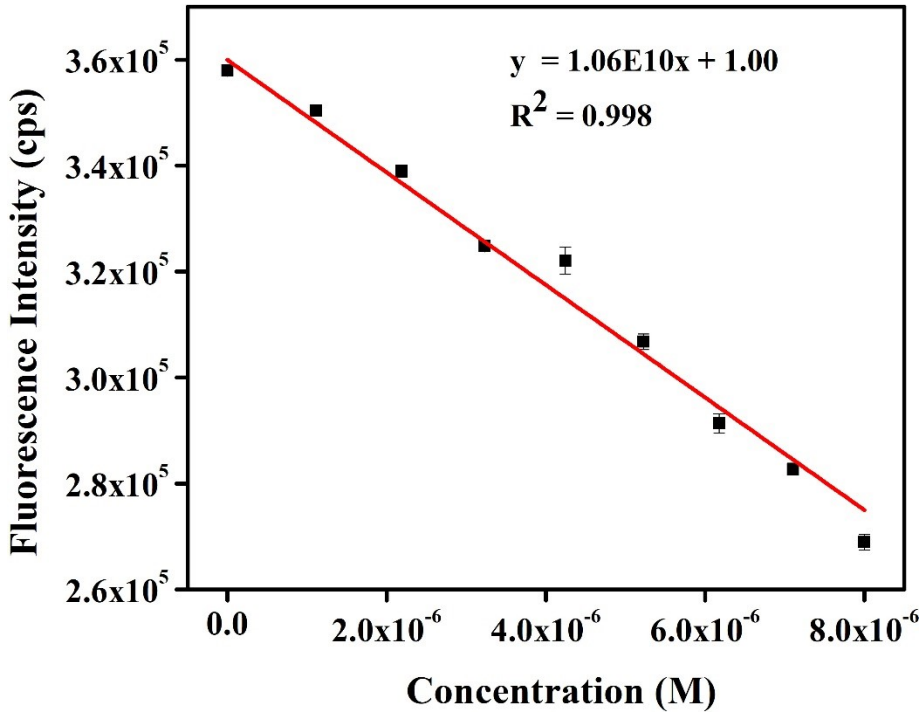

Figure S68. Change in fluorescence emission intensity of activated **1′** in methanol as a function of benfluralin concentration.

Table S3. Calculation of standard deviation of fluorescence intensity and limit of detection towards benfluralin.

Blank Readings	**Fluorescence Intensity (cps)**
Reading 1	337658.23
Reading 2	337486.73
Reading 3	337335.99
Reading 4	337327.85
Reading 5	336718.35
Reading 6	337386.521
Standard Deviation (σ)	291.23
Slope form Graph (K)	1.06E+10
LOD	82.4 nM

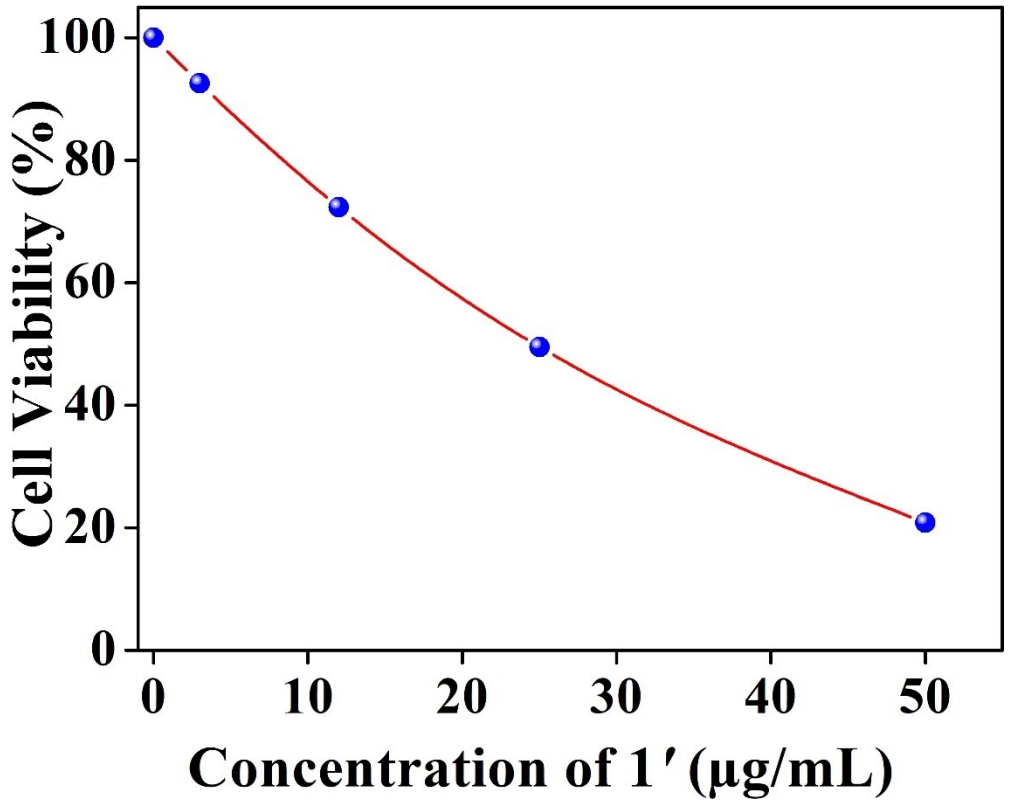

Figure S69. Cell viability assay for probe **1′** treated MDAMB-231 cells.

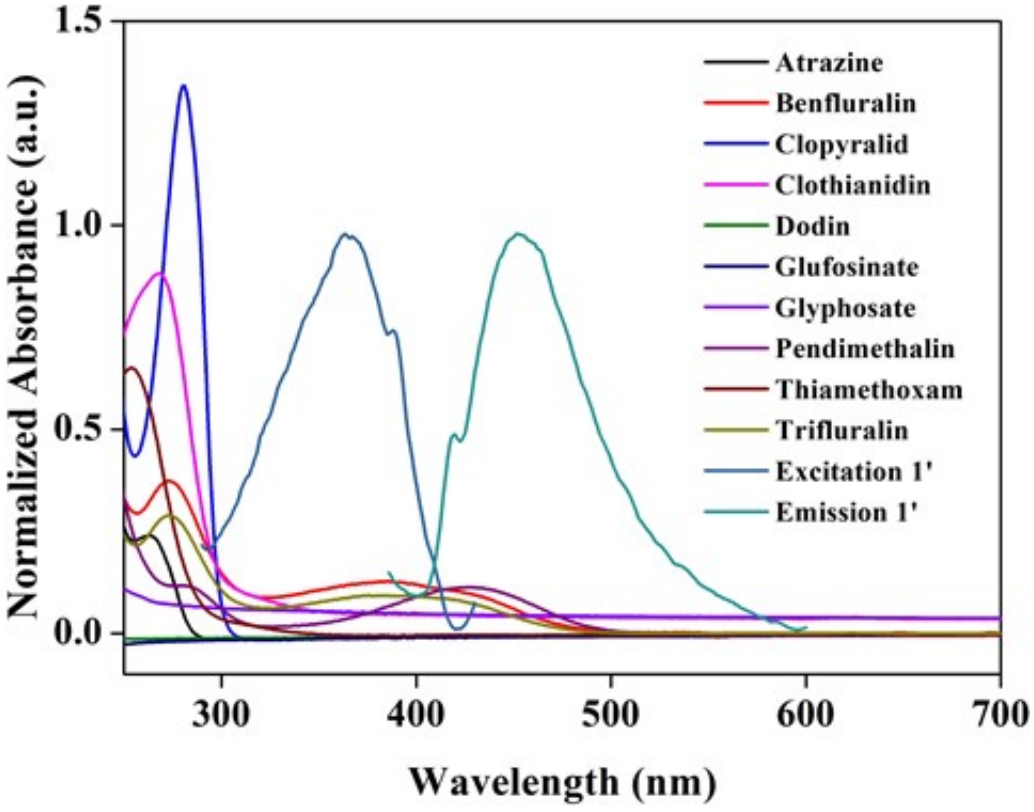

Figure S70. UV-Vis spectra of all competitive analytes of benfluralin and excitation and emission spectra of **1′**.

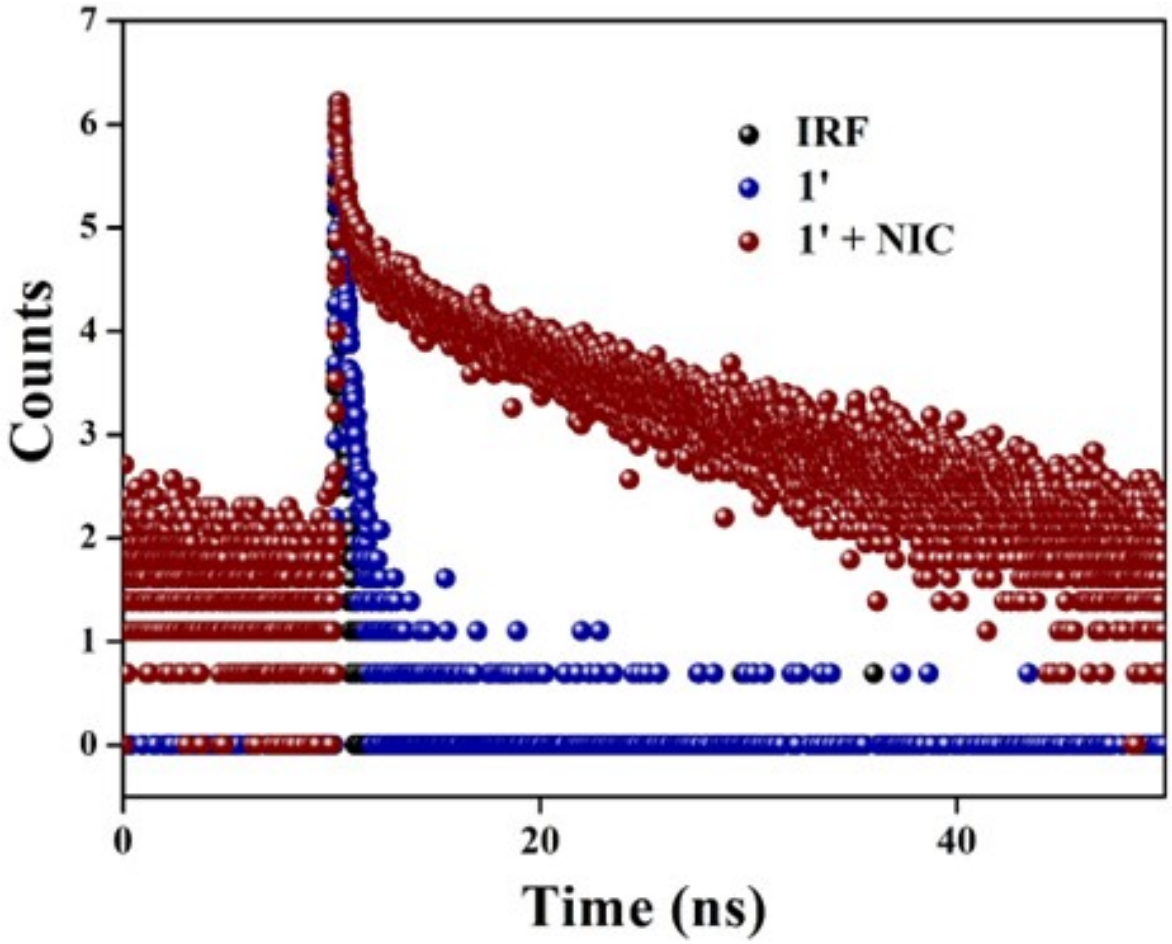

Figure S71. Fluorescence lifetime decay profile of **1′** in absence and presence of nicotine (λ_{ex} = 375 nm, monitored at 432 nm). Here, IRF = instrument response function.

Table S4. Fluorescence lifetime of **1′** before and after addition of nicotine (λ_{ex} = 374 nm, pulsed diode laser).

Volume of Nicotine Solution Added (μL)	a_1	a_2	τ_1 (ns)	τ_2 (ns)	$<\tau>^*$ (ns)	χ^2
0	56.849	43.151	0.045	0.296	0.515	0.94
100	4.121	95.879	0.256	11.485	11.02	1.15

Average lifetime $<\tau>^* = a_1\tau_1 + a_2\tau_2 + a_3\tau_3$

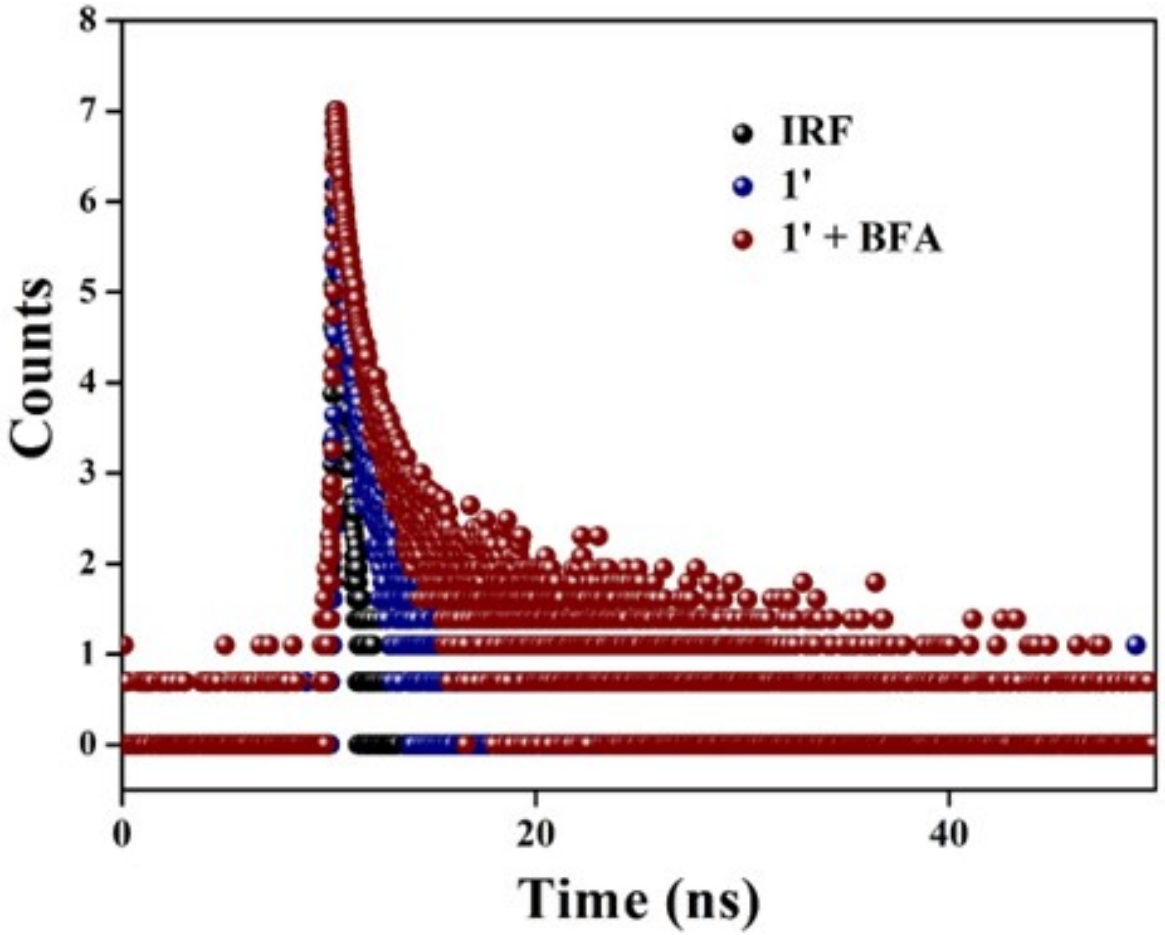

Figure S72. Fluorescence lifetime decay profile of **1′** in absence and presence of benfluralin (λ_{ex} = 374 nm, monitored at 447 nm). Here, IRF = instrument response function.

Table S5. Fluorescence lifetime of **1′** before and after addition of benfluralin (λ_{ex} = 374 nm, pulsed diode laser).

Volume of Benfluralin Solution Added (μL)	a_1	a_2	τ_1(ns)	τ_2(ns)	$<\tau>^*$ (ns)	χ^2
0	66.218	33.782	0.334	2.147	0.944	1.082
300	63.975	36.025	0.343	2.012	0.944	1.149

Average lifetime $<\tau>^* = a_1\tau_1 + a_2\tau_2 + a_3\tau_3$

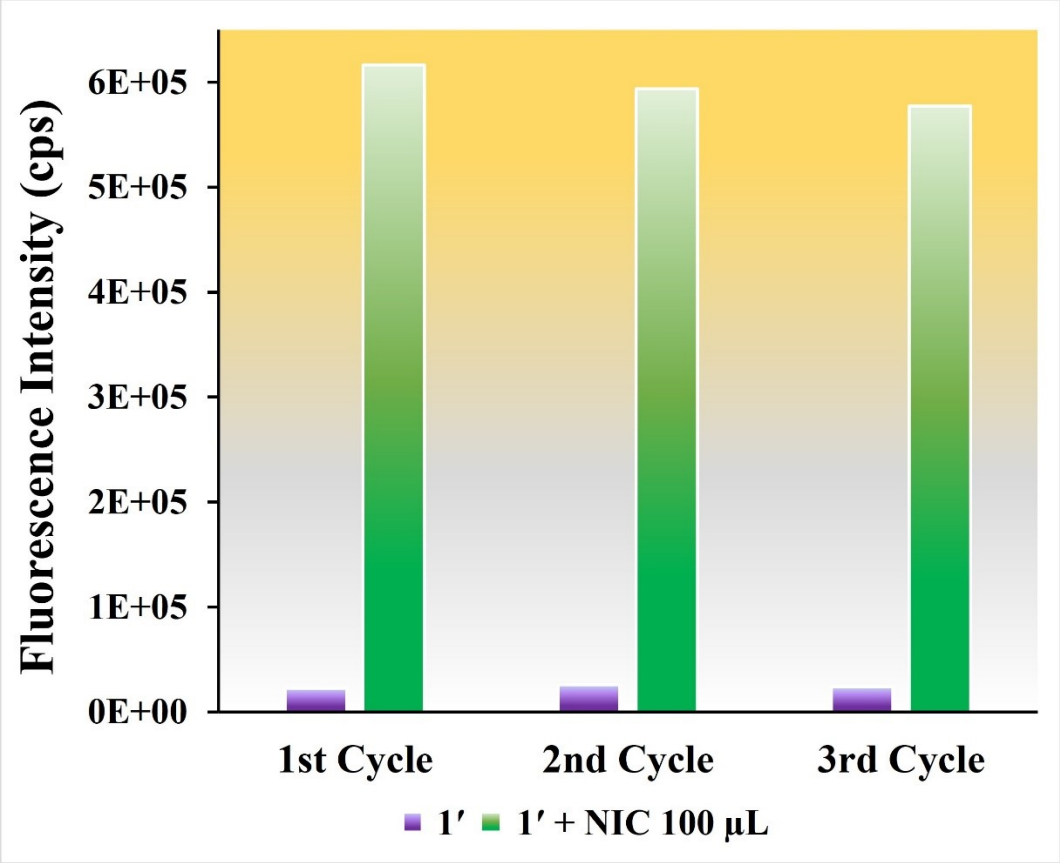

Figure S73. Recyclability test of probe **1'** for the sensing nicotine in aqueous medium.

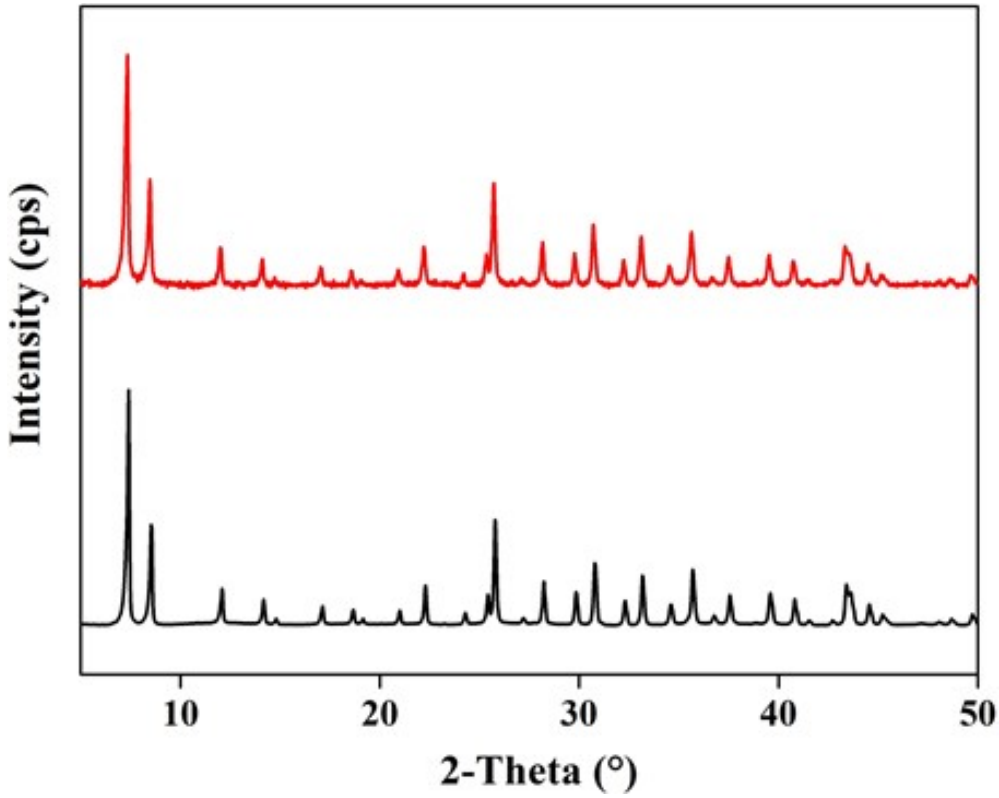

Figure S74. PXRD patterns of compound **1′** (black) after nicotine sensing (red).

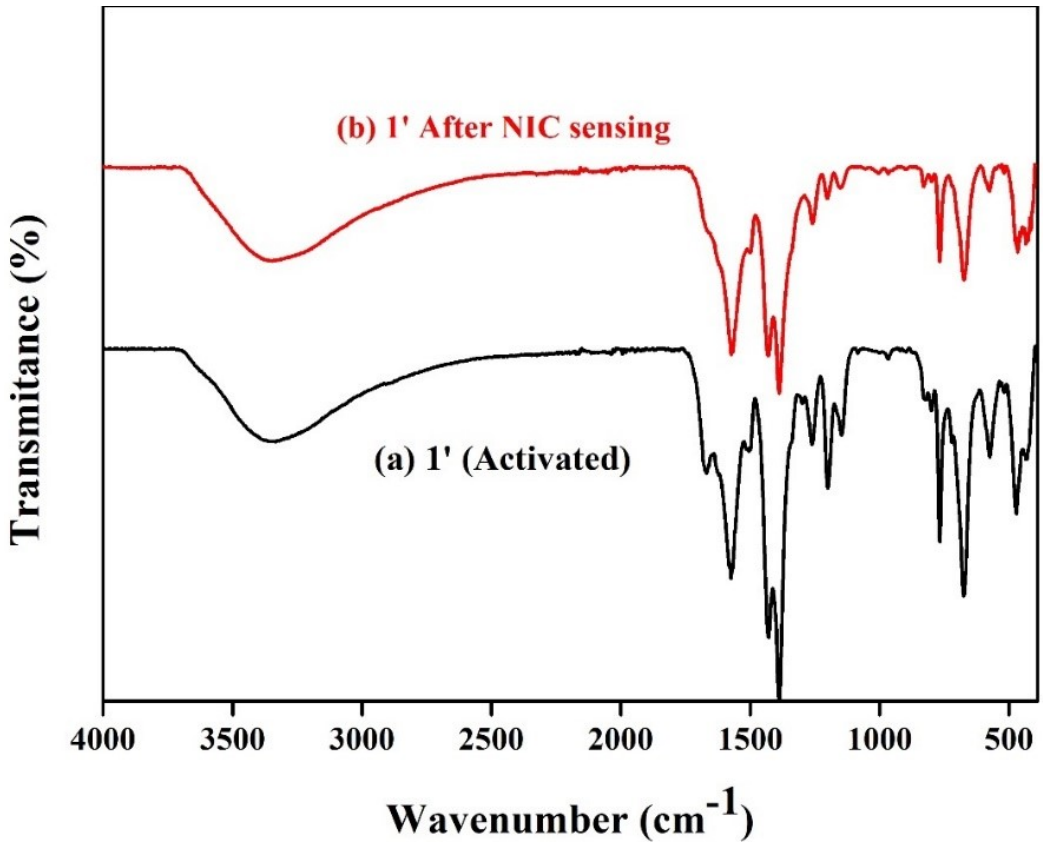

Figure S75. ATR-IR spectra of compound **1′** (black) after nicotine sensing (red).

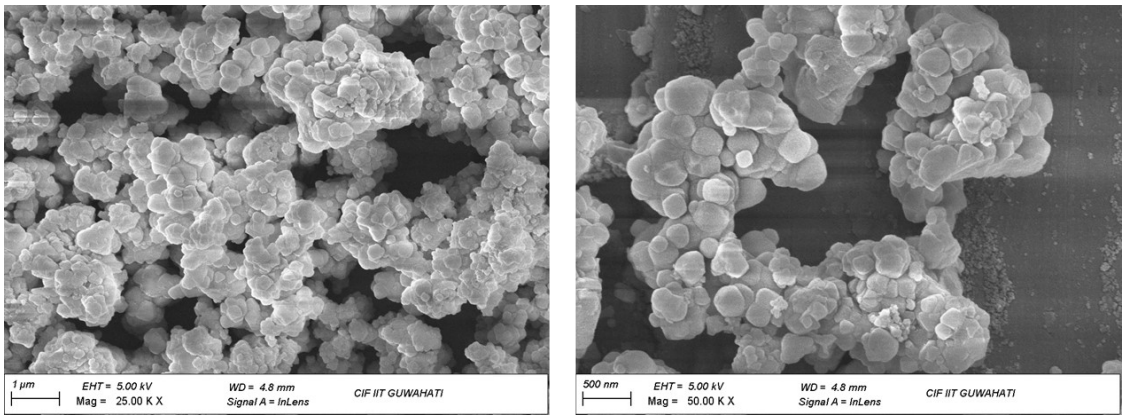

Figure S76. FE-SEM images of recycled **1** after nicotine sensing.

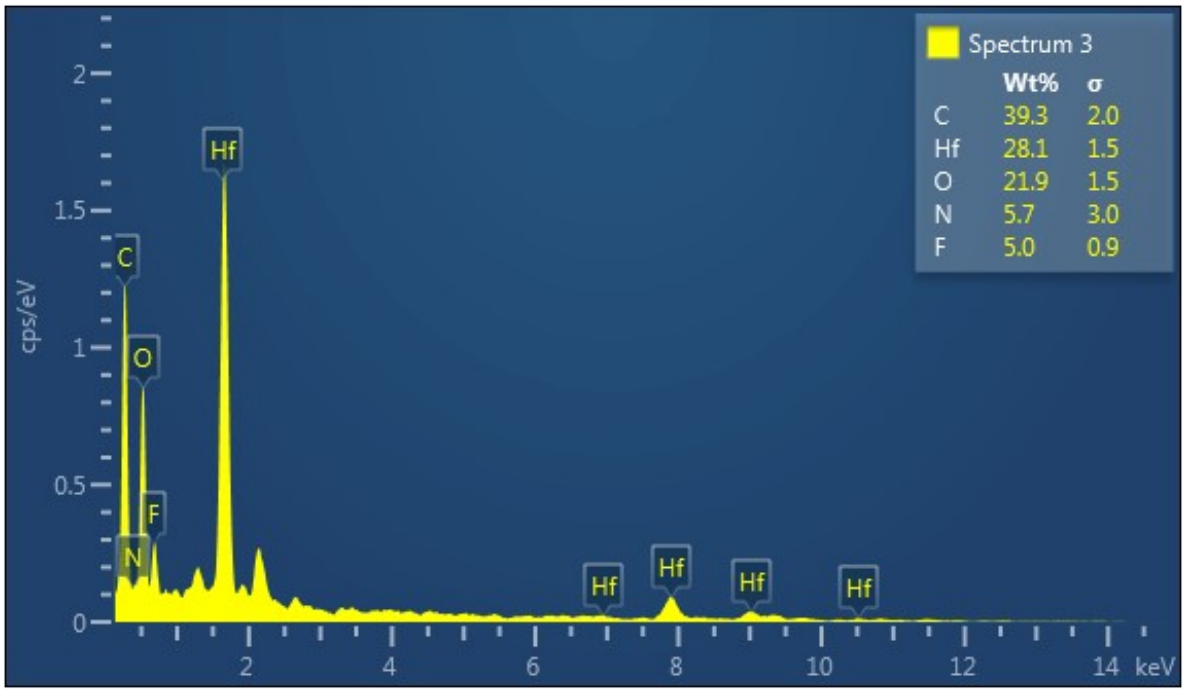

Figure S77. EDX spectrum of recycled **1** after nicotine sensing.

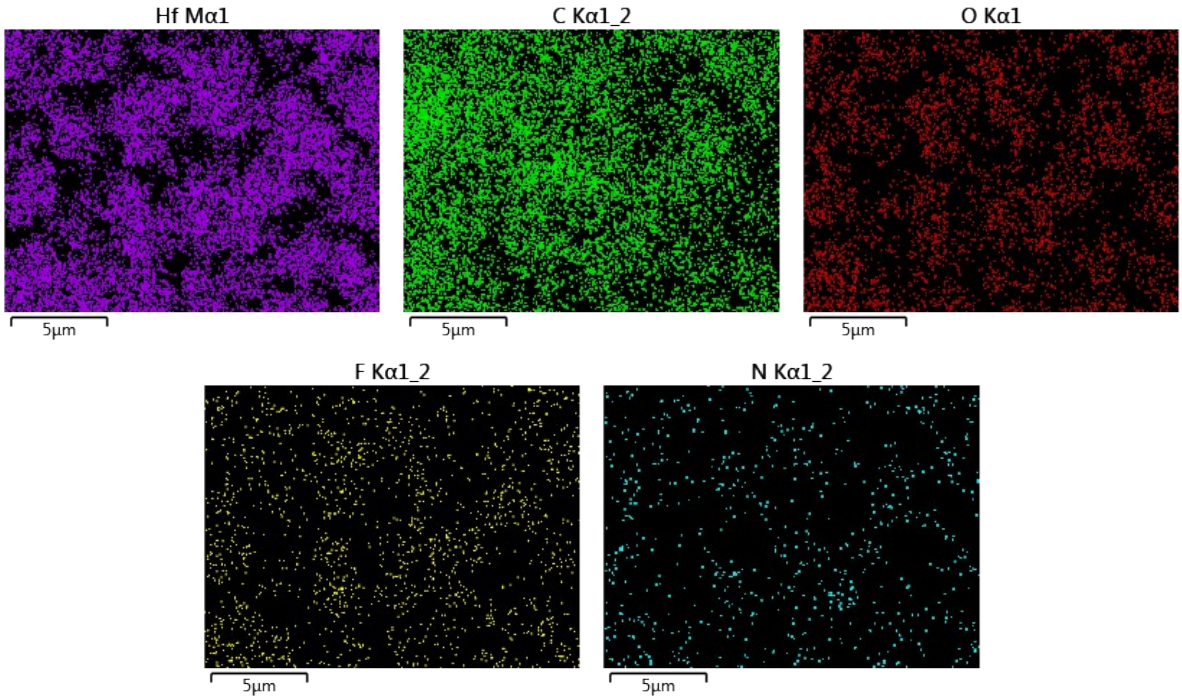

Figure S78. EDX elemental mapping of recycled **1** after nicotine sensing.

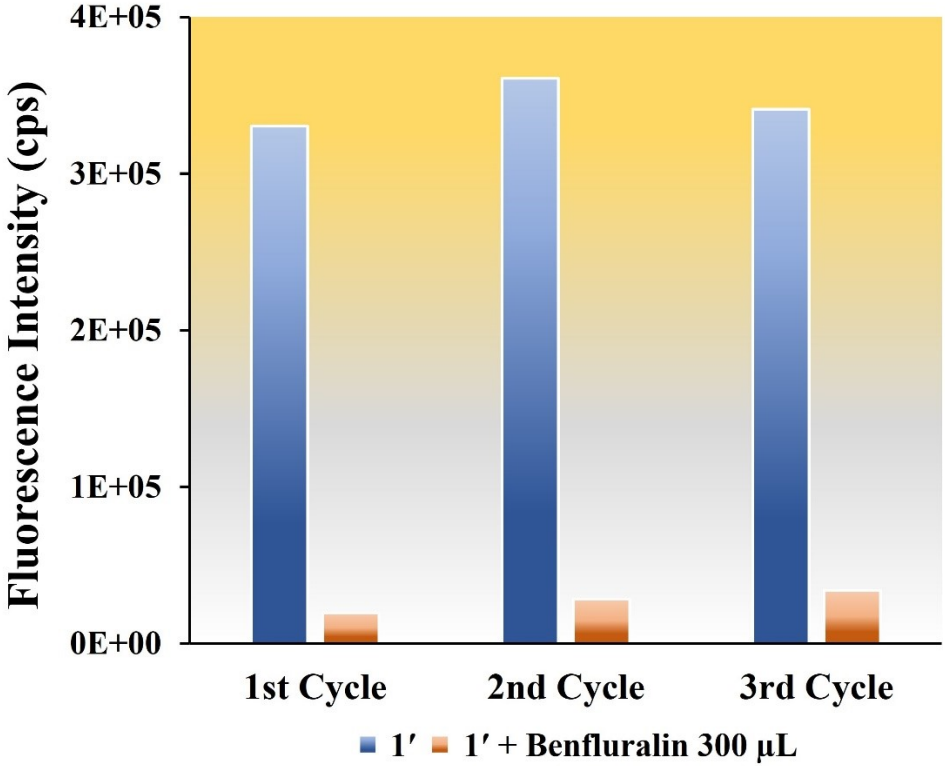

Figure S79. Recyclability test of probe **1'** for the sensing benfluralin in aqueous medium.

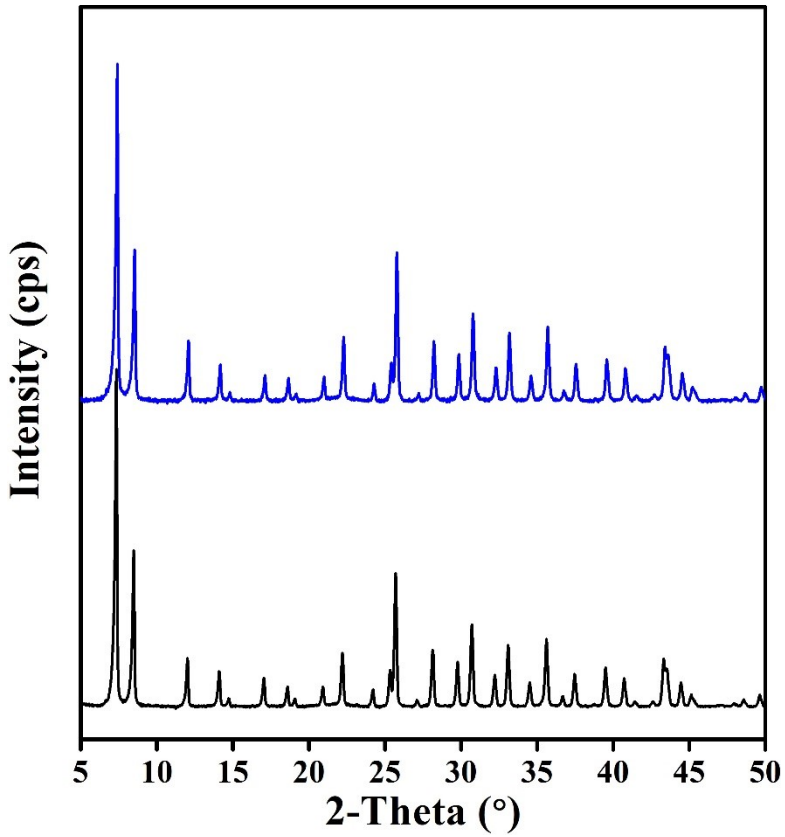

Figure S80. PXRD patterns of compound **1′** (black) after benfluralin sensing (blue).

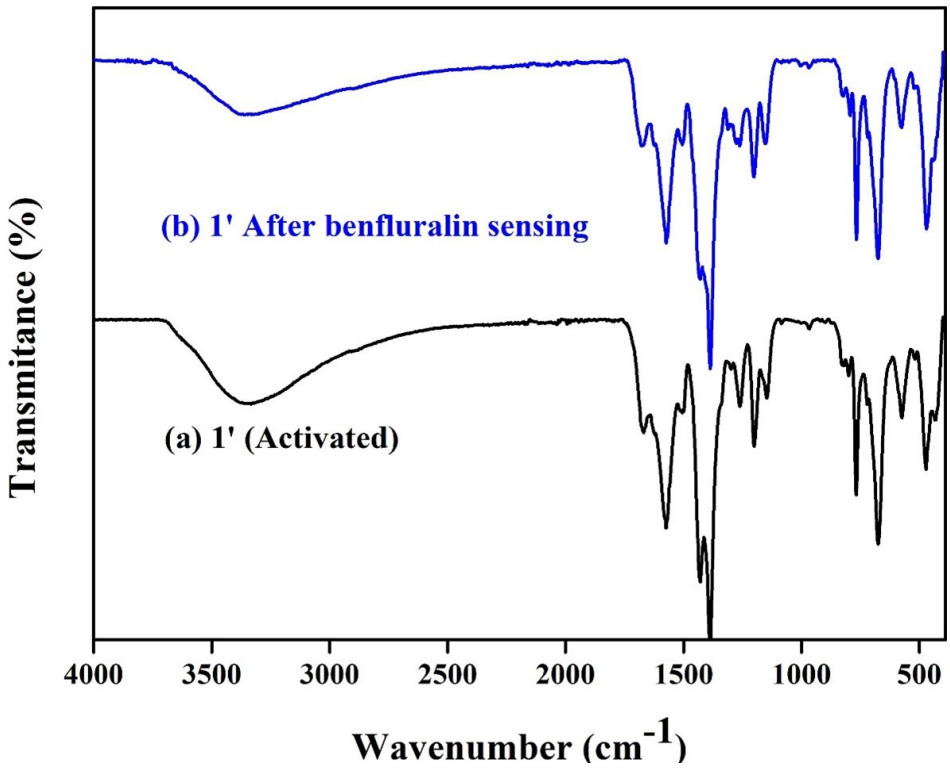

Figure S81. ATR-IR spectra of compound **1′** (black) after benfluralin sensing (blue).

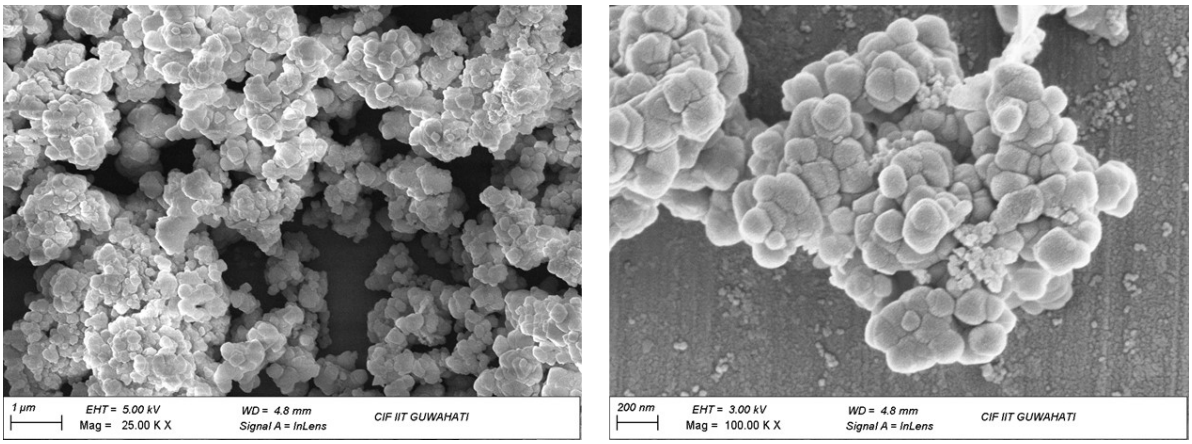

Figure S82. FE-SEM images of recycled **1** after benfluralin sensing.

Figure S83. EDX spectrum of recycled **1**⊃ after benfluralin sensing.

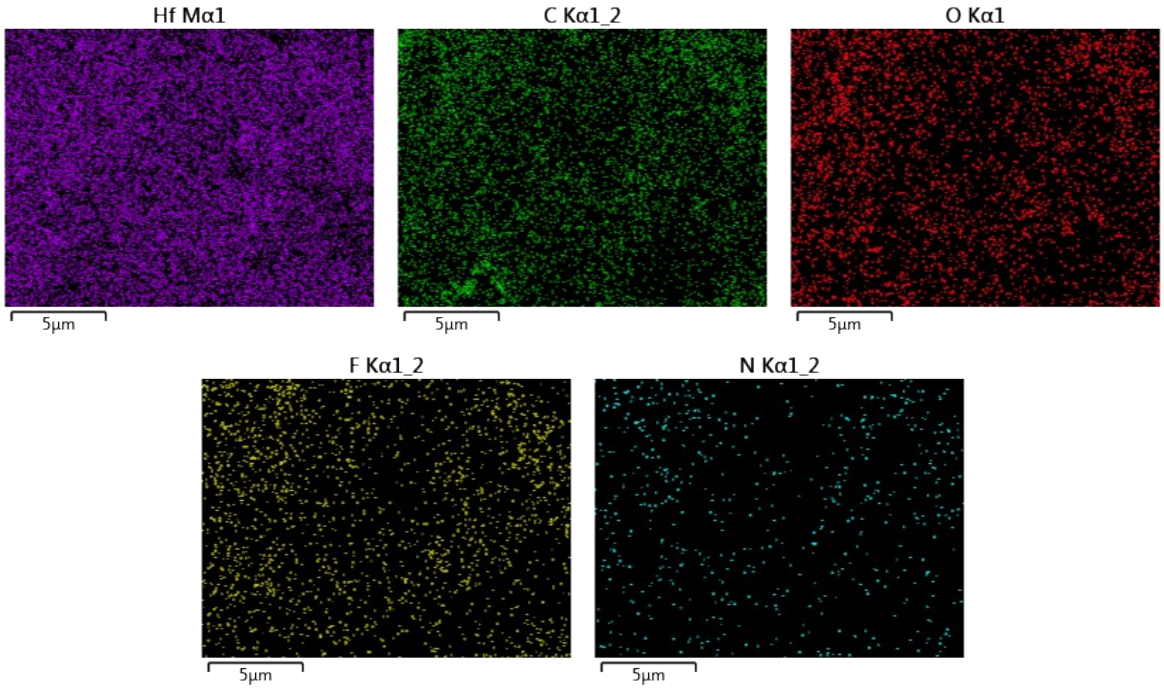

Figure S84. EDX elemental mapping of recycled **1**⊃ after benfluralin sensing.

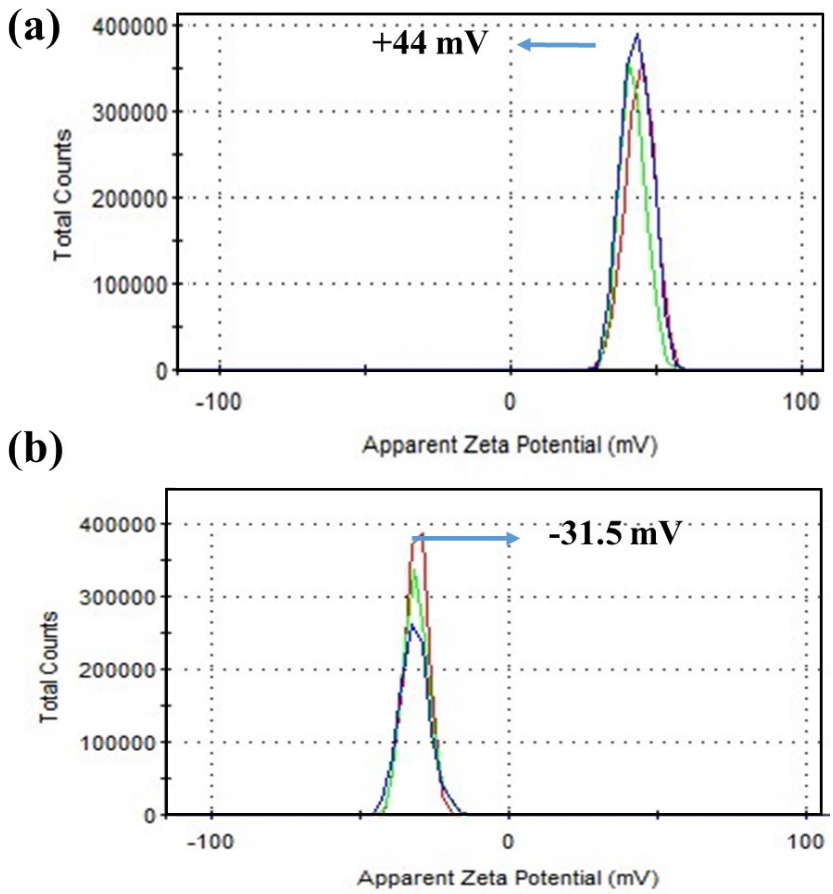

Figure S85. Surface zeta potential distribution of (a) **1′** and (b) **1′** + NIC in water (pH 7.0).

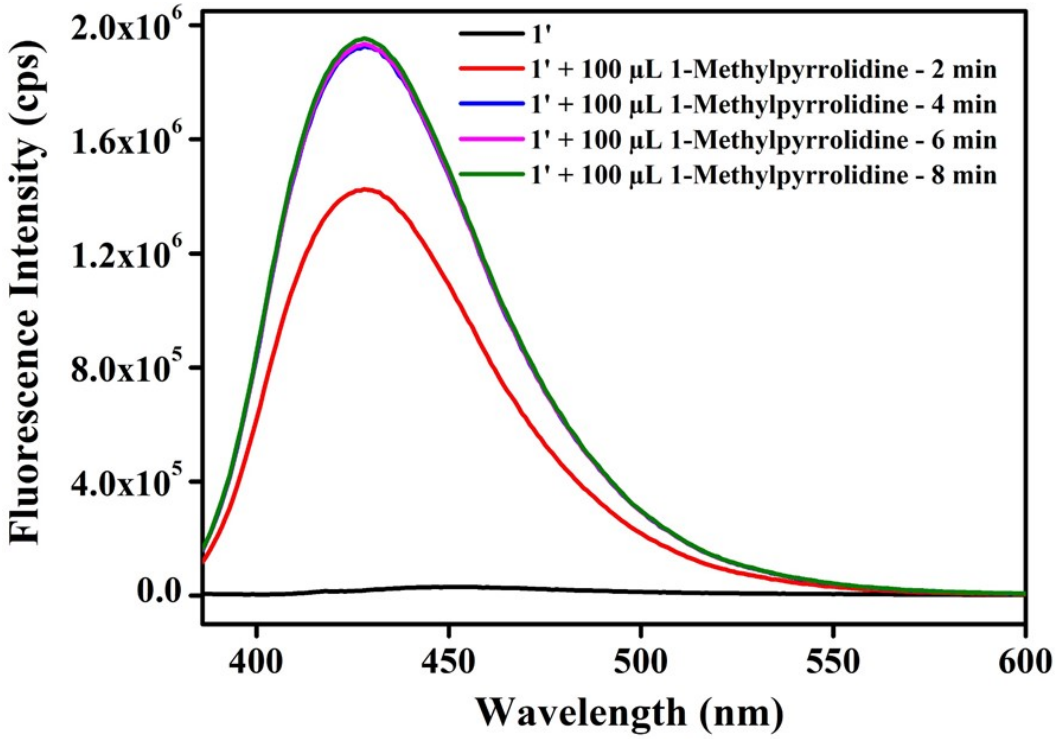

Figure S86. Change in fluorescence emission intensity of activated **1′** in aqueous medium upon addition of 100 µL of 10 mM 1-methylpyrrolidine (λ_{ex} = 366 nm and λ_{em} = 431 nm).

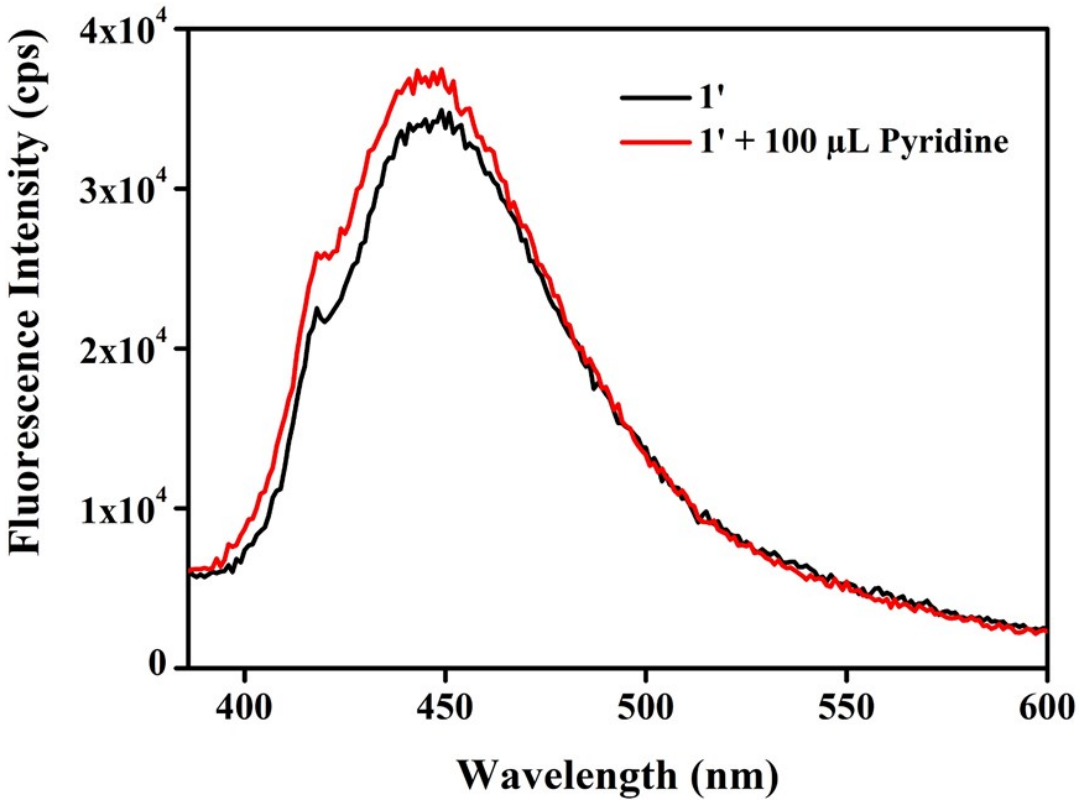

Figure S87. Change in fluorescence emission intensity of activated **1′** in aqueous medium upon addition of 100 µL of 10 mM pyridine (λ_{ex} = 366 nm and λ_{em} = 431 nm).

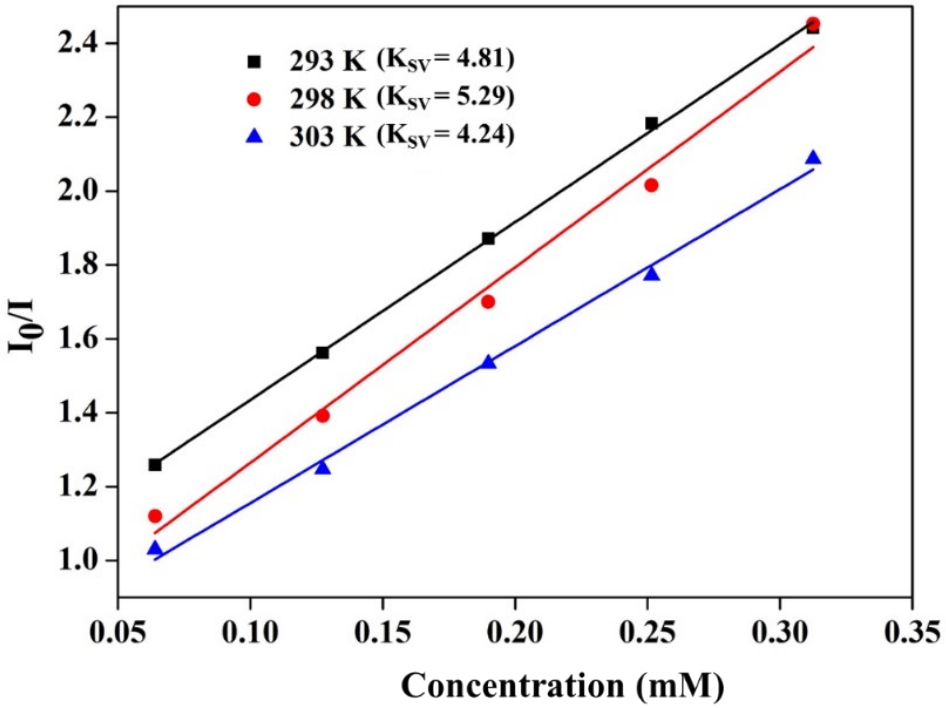

Figure S88. Stern–Volmer plots for the fluorescence emission quenching of **1′** in the presence of benfluralin solution at different temperatures.

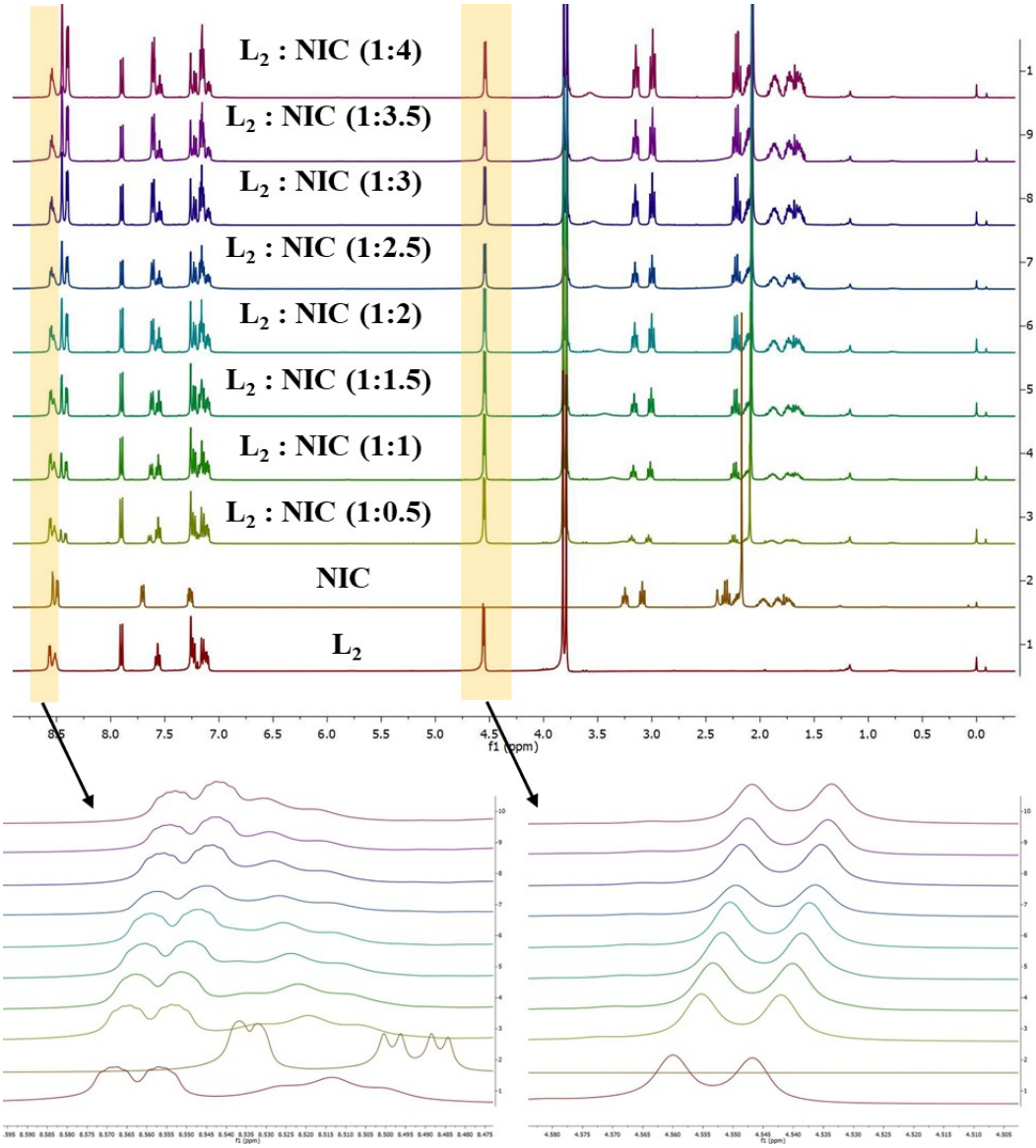

Figure S89. NMR titration experiment: a solution of NIC in $CDCl_3$ was incrementally added to the solution of the dimethyl 2-((pyridin-2-ylmethyl)amino)terephthalate (LE) in $CDCl_3$ medium and ^1H NMR spectra were collected.

Table S6. Comparison between the spiked and observed concentrations and recovery of nicotine in different biological samples

Biological samples	Spiked Conc. of Nicotine (μM)	Recovered Conc. of Nicotine (μM)	Recovery (%)
Human urine	78.51 151.51 220.5	77.79 150.07 221.03	99.0 99.0 99.7
Artificial sweat	78.51 151.51 220.5	76.6 147.61 218.48	97.56 97.42 99.0
Human serum	31.25 60.6 78.23	30.51 57.0 73.57	97.6 94.0 94.0

Table S7. Comparison between the spiked and observed concentrations and recovery of nicotine in environmental water samples.

Environmental water samples	Spiked Conc. of Nicotine (μM)	Recovered Conc. of Nicotine (μM)	Recovery (%)
River water	78.1	69.6	89.0
Lake water	78.1	74.0	94.8
Tap water	78.1	71.4	91.4
Mili-Q water	78.1	77.4	99.1

Table S8. Comparison of various probes previously reported in the literature for the fluorometric detection of nicotine.

Sl. No	Sensor Material	Sensing Medium	Response Time	LOD	Ref.
1	Copper and nitrogen doped carbon dots	phosphate buffer	-	10 μM	[2]
2	MB@UiO-66-NH_2	water	6 min	0.98 μM	[3]
3	MB-CB7 (cucurbit[7]uril)	NaAc–HAc buffer	20 min	0.31 μM	[4]
4	o-carborane-based fluorescent films	vapour phase	22 s	3 ppb	[5]
5	BITSH-1 MOF	ethanol	-	0.25 μM	[6]
6	Zr-BTDB-fcu MOF	water	-	280 nM	[7]
7	Eu(bpy)@HOF-215	water	2.2 s	0.039 μM	[8]
8	Zn porphyrin complex	water	<30 s	7.2 nM	[9]
9	Tb@MA-TMA/Zinc Film	gas	3 min	0.042 μM	[10]
10	**$[Hf_6(O)_4(OH)_4(C_{14}H_{10}O_4)(C_2F_3O_2)_4]$ (1′)**	**water**	**15 min**	**160.8 nM**	**this work**

Table S9. Comparison of various probes previously reported in the literature for the fluorometric detection of benfluralin.

Sl. No	Sensor Material	Sensing Medium	Response Time	LOD	Ref.
1	Surfactant assisted fluorescent probe	water	-	80 nM	[11]
2	**$Hf_6(O)_4(OH)_4(C_{14}H_{10}O_4)(C_2F_3O_2)_4]$ (1′)**	**methanol**	**5 s**	**82.4 nM**	**this work**

References

(1) Parker, C. A.; Rees, W. Correction of fluorescence spectra and measurement of fluorescence quantum efficiency. *Analyst* **1960**, *85* (1013), 587-600.
(2) Xu, X.; Chen, Z.; Li, Q.; Meng, D.; Jiang, H.; Zhou, Y.; Feng, S.; Yang, Y. Copper and nitrogen-doped carbon dots as an anti-interference fluorescent probe combined with magnetic material purification for nicotine detection. *Microchem. J.* **2021**, *160*, 105708.
(3) Yan, D.; Lou, Y.; Yang, Y.; Chen, Z.; Cai, Y.; Guo, Z.; Zhan, H.; Chen, B. Dye-modified metal–organic framework as a recyclable luminescent sensor for nicotine determination in urine solution and living cell. *ACS Appl. Mater. Interfaces* **2019**, *11* (50), 47253-47258.
(4) Zhou, Y.; Yu, H.; Zhang, L.; Xu, H.; Wu, L.; Sun, J.; Wang, L. A new spectrofluorometric method for the determination of nicotine base on the inclusion interaction of methylene blue and cucurbit [7] uril. *Mikrochim. Acta* **2009**, *164*, 63-68.
(5) Liu, K.; Zhang, J.; Xu, L.; Liu, J.; Ding, L.; Liu, T.; Fang, Y. Film-based fluorescence sensing: a "chemical nose" for nicotine. *Chem. Commun.* **2019**, *55* (84), 12679-12682.
(6) Leelasree, T.; Goel, S.; Aggarwal, H. MOF-based dual sensor for the electrochemical and fluorescence detection of nicotine. *ACS Appl. Nano Mater.* **2022**, *5* (11), 16753-16759.
(7) Mallick, A.; El-Zohry, A. M.; Shekhah, O.; Yin, J.; Jia, J.; Aggarwal, H.; Emwas, A.-H.; Mohammed, O. F.; Eddaoudi, M. Unprecedented ultralow detection limit of amines using a thiadiazole-functionalized Zr (IV)-based metal–organic framework. *J. Am. Chem. Soc.* **2019**, *141* (18), 7245-7249.
(8) Yang, C.; Yan, B. Dual-Function Platform Based on Postsynthetic Functionalization of a Water-Stable Hydrogen-Bonded Organic Framework: Ratiometric Sensing of Nicotine and Cotinine and Dynamic Anticounterfeiting for Information Encryption. *Inorg. Chem.* **2023**, *62* (49), 20458-20466.
(9) Mondal, S.; Ahmad, I.; Dey, N. Multifaceted Applications of Luminescent Metalloporphyrin Derivatives: Fluorescence Turn-On Sensing of Nicotine and Antimicrobial Activity. *ACS Appl. Bio Mater.* **2024**, *7* (4), 2346-2353.
(10) Hu, Z.; Yan, B. Facile fabrication of luminescent Tb@ HOF-based films as a highly sensitive platform for detecting nicotine and its metabolite cotinine via fluorescence sensing and a smartphone. *Journal of Materials Chemistry A* **2023**, *11* (9), 4739-4750.
(11) Qin, T.; Zhao, X.; Jia, T.; Si, S.; Xu, Z.; Liu, B.; Xu, H.; Zhao, C. A surfactant-assisted approach enables the fluorescence tracking of benfluralin in plants. *Spectrochim Acta A Mol Biomol Spectrosc* **2022**, *280*, 121517.